2017-05-30

Investigating the Role of PIR1 and CD200R1 in the Innate Immune Response to Viral Pathogens

Christopher R. MacKay
University of Massachusetts Medical School

INVESTIGATING THE ROLE OF PIR1 AND CD200R1 IN THE INNATE IMMUNE RESPONSE TO VIRAL PATHOGENS

A Dissertation Presented

by

CHRISTOPHER ROBERT MacKAY

Submitted to the Faculty of the

University of Massachusetts Graduate School of Biomedical Sciences, Worcester

in partial fulfillment of the requirements for the degree of

DOCTOR OF PHILOSOPHY

May 30, 2017

M.D./Ph.D. Program

INVESTIGATING THE ROLE OF PIR1 AND CD200R1 IN THE INNATE IMMUNE RESPONSE TO VIRAL PATHOGENS

A Dissertation Presented

by

CHRISTOPHER ROBERT MacKAY

The signatures of the Dissertation Defense Committee signifies

completion and approval as to style and content of the Dissertation

---

Evelyn A. Kurt-Jones, Ph.D., Thesis Advisor

Robert Finberg M.D., Member of Committee

Egil Lien, Ph.D., Member of Committee

Craig Mello, Ph.D., Member of Committee

Jennifer Wang, M.D., Member of Committee

Kate Jeffrey, Ph.D. (Massachusetts General Hospital), Member of Committee

The signature of the Chair of the Committee signifies that the written dissertation meets

the requirements of the Dissertation Committee

Neal Silverman, Ph.D., Chair of Committee

The signature of the Dean of the Graduate School of Biomedical Sciences signifies

that the student has met all graduation requirements of the school.

Anthony Carruthers, Ph.D., Dean of the Graduate School of Biomedical Sciences

M.D./Ph.D. Program

May 30, 2017

Abstract

After initially being infected with a virus, before an adaptive immune response can be mounted, the innate immune system of a cell recognizes and responds to certain patterns present in pathogenic molecules. I studied the role of two genes—PIR1 and CD200R1—on the innate immune responses in two different mouse models of viral infection, infection with the picornavirus EMCV (encephalomyocarditis virus) and infection with HSV-1 (herpes simplex virus) in a mouse model of herpes simplex encephalitis, respectively.

PIR1 is a putative RNA phosphatase that has been shown to play an important role in antiviral small RNA processing in *C. elegans*. It has also been shown to interact with the RIG-I-like receptor LGP2 in preliminary mammalian experiments. I sought to characterize the effect PIR1 has on the innate immune response to the virus EMCV in mice. By developing a PIR1-null mouse, I have found that the role of PIR1 in the progression of EMCV in mice is limited. However, *in vitro* studies show that PIR1 might play an important role in regulating foreign RNA recognition during the earliest time points post-infection.

CD200R1 is an anti-inflammatory signaling molecule that is expressed on myeloid-derived cells, and whose ligand is highly expressed within the central nervous system. I investigated the role of this receptor in an intracranial model of herpes simplex encephalitis. CD200R1KO mice show improved survival following direct intracranial infection with HSV. I found this increased survival can be attributed to decreased levels of viral replication in CD200R1KO compared to wild-type mice. Further investigation has shown that CD200R1 affects the signaling and upregulation of the pattern-recognition receptor TLR-2 (toll-like receptor 2), and thus CD200R1 may impact HSV-1 replication by affecting TLR2 signaling.

Contents

List of Tables

List of Figures

Abbreviations

5'pppRNA 5'-triphosphorylated RNA

avRNAi Antiviral RNA interference

BMDC Bone-marrow-derived dendritic cells

BSA Bovine serum albumin

CARD Caspase activation and recruitment domain

cDNA complementary DNA

CNS Central nervous system

CPE Cytopathic effect

DAB 3,3'-diaminobenzidine

DUSP Dual-specificity phosphatase

EMCV Encephalomyocarditis virus

HSE Herpes Simplex Encephalitis

IAV Influenza A Virus

IFN Interferon

IL Interleukin

IRES Internal ribosome entry site

ISG Interferon stimulated gene

LPS Lipopolysaccharide

MOI Multiplicity of infection

OD Optical density

PAGE Polyacrylamide gel electrophoresis

PAMP Pathogen-associated molecular patterns

PRR Pattern recognition receptor

qRT-PCR Quantitative reverse-transcriptase PCR

RNApolIII RNA polymerase III

SDS Sodium dodecyl sulfate

TBS Tris-buffered saline

TEMED Tetramethylethylenediamine

TNF Tumor necrosis factor

TSB Tryptic soy broth

CHAPTER I: Introduction

1.1 The Virus and the Human

As humans, we encounter potentially pathogenic viruses on a daily basis. While some pose little risk to our health, there are many which could be life-threatening if allowed to take hold within our cells. Fortunately, humans have evolved with both innate and adaptive immune systems, such that in an otherwise healthy host, viral infection may result only in a self-limited illness. For example, the Influenza A Virus (IAV) will manifests in an otherwise healthy person as several days of fever, myalgia, and lethargy, typically without long-term sequelae. However, when the immune systems are compromised—such as in the very young, the very old, pregnant women, those with chronic medical conditions or immunodeficiencies, and those receiving immunosuppressive therapies— this same virus can overwhelm the host, leading to severe disability and even death. For example, the CDC estimates that in the 2015-2016 flu season nearly 12,000 people died as a direct result of the influenza virus, a number that has ranged from 4,000-20,000 over the past five years (when accounting for secondary deaths from complications of infection, those figures balloon to 16,000-76,000 annually) [1]. While there is value in vaccine research and understanding the role of the adaptive immune system in resolving viral infections, there is still much we do not know about our most basic and vital innate immune responses, the first defense against infection from the viruses that surround us every day. Therefore, this dissertation explores the important roles of two proteins that function within the innate immune system - PIR1 and CD200R1.

1.2 Host Responses to Viral Infection

As mammals, our very first defense against any foreign virus or microbe in the environment includes a number of physical barriers such as our skin. However, if a pathogen overcomes this physical obstacle, infection can begin. In the case of viral infections, this process depends on cell entry, viral gene expression, and the manipulation of host components to promote self-replication. In order to combat this process and limit the negative effects of pathogenic viral infections, the host can mount an immune response. These many coordinated reactions, when effective, are capable of mitigating—if not eliminating—a viral infection. If the host is naive with respect to the infecting virus, the adaptive immune response can take a few days to weeks to develop and then reach a conclusion. Therefore, the immediate innate immune response serves as a critical first-line defense against pathogenic infections in mammals.

1.2.1 Pattern Recognition by the Innate Immune System

Without having encountered a particular virus before, mammals are still capable of recognizing and responding to a viral infection through the function of pattern-recognition receptors (PRR). While pathogenic microbes are highly varied and constantly changing, they possess certain structural patterns that a cell is able to recognize as foreign. These pathogen associated molecular patterns (known as PAMPs) are themselves quite varied, and range from cell-wall components of bacteria to RNA molecules generated as replication intermediates during a viral infection. Animals have evolved to recognize these patterns as being associated with pathogenic organisms or tissue damage and respond accordingly.

As shown in Figure 1.1, in the hours to days following an infection a naive host is able to produce a range of cytokines, including the type 1 interferon (IFN) molecules IFN-β and IFN-α. This initial response, triggered by the PRRs of infected cells, is critical in hampering viral replication, and in affording the host the 4 to 5 days required to generate a virus-specific

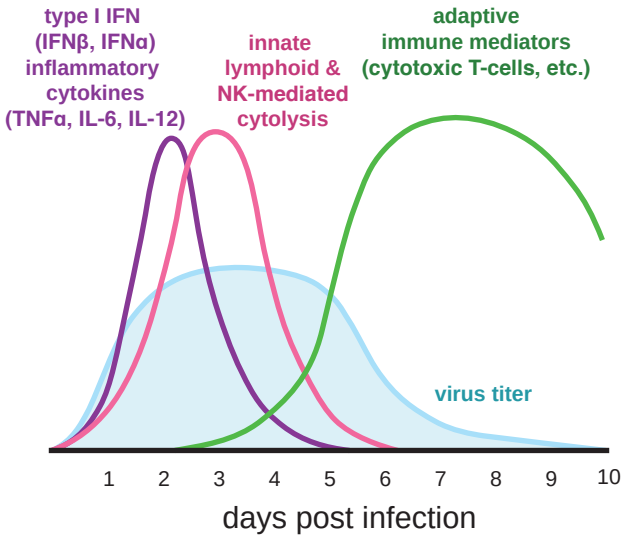

Figure 1.1: A schematic representation of a viral infection in a naive host. The innate (purple and pink curves) and adaptive (green curve) immune responses as well as the concomitant effects on viral titer (light blue shaded area) are shown following the infection of a naive host with a viral pathogen. Immediately upon infection, the PRRs of infected cells or of cells located near the site of infection recognize PAMPs generated by the infection and initiative the production of antiviral (IFN-α and IFN-β) and inflammatory (TNF-α, IL-6, IL-12) cytokines. This response promotes and directs natural killer cells and other innate lymphoid cells to begin targeting infected cells. These responses combine to halt the increase in viral replication, resulting in a plateau of viral titer. The inflammation and innate response also has the effect of kicking off the adaptive immune response. After several days of selection and expansion, virus-specific antibodies and cytotoxic T-lymphocytes are produced in sufficient numbers to mount a targeted and efficient removal of infected cells, dropping the viral titer until the infection is cleared. Adapted from Janeway's Immunobiology [2].

adaptive immune response, in the form of pathogen specific T-cells and B-cells.

Extracellular PAMP detection

The first interaction most cells have with a pathogenic microbe is extracellular. Many pattern-recognition receptors are located on the cell surface or the luminal side of endosomes. Some of the most well-studied surface PRRs are the Toll-like receptors, a family of evolutionarily conserved transmembrane proteins that are capable to sensing highly varied PAMPs, including bacterial or fungal cell-wall components, viral proteins, and nucleic acids (review by O'Neill et al. [3]).

The first TLR protein identified in mammals was TLR4, also known as the LPS (lipopolysaccharide) receptor, for its significant contribution to sepsis following the inoculation of mice with LPS [4,5]. Subsequent work identified ten total TLR proteins in humans, and 12 in the mouse. Of these TLR2, as an example, has been found to recognize various bacterial and viral molecules.

Toll-like receptor 2 TLR2 is a known to be activated by bacterial lipoproteins as part of a heterodimer with either TLR6 to respond to diacylated lipoproteins [6] or TLR1 to respond to triacylated lipopoteins [7]. TLR2 has since been shown to bind and respond to a wide range of bacterial and viral PAMPs including viral glycoproteins present on the viral envelope of Herpes Simplex Virus (gH/gL and gB) [8]. This interaction also involves an interaction on the cell surface with the the $\alpha v\beta 3$ integrin [9–11]

Upon binding to its ligand, TLR2—with one of its recognition partners TLR1 or TLR6—signals via the intracellular activation of MyD88 [12]. MyD88 activation then leads to the phosphorylation of IRAK-1, IRAK-2, and IRAK-4 [13,14]. These IRAK proteins interact with TRAF6 [15], leading to the production of IKK complexes capable of degrading I$\varkappa$B, resulting in the activation of NF-$\varkappa$B which translocates to the nucleus and turns on the expression of several proinflammatory cytokines which are able to bring about a larger response against the infecting pathogen[16].

Negative regulation of innate immune signaling

While pattern recognition receptors are capable of recognizing pathogens and initiating a response, too much inflammation can be detrimental, and for this reason many mechanism exists to negatively regulate inflammatory processes. Some of these mechanisms include negative regulators of certain pathways, like the expression of decoy pattern recognition receptors which capable of binding and neutralizing immunostimulatory molecules before they activate [17,18]

Other mechanisms of negative regulation focus on the immune cells which normally respond robustly to pathogenic stimuli. These cell-based negative regulators induce an anti-inflammatory state within a given cell limiting its capacity to induced inflammation. One such negative regulator CD200R1, is capable of inducing an anti-inflammatory state within a cell prior to stimulation with a pathogenic ligand and plays an important role in limiting inflammatory responses within the central nervous systems (CNS)

CD200:CD200R1 signaling CD200R1 is a cell-surface protein that is expressed on many different myeloid-derived cells including macrophages and neutrophils, but especially microglia within the CNS. Upon engagement with its ligand CD200, CD200R activates an intracellular signaling pathway that ultimately limits the inflammatory capacity of these myeloid-derived immune cells.

CD200R1 is the best understood of the putative receptors for CD200. Aside from an extracullar domain responsible for ligand binding and a transmembrane region, CD200R1 has a cytoplasmic tail responsible for conveying it signal following ligand binding. When CD200R1 binds it ligand, its cytoplasmic tail becomes phosphorylated, resulting in the recruitment of the signal mediators Dok1, Dok2, and SHP-1 [19,20]. Ultimately the phosphorylation of Dok1 and/or Dok2 and the activation of SHP-1 stimulates RasGAP [21] leading to a reduction in TNFα and NO production following TLR stimulation [22] and an negative regulation of NF-ϰB activation [23].

The result of these anti-inflammatory signaling events are macrophages and neutrophils that are less capable of responding to pathogenic stimuli. In this way, CD200:CD200R1 signaling is an important limiting factor in the progression of several autoimmune disease in mouse models of arthritis, multiple sclerosis, and inflammatory bowel disease [24,25]. However, in the case of pathogenic infections, this negative regulation can sometimes be deleterious, as is the case with mice infected with *L. amazonensis*. In this case, CD200-/- mice have improved disease outcomes and are better able to combat the infection, due to a stronger oxidative response against this typically indolent pathogen [26].

The role of CD200R1 in limiting inflammation is most pronounced in regions where too much inflammation can be detrimental, like the central nervous system. Within the CNS, CD200:CD200R1 signaling is a critical factor in reducing inflammation and disease severity in mouse models of both *N. meningitidis* septicemia and [27] and *Toxoplasma* encephalitis [28]. In the case of both of these infectious, the anti-inflammatory signaling of CD200R1 within the CNS has the effect of protecting the CNS from too much toxic inflammation, resulting in less damage to brain cells and a less severe disease course. Molecules like CD200R1 are critical moderators of the innate immune response, and as such help keep inflammation from becoming too harmful.

Intracellular response and Cytosolic RNA Receptors

While TLRs are important in alerting cells to extracellular PAMPs, viruses and other intracellular pathogens do inevitably find a way to enter a cell. For this reason cells also express certain cytoplasmic PRRs capable of detecting intracellular signs of infection. While there are exceptions, many of the intracellular PRRs recognize nucleic acids. Certain DNA and RNA structures—like 5'-triphosphorylated RNA, long dsRNA, naked DNA—are common to pathogenic organisms, and when these are encountered within the cytoplasm they are recognized as signs of an infection. Upon detection of foreign nucleic acids, these receptors—much like the TLR receptors—kick off a signaling cascade to respond to the

infection. Cytosolic sensors exist that recognize both DNA and RNA, and ultimately they again induce the production of type 1 IFN signaling, to reprogram host cells and limit viral replication (cytosolic nucleic acid receptors are reviewed in [29]). I will focus on RNA sensors here, as they play a significant role in later parts of this dissertation.

During the course of replication, many viruses introduce virus-derived RNA molecules into the cytoplasm of the infected cell. While the cytoplasm of a given cell is full of host-derived RNA molecules (mRNAs, tRNAs, and others), certain sensors are able to properly discriminate between endogenous RNA and foreign RNA and activate the type 1 IFN response accordingly.

RIG-I-Like Receptors Foreign RNA present in the cytoplasm can be detected by the RIG-I-like receptors. This family of DExD/H RNA helicases includes RIG-I, MDA5, and LGP2 [30]. Together these proteins serve as sensors for foreign RNA, binding to specific RNA structures like 5'-triphosphorylated RNA and dsRNA and setting off a signaling cascade that culminates in the expression of antiviral type I IFNs. RIG-I and MDA5 each contain two CARD (Caspase activation and recruitment domain) domains on their N-termini which are used to induce downstream signaling. Upon binding to stimulatory RNA, these sensors undergo a change in conformation, leading to the activation of their CARD domains. Their CARD domains are dephosphorylated by PP1α/γ and the second of their 2 CARD domains also undergoes K63-ubiquitination [31,32]

Upon activation, MDA5 and RIG-I both colocalize with their signaling adaptor MAVS, located on the mitochondrial outer membrane [33–36]. The activated RLR CARD domains interact with the CARD domain on MAVS to initiate the formation of MAVS fibrils, which then serve as scaffolds for the recruitment of subsequent molecules in the signaling cascade [37]. Ultimately MAVS activation leads to the phosphorylation, dimerization, and nuclear translocation of the transcription factor IRF3. IRF3 then binds to the promoter regions of type 1 IFN genes—IFN-β and the many IFN-α genes. The expression and subsequent secretion of type 1 IFN cytokines leads to the activation of the type 1 IFN receptor (IFNAR1),

the induction of the type 1 IFN cascade, and the expression of hundreds of interferon-stimulated genes (ISGs) (reviewed in [38]) (Figure 1.2). Ultimately the expression of ISGs result in making the cell less hospitable for viral replication.

RIG-I can be stimulated by several different RNA structures. The most widely studied is 5'-triphosphorylated RNA (5'pppRNA), although various other motifs and secondary structures found during viral infection have been shown to activate RIG-I as well (reviewed in [39]). 5'pppRNA is often generated during viral replication, while endogenous RNA in the cytoplasm is capped. This 5'ppp motif serves as marker of foreign RNA. Upon binding to RNA, the RIG-I CARD domain is rearranged in such a way to activate it. This conformational change, along with dephosphorylation and ubiquitination of RIG-I, leads to the activation of MAVS. RIG-I has also been shown to bind longer RNA molecules and form filamentous aggregates along their length. These filaments are also capable of activating MAVS with polyubiquitination [40].

MDA5 activation occurs in a similar manner, with MDA5 forming filamentous aggregates along the length of dsRNA molecules, leading to CARD domain aggregation and ultimately to MAVS activation [41–43]. MDA5 has been shown to recognize long segments of duplex RNA. It is thought that MDA5 regularly samples and moves along duplex RNA molecules via ATP-hydrolysis [44]. When it encounters an RNA molecule that is particularly long, it is able to reside on the molecule for long enough to nucleate a MDA5 filament capable of signaling downstream. It should be noted, however, that the most commonly studied ligands for MDA5, polyIC, is a synthetic homopolymer that does not actually form clean, uniform duplexes. In fact, work by Pichlmair et al. have shown that polyIC exists as a high-molecular weight RNA complex, thought to resemble a tangled string. Furthermore these larger complexes actually are MDA5-stimulatory, with similar RNA structures isolated from virus-infected cells giving a similar effect [45]. This suggests that there is some role in having dsRNA segments interspersed with other secondary and tertiary structural elements for optimal MDA activation. Finally, while MDA5 is the predominant sensor for polyIC,

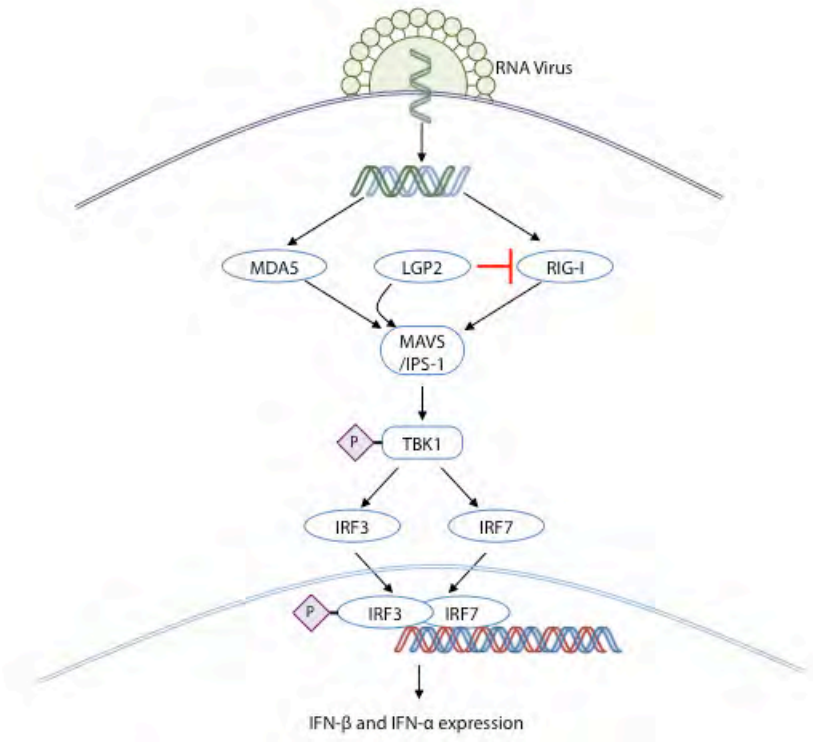

Figure 1.2: The RIG-I like receptor pathway for the recognition of virus-derived RNA molecules. Virus-derived RNA molecules carry certain structural patterns which are detectable by the RLR proteins, serving as cytosolic PRRs. RIG-I is known to bind to triphosphorylated RNA and small RNA molecules. MDA5 is known to recognize long dsRNA and RNA with complex tertiary structures. LGP2, the enigmatic third member of the RLR family, is currently thought to bind to dsRNA and promote the activation of MDA5, while inhibiting RIG-I activation in certain contexts. Upon activation, both RIG-I and MDA5 converge on the signal adapter MAVS, which is activated and subsequently triggers the phosphorylation, dimerization , and translocation of the transcription factors IRF3 and IRF7. These transcription factors turn on many important genes, chief among them the type 1 IFN molecules IFN-β and IFN-α.

it also appears that the helicase Dhx15 plays a small, though not yet fully defined, role in activating MAVS in response to polyIC stimulation in some cells types [46]. The function of Dhx15 appears to be independent of MDA5.

LGP2 is the enigmatic third member of the RLR family. Missing the critical CARD domains used by RIG-I and MDA5 for MAVS activation, LGP2 appears to play a role in facilitating the activation of the other RLRs, depending on the ligand. Recent studies have suggested that LGP2 functions to stabilize MDA5 binding to dsRNA molecules, when present at the correct stoichiometric ratio [47]. Too much or too little LGP2 binding however results in negative regulation of MDA5 signaling. Because of its enigmatic role in RLR signaling, several groups have sought to identify which RNA structures or motifs are bound by LGP2. LGP2 has been found to bind to triphosphorylated RNA, blunt-ended RNA, dsRNA, and ssRNA, among others [48–52]. Additionally, pulldown experiments have demonstrated that LGP2 binds to certain specific segments of viral RNA. In the case of EMCV, a well-studied agonist of MDA5 and LGP2 [53,54], LGP2 has been shown to preferentially interact with the L-region of the EMCV genome on the anti-sense (negative) strand of viral RNA [55].

While MAVS filament formation and signaling takes place near the surface of the mitochondria, the specific location where signaling occurs within the cells is still up for debate. Some recent evidence has suggested that RLR signaling takes place in or adjacent to RNA stress granules—punctate structures formed in the cytoplasm of a cell in response to stressful stimuli (oxidative stress, heat shock, etc.). Stress granules are thought to serve as important mediators of RNA regulation and processing. A number of recent studies have found that RLR receptors relocate to stress granules upon stimulation with RNA ligands [56,57]. However, at least one report has found that RLR localization to stress granules is not required for MAVS activation [58], suggesting that stress granules might not be critical loci of RLR signaling.

1.2.2 Antiviral small RNAs

While the prominent antiviral signaling pathways in mammals revolves around the production of type 1 IFN and other cytokines that are capable of signaling in an autocrine and paracrine manner, another pathway dependent on small RNAs can contribute to the innate response. Antiviral small RNAs are critical to the innate immune response in worms and flies, and while they are not as critical to mammals, their full role is still under investigation.

The antiviral small RNA response in C. elegans

The nematode *C. elegans* employs a small RNA pathway to combat viral infections. Upon infection, small RNA processing enzymes DCR-1 and DRH-1 along with RDE-3 bind to and process viral dsRNA into primary antiviral RNAs that average 23nts in length and resemble canonical siRNAs [59]. These primary antiviral RNAs are then loaded into complexes with the argonaute protein RDE-1. These complexes recognize long, unprocessed segments of viral RNA and recruit RNA-dependent RNA polymerases (RdRPs). These RNA polymerases then generate short, complementary RNA molecules using the length of the targeted molecule as a template [60,61]. The small secondary antiviral RNA molecules that are generated are called 22G RNAs since they are predominantly 22nts in length and usually begin with a guanosine. These 22G RNAs are thought to be the effector antiviral RNA molecules responsible for targeting and inhibiting viral RNA replication [59].

In *C. elegans*, the RLR orthologue and Dicer-associated protein, Dicer-related helicase 1 (DRH-1), is essential for the Dicer-dependent cleavage of viral dsRNA into primary vsiRNAs. Guo et al. recently demonstrated that worms lacking DRH-1 are unable to mount an antiviral RNAi response against Orsay virus [62]. Intriguingly, the antiviral RNAi response in these DRH-1-null worms can be rescued with a chimeric DRH-1 protein consisting of the helicase and C-terminal domains of human RIG-I and a worm-specific N-terminal domain [62]. More recently it has been shown that DRH-1-mutant worms are able to produce some

primary avRNAs, however instead of being dispersed along the length of the viral genome, they were predominantly from the RNA termini, suggesting the DRH-1 plays a role in facilitating dicer translocation along foreign RNA molecules [63].

Virus-derived dsRNA is cleaved by Dicer to create primary viral small interfering RNAs (vsiRNAs). Dicer's DExD/H helicase domain appears to be important for the processing of siRNA from a dsRNA precursor, while being dispensable in the processing of pre-miRNAs into miRNAs [64,65]. These primary vsiRNAs are then thought to recruit RNA-dependent RNA polymerase (RdRP) complexes to viral RNA [60,66,67]. RdRP complexes produce large amounts of single-stranded anti-sense secondary vsiRNA, which are then incorporated in RISCs, where they can target viral RNA for silencing [68]. Worms lacking an active Dicer-dependent RNAi pathway are susceptible to infection by several natural and non-natural viral pathogens, including single-stranded RNA viruses such as insect Flock house virus, mammalian vesicular stomatitis virus (VSV), and Orsay virus, which naturally infects C. elegans [61,69–72].

The antiviral small RNA response in D. melanogaster

Like the worm, the antiviral immune response in *D. melanogaster* involves the production of antiviral small RNAs that are capable of blocking viral replication and gene expression. While similar in many ways to the avRNAi response in the worm, the antiviral response in *D. melanogaster* has a number of important differences. Flies have two different dicer genes (Dicer-1 and Dicer-2) that each have a unique role in processing small RNA ligands. Dicer-1, in association with its RNA-binding partner Loquacious, is known to process pre-miRNAs into functional miRNAs [73]. Dicer-2, with its RNA-binding partner R2D2, is responsible for cleaving in a processive manner long dsRNA ligands into siRNA molecules [74]. It is in this capacity that Dicer-2 is thought to function in the antiviral response, by selectively binding to the ends of virus-derived dsRNA and processively cleaving off antiviral siRNAs. Flies lacking Dicer-2 are susceptible to viral infections and are unable to mount a proper

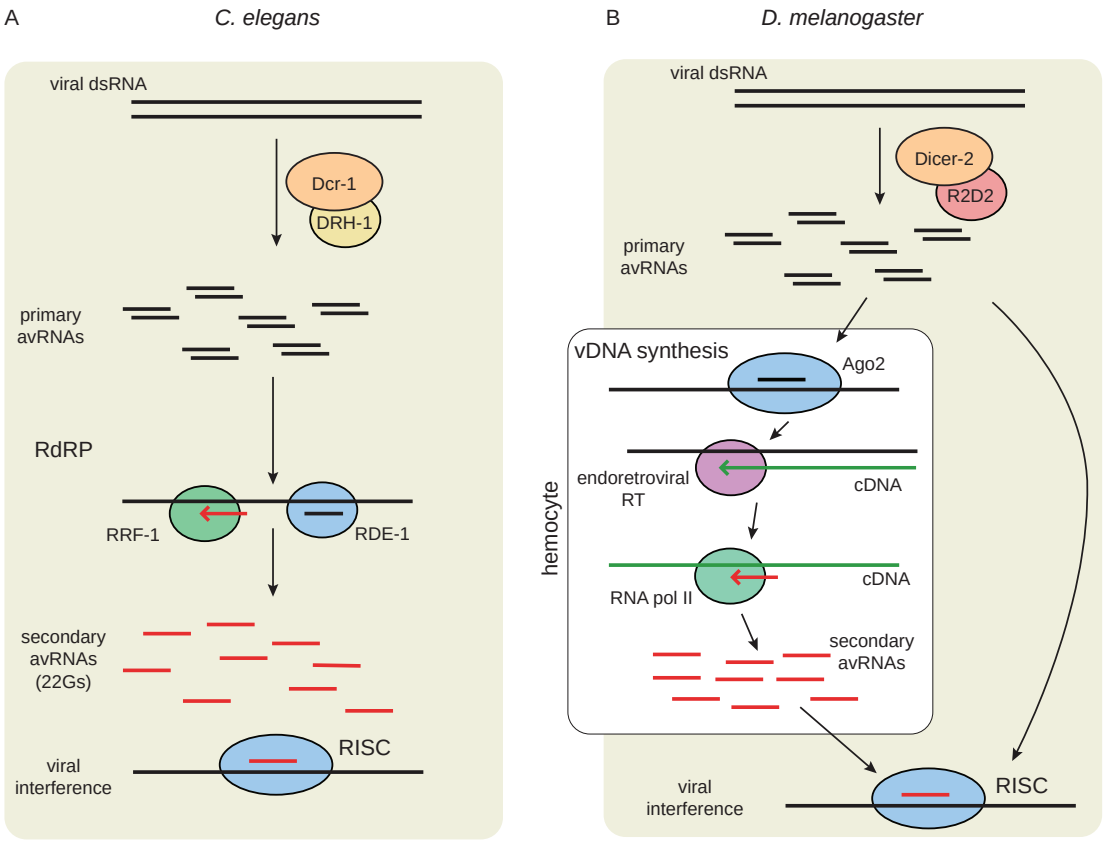

Figure 1.3: Antiviral small RNA pathways in the model organisms *C. elegans* and *D. melanogaster*. (A) *C. elegans*: Virus-derived dsRNA is processed by the dicer protein DCR-1 producing primary antiviral RNA molecules that are short and double-stranded. These primary avRNAs are then employed by the argonaute protein RDE-1 to target other viral RNA molecules for RNA-dependent RNA polymerization. RdRP products derived from all along the viral RNA molecule are produced. The secondary avRNAs are generally 22nt longs, single-stranded, and beginning with a `G`. The secondary avRNAs are then used by other argonaute molecules to carry out antiviral inhibition of viral RNA. (B) *D. melanogaster*: Virus-derived dsRNA is processed by Dicer-2 into primary antiviral RNA molecules. These avRNAs can complex with an argonaute protein and form a RISC complex to targets viral RNA. If this complex is taken up by a circulating hemocyte it can lead to the reverse transcription of viral RNA in to DNA, and then the *de novo* transcription of new RNA molecules capable of interfering with viral RNA.

antiviral small RNA response [75–77].

Unlike worms, flies do not have a bonafide RdRP enzyme. However, flies do appear to utilize an amplification step in order to enhance their antiviral RNA interference response. This is accomplished through the synthesis of a cDNA intermediate generated by reverse transcribing viral RNA as carried out by endogenous transposon-associated reverse transcriptases [78]. This reverse transcription reaction is thought to occur selectively in hemocytes, a class of circulating cells in the fly. These hemocytes can take up viral RNA and use it as a template to generate complementary viral DNA. This cDNA is then used as a stable and persistent template from which secondary antiviral RNAs are transcribed. The secondary avRNAs are then thought to be transported from the hemocyte to an infected cell. Since these secondary avRNA molecules are *de novo* RNA products produced in the cytoplasm, they are uncapped on the 5'-end [79].

Primary or secondary antiviral small RNAs, following synthesis, are then loaded into an argonaute complexs [80]. Interestingly—as is the case in *C. elegans*— the avRNAi pathway in *D. melanogaster* appears to be distinct from the exogenous dsRNAi pathway. In the case of flies, the avRNAi pathway engages Dicer-2 and leads to the production of antiviral siRNA molecules, but it also induces the production of antiviral molecules which activate Jak/STAT signaling [81]. This Jak/STAT signaling is not observed when non-viral exogenous dsRNA is introduced, again suggesting that exogenous dsRNAi and avRNAi pathways, while overlapping, are not identical.

A mammalian antiviral small RNA response As there is no known mammalian RdRP, it was initially thought that mammals did not have a antiviral small RNA response, as they lacked any mechanism for amplifying the antiviral effect. It was also supposed that as mammals adapted the type 1 IFN response, they evolutionarily lost the small RNA response, given that the IFN response is capable of significant signal amplification at each step along the signaling pathway, and is an effective antiviral defense.

However, several recent studies have shown that mammals—specifically mice and human cells—do in fact utilize smalls RNAs to mount an antiviral response. The picornavirus EMCV was used to demonstrate that under certain circumstances, antiviral RNA molecules are produced and do have an important anti-viral role [82] in a mammalian system. Maillard et al. showed that mouse stem-cells do produce EMCV-derived small RNAs, which can be loaded into RISC complexes, suggesting that avRNAi could be used to mount an antiviral response. More recent work by Li et al. shows that small RNAs derived from Influenza A virus are associated with Argonaute proteins in mouse cells and have an important role in regulating viral RNA [83]. In these somatic mammalian cells, small RNA molecules generated from longer dsRNA molecules are able to inhibit viral replication.

Even more recently, it was demonstrated that the mammalian avRNAi response does interact with the type 1 IFN response, with type 1 IFN signaling serving as a potent antagonist to avRNAi production [84]. Antiviral RNAs derived from exogenous dsRNA were detectable only after type 1 IFN signaling was abrogated (either by mutating MAVS or neutralizing IFNAR). It was further demonstrated that type 1 IFN signaling negatively regulates antiviral RNAi in mammalian cells. It has been found that type 1 IFN can negatively regulate RISC activity by inducing the p(ADP)-ribosylation of Argonaute or other RISC components [85,86].

Taken together, the literature to date suggests that mammalian cells have two competing antiviral response pathways: the antiviral small RNA response pathway and a cytokine-driven type 1 IFN response pathway. The evidence also suggests that the type 1 IFN response is the dominant antiviral pathway, and is capable of suppressing the small RNA pathway. Moreover, it is evident that the mammalian antiviral small RNA response is not capable of compensating for a missing type 1 IFN antiviral response, as animals lacking MDA5, MAVS, IFNAR, and others type I IFN signaling components are significantly more susceptible to many viral infections. This suggests that while active, the mammalian small RNA antiviral response is insufficient to protect against most common mammalian

pathogens, at least in the context of laboratory infections of model organism with pathogenic viruses.

However our interactions with viruses are not limited just to those that make us sick. Just as the body of knowledge regarding the gut and the environmental microbiomes has exploded in recent years, so has our understanding of the human virome, the countless viruses and phages that we encounter on a daily basis (well reviewed in [87]). Eukaryotic viruses, phages, and endogenous retroviruses are prevalent in our genome, gut, and elsewhere throughout out bodies. These indolent sources of viral RNA might be a reason why mammals have held on to the avRNAi pathway.

1.3 Conclusions

The innate immune response to viral infections in mammals is multifaceted, with cells expressing a repertoire of PRRs, waiting to raise the alarm and launch an IFN response, and with a small RNA response that can process and utilize viral RNA to launch a more widespread, cytokine-driven type 1 IFN response. However, we are still just understanding the varied and intricate interactions that lead to this common innate response. In this dissertation, I will present my work on two such important aspects of the innate immune system in mammals. The first examines the role of the phosphatase PIR1 in the early viral detection of mammals (Chapter 2). The second explores the surprising role of the anti-inflammatory molecule CD200R in viral replication, specifically during HSV encephalitis (Chapter 3).

CHAPTER II: Investigating the role of PIR1 in the innate immune response to EMCV

In addition to contributing to the design, analysis, and interpretation of the experiments herein, I was assisted in processing experimental samples and carrying out certain assays. Michael King helped perform the western blot analysis on cell lysates, ELISA tests on serum and tissue culture supernatant, and genotyping of mice by complementary DNA and genomic DNA. Anna Cerny assisted in mouse husbandry and genotyping of mice by complementary DNA.

I designed the PCR primers presented in Table 2.2 and Table 2.4. I also developed the PCR protocol used in Figure 2.6 and Figure 2.8 and generated the samples analyzed in each. I performed the PCR experiments presented in Figure 2.8. I generated the visual representation of the SNP data generated by Jackson Laboratories (www.jax.org) displayed in Figure 2.5.

I generated the samples and performed the assays presented in Figure 2.9, Figure 2.10, Figure 2.11, Figure 2.13, Figure 2.14, and Figure 2.16. I generated the samples analyzed in Figure 2.12 and Figure 2.15.

2.1 Introduction

2.1.1 PIR1 - protein that interacts with RBP 1

PIR1 (Phosphatase that interacts with RNA/RNP-1) is a member of protein phosphatase family known as dual-specificity phosphatases (DUSP), and is highly conserved in animals as far ranging from nematodes to humans. While PIR1 (also known as DUSP11) shares a conserved `HCXXGXXRXG` catalytic active site motif with other DUSP family protein phosphatases [88], PIR1 is unique for its ability to bind with high affinity to *in vitro* transcribed mRNA molecules[89]. Additionally, PIR1 stands out from other atypical DUSPs as it shares significant sequence homology with the RNA phosphatase RNGTT/MCE1 (RNA Guanylyltransferase And 5'-Phosphatase, or mRNA Capping Enzyme 1), homology that is not shared by any other members of the DUSP family [90].

Beyond homology, PIR1 can function as an RNA phosphatase, while the other DUSP family members are exclusively protein phosphatases. In solution, human PIR1 acts as a γ- and β-phosphatase for short RNA molecules, producing 5'-monophosphorylated products from 5'-triphosphorylated substrates [91]. Experiments performed by Deshpande et al. using human PIR1 showed that in solution PIR1 has a several orders of magnitude greater activity for dephosphorylating RNA molecules than it does for dephosphorylating peptides [91]. These findings suggested that PIR1 could potentially act as an RNA phosphatase within the cell.

As seen in Figure 2.1, the PIR1 protein has a catalytic domain, N- and C-terminal arginine rich motifs (ARM), and a proline rich motif (PRM). PIR1 also has a predicted nuclear localization sequence (NLS), and 2 predicted α-helices [89,92]. The ARMs have been suggested to serve as RNA-binding domains [89] and might facilitate viral RNA recognition. Likewise, the PRM has been hypothesized to function as an SH3-binding domain [89], and could facilitate protein-protein interactions critical for the assembly of an RNA-detection complex.

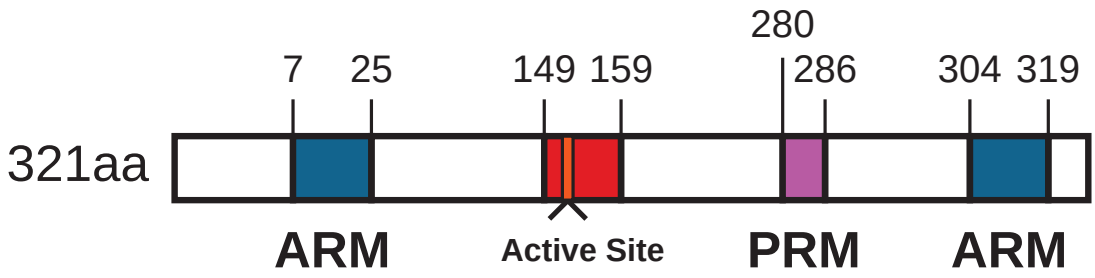

Figure 2.1: A domain schematic of the mouse PIR1 protein, demonstrating two arginine rich motifs (ARMs), a catalytic domain, the catalytic phosphatase active site, and a proline rich motif (PRM).

PIR1 is a well-conserved protein present throughout the animal kingdom, with the human and worm version sharing substantial similarity. When aligned with one another these two proteins show a 60.8% similarity (138 of 227 aligned amino acids) and 41% identity (93 of 227 aligned amino acids) (Figure 2.2). Of note is the high degree of conservation around the catalytic active site (C152 in the human gene, shown in blue in Figure 2.2), with this region of the enzyme showing a high degree of identity between the worm and human version of the protein (shown in red in Figure 2.2).

This level of conservation between the worm and human versions of the PIR1 protein, especially around the catalytic domain suggests that its catalytic function is also conserved between these two species. The human protein, as seen in Figure 2.2 does have a substantial C-terminal domain, that the worm protein is lacking which might suggest differences in how these two proteins interact and in which pathways they function in. More work will be needed to better isolate and characterize each of the potential domains in the mammalian PIR1 protein, including the C-terminal domain.

PIR1 in C. elegans

Work by Duchaine et al. first hinted at a role for PIR1 in *C. elegans* in small RNA processing. Using a proteomic approach, they sought to identify what proteins were interacting with DCR-1, the dicer protein found in worms. PIR-1, among other proteins, was found to interact with DCR-1 [93], leading the way for further investigation into what role PIR1 might have in small RNA pathways.

Using a *pir-1* mutant, Daniel Chaves Ph.D. (working in the lab of Craig Mello Ph.D) in his doctoral dissertation demonstrated that, in the nematode, PIR1 plays a critical roles in spermatogenesis, animal development, and antiviral immunity [94]. Specifically, with respect to the its role responding to viral infection, Chaves showed that *pir-1* mutant worms are unable to control replication of the natural nematode pathogen Orsay virus. Without PIR1 expression, this RNA virus is able to replicate to levels that are several orders of

```
C. elegans pir-1    1 MSNYHHNHNYQHRPRGY------ERLPGKRLPDRWNIYDNVGRDIDGTRF     44
                      ||.:||..:...|.|.:      ::..|..:|:||..|..||:.:.||||
H. sapien PIR1      1 MSQWHHPRSGWGRRRDFSGRSSAKKKGGNHIPERWKDYLPVGQRMPGTRF     50

C. elegans pir-1   45 VPFKTPLDSSFFDGKNMPVELQFGVKTLISLAQQANKQIGLVIDLTNTDR     94
                      :.||.||..||  .|.:..|..|....|.:..::.|:::||:||||.|.|
H. sapien PIR1     51 IAFKVPLQKSF--EKKLAPEECFSPLDLFNKIREQNEELGLIIDLTYTQR     98

C. elegans pir-1   95 YYKKTEWADHGVKYLKLNCPGHEVNEREDLVQDFINAVKEFVNDKENDGK    144
                      |||..:..: .|.|||:...||:|.:.|.:.: |.:||..|:.:.::::.|
H. sapien PIR1     99 YYKPEDLPE-TVPYLKIFTVGHQVPDDETIFK-FKHAVNGFLKENKDNDK    146

C. elegans pir-1  145 LIGVHCTHGLNRTGYLICRYMIDVDNYSASDAISMFEYYRGHPMEREHYK    194
                      ||||||||||||||||||:|||:.....|||.:|...|||.:||::|.
H. sapien PIR1    147 LIGVHCTHGLNRTGYLICRYLIDVEGVRPDDAIELFNRCRGHCLERQNYI    196

C. elegans pir-1  195 KSLYEAERKKKYGKSSGKSSGNSADSTISSEQLHRNNSQ-----------    233
                      :.|.....:|.:..|..:|| :..||....:.:|....:
H. sapien PIR1    197 EDLQNGPIRKNWNSSVPRSS-DFEDSAHLMQPVHNKPVKQGPRYNLHQIQ    245

C. elegans pir-1  234 --------------------------------------------------    233

H. sapien PIR1    246 GHSAPRHFHTQTQSLQQSVRKFSENPHVYQRHHLPPPGPPGEDYSHRRYS    295

C. elegans pir-1  234 ----------------------------------    233

H. sapien PIR1    296 WNVKPNASRAAQDRRRWYPYNYSRLSYPACWEWTQ    330
```

Figure 2.2: A pairwise alignment of the human and worm PIR1 protein sequences. The sequences were aligned using a global pairwise alignment algorithm and the BLOSUM62 substitution matrix. The highly similar alignment positions are denoted by a `:` and identical alignment positions are denoted by a `|`. The catalytic active site (C152) is shown in blue, and the highly conserved region adjacent to the catalytic active site is shown in red. Sequences used are the human NCBI reference sequence: NP_003575.2 and the *C. elegans* sequence WP:CE48135 from wormbase.com (http://wormbase.com). The sequences are aligned using the Needleman–Wunsch algorithm with the EBLOSUM62 substitution matrix, a gap-open penalty of 10.0, and a gap-extend penalty of 0.5.

magnitude greater than wild-type animals. Deep sequencing studies showed that the *pir-1* mutant worms are capable of generating many virus-derived small RNA. The *pir-1* mutant animals also had significantly higher levels of primary antiviral small RNAs (these are dsRNA molecules that average 23nt in length, and show hallmarks of being produced by the Dicer cleavage of viral dsRNA). However, the *pir-1* mutant animals had significantly lower relative levels of 22G RNAs (secondary avRNAs that carry out antiviral RNA inhibition, as described in Section 1.2.2 on page 12), relative to the amount of viral RNA within the cell [94]. Since these 22G RNAs, being RdRP products, are initially 5'-triphosphorylated, one potential role for PIR1 in this pathway might be in the dephosphorylation of these triphosphorylated 22G RNAs.

Taken together the data presented by Chaves demonstrates that PIR1 plays a critical role in facilitating a robust and effective antiviral small RNA response. Chaves suggests that PIR1 exerts its effect by promoting the production of effective secondary 22G avRNAs early on in the course of an infection [94]. How the RNA phosphatase activity of PIR1 affects this process is not yet well understood, but it could be that PIR1 facilitates the detection, shuttling, or processing of triphosphorylated 22G avRNAs thereby promoting their efficacy. It is also possible that the processing of triphosphorylated 22G avRNA molecules into their monophosphorylated form by PIR1 renders them better suited to carry out antiviral RNAi either by increasing the efficiency of loading 22G avRNAs into their appropriate Argonaute protein complexes or by increasing the inhibitory activity of these argonaute complexes once formed. When first discovered, it was noted that PIR1 binds to RNA molecules with high affinity [89], raising the possibility that the function of PIR1 might not be directly linked to its phosphatase activity, but rather to its RNA-binding activity. Further investigation is needed to better understand the true mechanism for the PIR1 phenotype in *C. elegans*.

PIR1 in the mammalian system

Human PIR1 is similar in sequence to *C. elegans* PIR1, with 75% amino acid similarity along the length of the expressed protein. Human PIR1 has been shown to bind RNA with high affinity and dephosphorylates the 5'-end of RNA molecules [89,91]. The crystal structure of the core phosphatase domain of human PIR1 was recently solved and showed that PIR1 does share many structure and ligand-bindings similarities with other RNA phosphatases, further supporting the hypothesis that PIR1 functions as a RNA phosphatase [92].

A number of additional studies have implicated PIR1 in RNA metabolism pathways. In the study first describing the PIR1 gene, Yuan et al. showed by confocal microscopy that a labelled PIR1 protein is expressed in the nucleus, where it colocalizes with the the splicing factor SC35 [89]. This same study also showed PIR1 interacting with the splicing factors 9G8 and SRp30C using yeast two-hybrid analysis [89]. Another study, looking at the regulation of PIR1 by the tumor suppressor p53, showed PIR1 interacting with yet another splicing factor, SAM68 [95].

There are several sources of triphosphorylated RNA in a mammalian cell, with the most well-studied being virus-derived RNA molecules. Many viruses produce triphosphorylated RNA as a product of RNA-dependent RNA polymerization. These 5'-ppp-containing RNA molecules are recognized as foreign since the vast majority of host RNAs found in the cytoplasm have a 5' cap or are monophosphorylated. Ultimately, these 5'-ppp viral RNA molecules activate the RLR:IFN antiviral pathway. Since RLR proteins are orthologous to the helicases DRH-1 and DRH-3, which are known to interact with PIR1 and are critical for antiviral siRNA production in *C. elegans*, the link between RLR signaling and PIR1 was investigated, again by the Mello Lab. Expression and co-immunoprecipitation experiments by Darryl Conte Ph.D. showed that in unstimulated human HEK293T cells, PIR1 selectively interacts with the RLR protein LGP2 and Dicer (Figure 2.3).

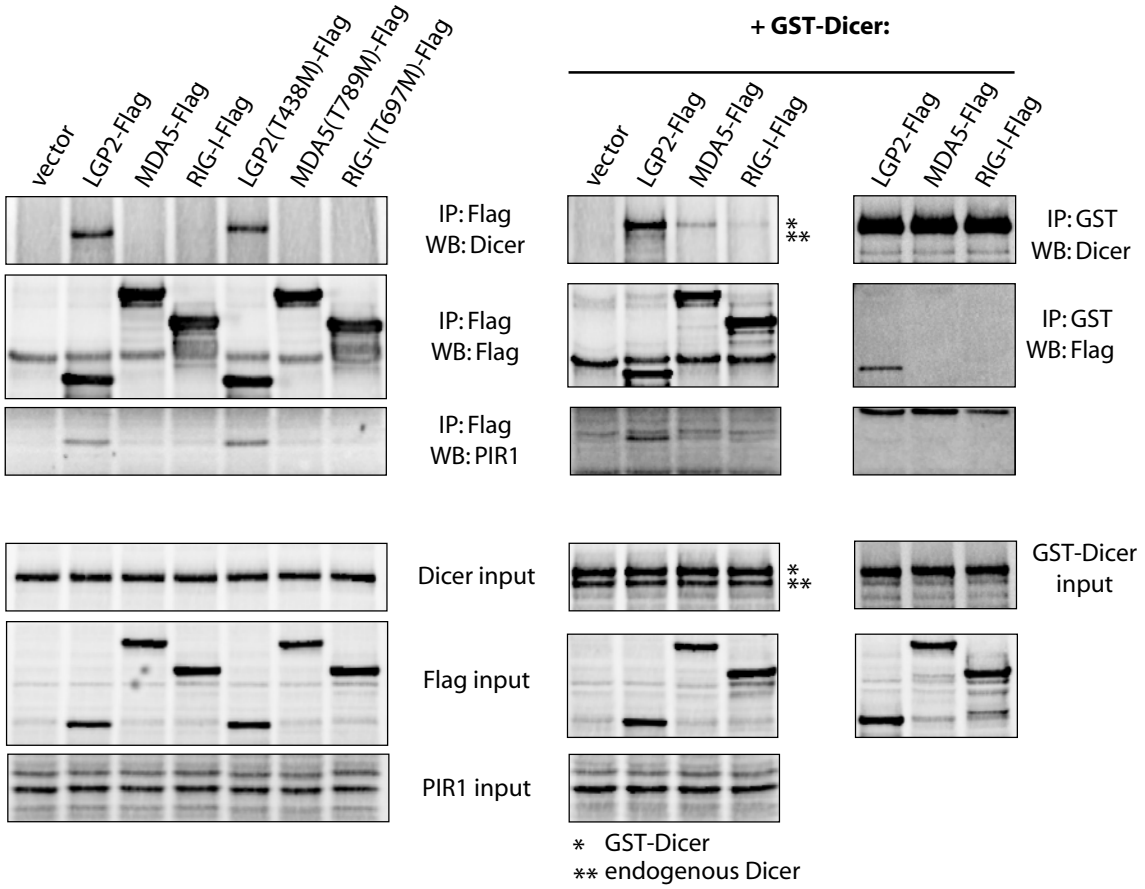

Figure 2.3: Initial human PIR1 overexpression and co-immunoprecipitation experiments performed by Darryl Conte Ph.D. show that PIR1 selectively immunoprecipitates with human LGP2. (reproduced with permission from Darryl Conte Ph.D. UMass Medical School Worcester, MA)

Aside from a potential role in RLR signaling, PIR1 has recently been shown to have an effect on the production or maturation of certain RNA polymerase III products, including miRNAs produced from viral DNA and various host RNAs [96]. These recent findings point to a role for PIR1 is the maturation of atypical miRNAs or other small non-coding RNAs.

Therefore, for this dissertation work I set out to examine the critical roles of PIR1 in the innate immune response to viral infection using a PIR1KO mouse.

2.1.2 The replication cycle of Encephalomyocarditis Virus

Given PIR1 was shown to interact directly with the RLR LGP2 by co-immunoprecipitation (Figure 2.3), I sought to investigate the role of PIR1 in the mouse innate immune response to encephalomyocarditis virus (EMCV), a response that is known to be dependent on LGP2 [54].

EMCV is a picornavirus (positive sense, single-stranded RNA, unenveloped), that naturally infects rodents. EMCV also is known to infect pigs, a potential threat to livestock, but a more serious threat to humans as porcine xenotranplantation continues to be examined as a potential solution for a broad range of human disease [97]. In the study of the mammalian innate immune response, EMCV is widely used as a selective agonist of MDA5-dependent, but not RIG-I-dependent, IFN induction. Groundbreaking work by Kato et al. used EMCV to show that MDA5 and RIG-I detect and respond to different RNA ligands and infections, and therefore are not redundant despite the fact that they both activate the the signaling-adaptor molecule MAVS [53].

EMCV infection begins with viral entry into a host cells. The mechanism of entry is not well understood, but it is clear that EMCV has tropism for certain tissues—including the heart, brain, and the pancreas—and that this tropism can be virus strain specific [98]. VCAM-1, which is highly expressed within the heart, is one of several molecules implicated in EMCV entry [99]. Following the introduction of the positive sense EMCV genome into the cytoplasm of the host cell, the genome recruits host translation machinery and begins

producing viral protein. This process is cap-independent given an internal ribosome entry site (IRES) in the 5'-UTR of the genome [100]. In total, the EMCV genome is roughly 7.8kb in length and encodes for 13 proteins, with at least one of them being in a different reading frame (called 2B* [101]).

The EMCV genome is covalently linked on the 5'-end to the viral protein VpG (a.k.a. protein 3B). However, during ribosome binding this VpG protein cap is removed by the host protein TDP2 [102]. The requirement of VpG removal for viral gene expression is virus specific, but for several picornaviruses, it has been shown that VpG removal increases the efficiency of viral translation [103]. Translation generally occurs along the entire length of the genome, generating a polyprotein that is subsequently processed by the protease 3C into mature proteins. The protease 3C is an active and promiscuous protease capable of cleaving many host proteins including RIG-I [104].

Following viral gene translation, genome replication takes place. Replication occurs in the cytoplasm in membrane vesicles formed through the rearrangement of the endoplasmic reticulum. In order to generate negative strand molecules via RNA-dependent RNA polymerization (RdRP), translation must stop on the positive strand [105]. Once translation has ended, the positive strand is positioned to allow for the template-driven addition of two uridine bases to a VpG molecule [106]. The subsequent VpG-pUpU is then used as a primer for RNA synthesis by the RNA polymerase $3D^{pol}$, beginning at the poly(A) tail on the 3'-end of the positive strand. As the negative strand is synthesized a double-stranded RNA intermediate—known as the replicative form (RF)—is generated [107]. Each negative-sense genome is then used as a template for the synthesis of several positive-sense genomes simultaneously. The resulting RNA molecule, which consists of a single negative-sense molecule associated with several positive-sense molecules at various stages of synthesis, is known as the replicative intermediate (RI).

The final steps of replication involve the formation of viral capsids around a viral genome. While the exact mechanisms of viral assembly are not yet well understood, it is known

that only VpG-linked positive strand genomes are loaded into virions [108]. After virion maturation, the exact mechanism by which mature, infectious virions egress are also not well understood. As described by Carocci et al., several hypotheses have been put forward explaining EMCV egress, including direct physical membrane rupture by an overabundance of virions or the formation of membrane pores using viral proteins [109].

2.1.3 EMCV Pathogenesis in Mice

Rodents are thought to be the natural host of EMCV, especially rats, in which infection can result in an asymptomatic and prolonged infection [106]. In mice, the illness caused by EMCV is dependent on the strain of virus used and amount of inoculum administered. Several strains, including EMCV-D, are well studied for their ability to induce diabetes. EMCV is also capable of infecting many other organs in the mouse, but generally most strains of EMCV cause encephalitis, limb paralysis, and myocarditis. Viral infection of the mouse myocardium leads to necrosis of the myocardium and an infiltration of immune cells. It is thought that NF-$\varkappa$B-mediated inflammation during the subsequent immune-cell infiltration reaction leads to more severe disease in the heart [110–114]. The type I IFN response has been shown to help slow the loss of cardiac function, following EMCV infection [53], suggesting that viral damage and the resulting inflammation together contribute to the observed myocarditis.

In the central nervous system, EMCV causes encephalitis and focal lesions within the spinal cord. With a high dose of virus, paralysis is evident by 3 to 4 days post infection regardless of the route of infection. In the brain, necrosis and gliosis are present, along with cellular infiltration and perivascular cuffing typical of central nervous system inflammation reactions [115–117]. The ultimate cause of mortality in the mouse is likely a combination of the encephalitis and myocarditis, however certain strains of EMCV strains are capable of replicating in the heart without causing encephalitis [115], and some strains will infect the mouse pancreas and cause diabetes before the either encephalitis or myocarditis can

manifest [118].

EMCV Detection by the Innate Immune System

EMCV was found to be a potent agonist for MDA5 [53], and subsequently LGP2 [119], and much work has been done investigating how EMCV induces MDA5 activation and type I IFN production. The exact mechanism of how EMCV activates this pathway, however, is still not completely understood. RNA isolated from EMCV-infected cells and analyzed for MDA5-stimulatory activity, showed that high molecular weight RNA complexes were potent agonists of MDA5 signaling [45]. Further studies demonstrated that viral replication is required for viral MDA5 ligand production. Additionally isolated RI and RF viral RNAs were found to induce MDA5 activation [120]. Finally, using immunoprecipitation, it was shown that a small segment of the antisense sequence of the Leader protein was bound with high affinity to LGP2 and was capable of activating IFN signaling in primary mouse fibroblasts [55]. Together it appears that during virus replication, EMCV generates several RNA species that can be detected by MDA5 and LGP2.

At the same time, EMCV actively antagonizes these RLR:MAVS-driven detection mechanisms. The viral protease 3C cleaves RIG-I, rendering it inactive [104]. Expression of a un-cleavable RIG-I variant results in RIG-I activation following EMCV infection and a more robust IFN response. How EMCV activates RIG-I is unclear, and it is unknown whether this activation is through the generation of EMCV-derived triphosphorylated RNA, short dsRNA, or another RIG-I ligand. The Leader protein also actively antagonizes type I IFN activation by directly interfering with IRF3 dimerization, preventing proper IRF3 activation and translocation to nucleus [121]

2.1.4 Investigating the role of PIR1 in the mammalian innate immune response

Given that PIR1 was previously shown to interact selectively with LGP2 (Figure 2.3), and that the type I IFN response to EMCV is dependent on LGP2 [119], I sought to

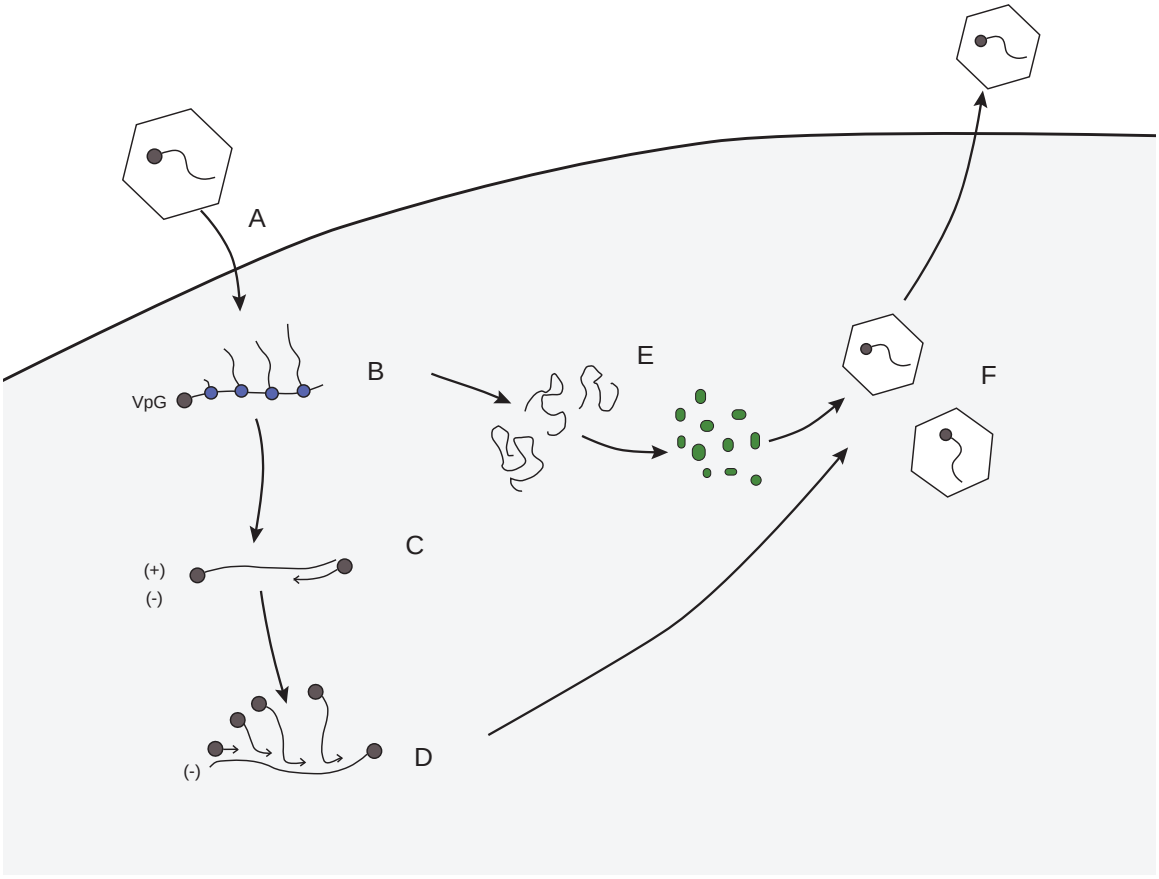

Figure 2.4: A schematic representation of the replication cycle of encephalomyocarditis virus (EMCV). (A) viral entry. (B) polyprotein synthesis. (C) negative strand synthesis. (D) positive strand synthesis. (E) polyprotein processing and cleavage. (F) viral assembly. (G) viral egress.

investigate the role of PIR1 in the mammalian innate immune response by examining EMCV infection in a PIR1-null mouse. I also examined here the effects of loss of PIR1 on RLR signaling using PIR1-null bone-marrow-derived dendritic cells *in vitro*. Finally, I began investigations into the role of PIR1 in small RNA regulation.

2.2 Materials and Methods

2.2.1 Generating a PIR1 gene trap mouse strain

Embryonic cells containing a putative null allele containing a gene-trap insertion within the Dusp11 locus were purchased from the International Gene Trap Consortium (gene-trap.org). The strain purchased was identified as $Dusp11^{Gt(BB0198)Wtsi}$. The 129P2/OlaHsd-derived cells carried a gene trap insertion in the Dusp11 locus on chromosome 6. This allele is called the PIR1KO allele going forward.

A mouse strain was generated from the embryonic cells by the Transgenic Mouse Core Facility at the University of Massachusetts, ultimately resulting in mice heterozygous for the gene trap allele, which were then crossed with C57BL6/J mice for up to 11 generations. Unless noted otherwise, all experiments presented herein were conducted with N=11 backbred PIR1KO mice and C57BL6/J bred in house as wild-type control.

2.2.2 Genotyping the PIR1 gene trap

Genotyping via complementary DNA

A blood sample was collected via tail bleed from weanling mice. Approximately 6 drops of blood were collected directly into 50 µL of heparin 50 U/mL, and stored on ice until processing. Blood samples were centrifuged at 800×g for 5 minutes at room temperature. The supernatant was removed, the cell pellet was resuspended in 500 µL of Red Cell Lysis Buffer, and cells were incubated for 5 minutes at room temperature. The cells were collected by centrifugation for 10 minutes. The supernatant and the top layer of the pellet were then removed. The cell pellet was again resuspended in 500 µL of Red Blood Cell Lysing Buffer (Sigma Aldrich; sigmaalrich.com; cat: R7757), and incubated at for 5 minutes as room temperature. The cells were spun at 500×g for 10 minutes, and then washed in PBS. The cells were pelleted a final time at 500×g, and the pellet was resuspended in 350 µL of RLT lysis buffer (Qiagen RNeasy RNA Isolation Kit).

RNA isolation was then carried out according to the manufacturers specifications for the RNeasy RNA Isolation Kit (Qiagen). Following isolation, the RNA was eluted once with 30 µL of RNase free H_20.

Complementary DNA (cDNA) was made using the Quantitect Reverse Transcription Kit (Qiagen). 12 µL of RNA sample was used as starting material. PCR amplification of a wild-type transcript (expressed from a wild-type *Dusp11* allele) and a gene trapped transcript (expressed from a gene-trap allele) was conducted, along with amplification of a housekeeping gene as a control. The PCR master mix included, per reaction: 1 µM forward primer, 1 µM reverse primer, 25 µL of HotStart Taq 2x Master Mix (Qiagen), 2.5 µL of cDNA, and H_20 to bring the reaction volume to 50 µL. PCR was performed with the following conditions: 95°C for 5 mins; 38 cycles of 94°C for 30 seconds, 60C for 30 seconds, and 72C for 1 minute; 72°C for 10 minutes, and 4°C indefinitely.

PCR samples were then analyses via a 1.2% agarose gel. 5.56 µL of 10× loading buffer was added each samples, and 20 µL of this mixture was loaded into each lane. 10 µL of ethidium bromide was added to the gel box, and the gel was run at 100 V for 30 minutes. The gel was then imaged using a UV gel box.

Genotyping via genomic DNA

Tail tissue samples were collected from weanling mice. DNA was extracted from this tissue using the DNeasy kit (Qiagen, qiagen.com, cat: 69504) according to the manufacturers instructions. The DNA as eluted in 100 µL of AE buffer as supplied by the kit.

For each animal three reactions were set up: a control reaction, a wild-type reaction and a gene-trap reaction. A master mix was made consisting of: 25 µL of HotStarTaq Master Mix (Qiagen; qiagen.com; cat: 203443), 500 nM forward primer, 500 nM reverse primer, 2 µL of tail DNA, and enough H_2O to bring each reaction to 50 µL. PCR was run with the following conditions: 95°C for 5 mins; 30 cycles of 94°C for 30 seconds, 55°C for 30 seconds, and 72°C for 1 minute; 72°C for 10 minutes, and 4°C indefinitely.

Table 2.1: PCR primers used for PIR1 mouse genotyping by complementary DNA. To detect the wild-type allele, the primers used are: DUSP11 F1, and DUSP11 R1. To detect the gene-trap allele, the primers used are: DUSP11 F1, and Genetrap R2.

Primer	Sequence	Target
Dusp11 F1	AGAAGGGCAGAAACCACATC	dusp11, exon1
Dusp11 R1	GTAGGATCTGCTGAGTCTTC	dusp11, exon8
Genetrap R2	GTAGCCAGCTTTCATCAACAT	LacZ gene, in pg101xr plasmid

PCR samples were then analyses via a 1.2% agarose gel. 5.56 µL of 10× loading buffer was added to each sample, and 20 µL of this mixture was loaded into each lane. 10 µL of ethidium bromide was added to the gel box, and the gel was run at 100 V for 30 minutes. The gel was then imaged using a UV gel box.

Sequencing Intron 1

Primer sequences were designed using NCBI Primer-BLAST [122]. The target sequence used was NC_000072.6 (*Mus musculus* strain C57BL6/J chromosome 6, GRCm38.p2 C57BL/6J, NCBI Reference Sequence) from position 85,961,962 to position 85,958,583, which is a 3379 bp segment of the Dusp11 locus on chromosome 6. The primer query included checks against the remainder of the *M. musculus* genome to reduce the risk of spurious PCR products when gDNA is used. The other Primer-BLAST parameters are listed in Table 2.3. The primers generated are listed in Table 2.4

2.2.3 Mouse cell line generation

Bone-marrow-derived dendritic cells

Bone-marrow-derived dendritic cells (BMDCs) were generated from 6 to 8 week old mice using a protocol adapted from the one used by Lutz el al. [123] and Brandt et al. [124].

Mice were euthanized then, rinsed with 90% ethanol to reduce fur contamination, then dissected to isolated the tibias and femurs. Each bone was cut on either end using sterile scissors, and flushed with RPMI1640 media using a 25G needle. Bone marrow was then passed through a 70 µm cell strainer, and centrifuged for 5 minutes at 300×g at room temperature. The supernatant was discarded, and the cell pellet was resuspended in 1 mL of Red Cell Lysing Buffer (Sigma Aldrich; sigmaalrich.com; cat: R7757), and incubated at for 5 minutes as room temperature. After incubation for 1 minute at room temperature, 15 mL of RPMI1640 was added, and the cells were centrifuged again for 5 minutes. This was repeated

Table 2.2: PCR primers used for PIR1 mouse genotyping by genomic DNA. To detect the wild-type allele, the primers used are: dusp11intr1–4F, and dusp11intr1–4R. To detect the gene-trap allele, the primers used are: dusp11intr1–4F, and Genetrap R2.

Primer	Sequence	Target	Reaction
dusp11intr1–1F	AACCAGCATTATGGCCGACA	dusp11, exon1	control
dusp11intr1–1R	CTCAAAGGACACCTCCGCTT	dusp11, intron1 5' side	control
dusp11intr1–4F	ACGAGGCTGGGTTTGTTAGG	dusp11, intron1 3'side	wild-type, gene trap
dusp11intr1–4R	TGAAACGAGTCCCAGGCATC	dusp11, exon2	wild-type
Genetrap R2	GTAGCCAGCTTTCATCAACAT	LacZ gene, in pg101xr plasmid	gene trap

Table 2.3: A table of parameter used with the program Primer-BLAST to generate overlapping PCR primers that span Intron 1 of the mouse Dusp11 gene.

Parameter	Value
Min total mismatches	2
Min 3' end mismatches	2
Defined 3' end region length	5
Mismatch threshold to ignore targets	4
Misprimed product size deviation	4000
Max number of Blast target sequences	50000
Blast E value	30000
Blast word size	7
Max candidate primer pairs	50
Min PCR product size	200
Max PCR product size	1000
Min Primer size	15
Opt Primer size	20
Max Primer size	25
Min T_m	57
Opt T_m	60
Max T_m	63
Max T_m difference	3
Repeat filter	AUTO
Low complexity filter	Yes

Table 2.4: Primer pairs used in Figure 2.6 to determine the insertion location of the gene trap plasmid. These primer pairs target Intron 1 of the Dusp11 gene on chromosome 6 of the mouse genome.

Pair Number	Primer Name	Sequence (5'→3')	Product length
Primer pair 1	dusp11intr1–1F	AACCAGCATTATGGCCGACA	464
	dusp11intr1–1R	CTCAAAGGACACCTCCGCTT	
Primer pair 2	dusp11intr1–2F	GCAGGCTGACAAACCCTACT	225
	dusp11intr1–2R	TGTCGGCCATAATGCTGGTT	
Primer pair 3	dusp11intr1–3F	GTCAGCCAGTGTGTAGGCAT	483
	dusp11intr1–3R	CCTAACAAACCCAGCCTCGT	
Primer pair 4	dusp11intr1–4F	ACGAGGCTGGGTTTGTTAGG	309
	dusp11intr1–4R	TGAAACGAGTCCCAGGCATC	
Primer pair 5	dusp11intr1–5F	GATGCCTGGGACTCGTTTCA	519
	dusp11intr1–5R	CCACTTGAAGCCCTGTAGCA	
Primer pair 6	dusp11intr1–6F	AAGCGGAGGTGTCCTTTGAG	414
	dusp11intr1–6R	GCAAGCTGTCAGGCAAGTTC	
Primer pair 7	dusp11intr1–7F	GAACTTGCCTGACAGCTTGC	701
	dusp11intr1–7R	ATGCCTACACACTGGCTGAC	
Primer pair 8	dusp11intr1–8F	CCCTTTCTCCTGCCCACATT	346
	dusp11intr1–8R	AGCCTAACAAACCCAGCCTC	
Primer pair 9	dusp11intr1–9F	ACCCTACTTTCAGTGCGACG	985
	dusp11intr1–9R	CCACTCTGGGAAGGGAGAGA	
Primer pair 10	dusp11intr1–10F	GAGGCTGGGTTTGTTAGGCT	800
	dusp11intr1–10R	GAAGCCCTGTAGCACACGAT	
Primer pair 11	dusp11intr1–11F	ACATCCCCGAAAGGTAAGCG	711
	dusp11intr1–11R	TCCACTCTGGGAAGGGAGAG	
Primer pair 12	dusp11intr1–12F	ACTTTGCCCATGTTCACCCA	436
	dusp11intr1–12R	GAGCACACAGGTCTCCACAA	
Primer pair 13	dusp11intr1–13F	TTCAGGATGGACGTGATGGC	892
	dusp11intr1–13R	TGGGTGAACATGGGCAAAGT	
Primer pair 14	dusp11intr1–14F	TTGTGGAGACCTGTGTGCTC	597
	dusp11intr1–14R	GTTTGTGTCTCCCTGCCTGA	
Primer pair 15	dusp11intr1–15F	TGAACCCTTTACTTGCGGCT	251
	dusp11intr1–15R	GCCATCACGTCCATCCTGAA	
Primer pair 16	dusp11intr1–16F	TCTCCTGCCCACATTTTGCT	333
	dusp11intr1–16R	AAACCCAGCCTCGTGTCAAA	
Primer pair 17	dusp11intr1–17F	GTCCCTTGATCTCCGAAGCC	220
	dusp11intr1–17R	AGCCGCAAGTAAAGGGTTCA	
Primer pair 18	dusp11intr1–18F	ATTTGACACGAGGCTGGGTT	662
	dusp11intr1–18R	TGTTTGTGTCTCCCTGCCTG	
Primer pair 19	dusp11intr1–19F	CTTTCAGTGCGACGTGTGTC	289
	dusp11intr1–19R	CGCTTACCTTTCGGGGATGT	
Primer pair 20	dusp11intr1–20F	TCAGGATTCGGAAAGCGGAG	258
	dusp11intr1–20R	GGGCAGAGCATTCTGTCGAT	

as necessary until the cell pellet is no longer red. Finally, the cell pellet was resuspended in RMPI R10 media—RPMI 1640 Dutch Modification with sodium bicarbonate, 10% heat-inactivated FBS, 2 mM L-glutamine, 50 μM β-mercaptoethanol, 100 U/mL penicillin, 100 μg/mL streptomycin, 20 ng/mL recombinant murine GM-CSF (Peprotech; peprotech.com; cat: 315-03)—, and placed in the appropriate size tissue culture flasks with the appropriate volume of media: roughly 300 cm^2 per animal. The flasks were then incubated at 37°C with 5% CO_2.

After 3 days, the non-adherent cells were removed by swirling the flasks, removing the media, and replacing with a half-volume of fresh RPMI R10 media. The removed media was centrifuged at 350×g for 5 mins at room temperature, and then a half-volume of the old media was returned back to the culture flask. The remaining media and non-adherent cell pellet was discarded. The flasks were then incubated again at 37°C with 5% CO_2.

After 3 more days, the non-adherent cells were removed again, as described above. The flasks were then incubated again at 37°C with 5% CO_2.

After 2 more days, half of the media was exchanged while preserving non-adherent cells. Half of the media from each flask was removed and centrifuged at 300×g for 5 minutes. The supernatant was discarded, and the non-adherent cell pellet was resuspended in an equal volume of fresh R10 media. The flasks were then incubated again at 37°C with 5% CO_2.

After 1 or 2 more days, the cells were harvested, counted, and plated for stimulation. The media and non-adherent cells were removed from each flask, centrifuged at 350×g for 5 minutes, the supernatant was saved as *conditioned* media. 5mL of fresh RMPI1640 was added to each flask, and the cells were then scrapped off the bottom of the flask, and centrifuged at 350×g for 5 minutes at room temperature. The cells were then resuspended in 5mL of conditioned media and counted using a hemocytometer. Cells were plated at the appropriate for the experiment at hand in conditioned R10 media and incubated overnight at 37°C with 5% CO_2. The following day, the media was removed, and cells were stimulated per the stimulation protocols.

2.2.4 Preparation of EMCV stocks

The strain of encephalomyocarditis virus (EMCV) used was original purchased from ATCC (American Tissue Culture Collection, atcc.org): VR-129B. The strain was passaged four times on BHK-21 cells (ATCC).

To generate a highly-concentrated stock of EMCV, a monolayer of BHK-21 cells was inoculated with EMCV at a multiplicity of infection (MOI) of 0.01, and incubated for 24 hours at 37°C and 10% CO_2. At the point that roughly 90% of the BHK-21 cells exhibited cytopathic effect (CPE), the culture flasks were freeze-thawed three times. From this point the cell lysates were collected, centrifuged at 3,500×g for 15 minutes at 4°C. The supernatant was removed and passed through a 0.2 μm filter.

EMCV was then purified by pelleting through a sucrose cushion. Briefly, the filtered supernatant was placed in a 1 inch ultracentrifuge tube (Beckman Coulter; beckmancoulter.com; cat: 344058) and then underlaid with 2 mL of sterile 30% (w/v) sucrose in PBS. The samples were then ultracentrifuged using the SW32Ti ultracentrifuge rotor (Beckman Coulter; beckmancoulter.com; cat: 369650) at 174,900×g (32,000rpm) for 2 hours at 4°C.

After ultracentrifugation, the supernatant and sucrose were aspirated off, and the EMCV pellet was resuspended in PBS with 50 mM $MgCl_2$. This viral stock solution was then dispensed into 10 μL aliquots that were then stored at -80°C. One day later, two or three aliquots were thawed on ice and titered by a plaque assay on BHK-21 cells in order to determine the concentration of infectious EMCV by measuring plaque forming units per mL.

2.2.5 EMCV plaque assays

BHK-21 cells (ATCC) were seeded in a 12-well plate at a concentration of 5×10^5 cells/well in 2mL of DMEM complete (DMEM, 10% heat-inactivated FBS, 2 mM L-glutamine, 100 U/mL penicillin, 100 μg/mL streptomycin), and incubated overnight at 37°C in 10%

CO_2. The next day, the media was removed from the BHK21 monolayers, and 1 mL of 10-fold serially-diluted EMCV-containing sample (virus stock, tissue lysate, cell-culture supernatant, etc) was added to the cells, and incubated at 37°C in 10% CO_2 with hand-shaking every 20 minutes. After the one hour of inoculation, the virus-containing media was removed, and 1mL of agarose overlay was added on top. The overlay consists of 1× MEM and 2% low-melting-point agarose (w/v), which has been melted and then held at 42°C in a water bath prior to overlaying BHK-21 cells. The cells were then incubated at 37C in 10% CO_2. After 36 hours, the 0.5 mL of a 0.5% crystal violet (w/v) and 4% paraformaldehyde (w/v) in deionized H_2O was added on top of the agarose, and allowed to stain the cells for at least 2 hours at room temperature. At this point, the agarose overlays were removed, and the fixed monolayers were rinsed with water. The plates were then air dried, and plaques quantified using a light box to illuminate the monolayers for visual inspection.

2.2.6 SNP analysis of mouse lineages

Tail samples from weanling mice were collected in a microcentrifuge tube, and shipped on ice to the Jackson Laboratory (Bar Harbor, ME; jax.org). Personnel at Jackson Laboratory performed the gDNA isolation and SNP sequencing. SNP sequences were compared to those of both parental strains: C57BL6/J and 129.

The SNPs tested are listed in Table 2.5

2.2.7 Infection of mice with EMCV and collection of samples

For survival studies, 6 to 10 week old mice were inoculated via intraperitoneal injection with 1×10^5 pfu/mouse of EMCV in 200 μL of sterile PBS. After infection, the mice were then monitored once ever 12 hours for death or moribundity. Moribund mice were counted as dead, and euthanized.

For time point sample collection, mice were infected with EMCV via intraperitoneal injection. At the specified time points (6, 24, and 48 hours) mice were euthanized and

Table 2.5: Positions and rsID numbers for SNPs tested to assess backbreeding.

Chr	Location	Ref SNP ID	Chr	Location	Ref SNP ID	Chr	Location	Ref SNP ID	Chr	Location	Ref SNP ID
1	5215199	rs3708040	4	86563736	rs3659971	9	16021041	rs3719348	14	48792639	rs3659053
1	15968979	rs3684370	4	91021367	rs4136370	9	32541782	rs3716314	14	63543331	rs3702501
1	25731275	rs3666554	4	105891733	rs3664701	9	34646174	rs3659084	14	70097369	rs4230429
1	29774142	rs3695988	4	108237002	rs3664065	9	45669748	rs4227612	14	76489669	rs3664973
1	45504098	rs3654040	4	122489120	rs3702270	9	52358773	rs3654569	14	86443660	rs3666728
1	59272438	rs3687432	4	122489120	rs3702270	9	59238251	rs3685575	14	102295849	rs3686670
1	64459042	rs3697376	4	134927851	rs3679734	9	76102534	rs3685573	14	105343852	rs3656066
1	76386671	rs3699038	4	142898789	rs3718220	9	76938604	rs3676260	14	106254320	rs3677639
1	87687980	rs3678377	4	155091989	rs3680364	9	89297541	rs3709387	14	121343810	rs4230603
1	90636912	rs3670389	5	10671078	rs3676096	9	98249448	rs3692530	14	123545419	rs3685710
1	103425685	rs3720366	5	4082306	rs4225033	9	105983686	rs3657415	15	3219262	rs3687235
1	120375151	rs3680832	5	15336887	rs3673475	9	113824128	rs3721068	15	17000043	rs3726451
1	124137123	rs3676992	5	24922231	rs3664933	9	123551657	rs3706619	15	20138467	rs3662097
1	135256759	rs3022833	5	30708181	rs3023765	10	6998239	rs3724192	15	31846034	rs3023416
1	143991782	rs3663996	5	45444992	rs3663092	10	3496425	rs3090968	15	42657298	rs3667271
1	151052601	rs3710036	5	52211200	rs3655838	10	14976369	rs3701746	15	46631272	rs3024123
1	163725177	rs3706326	5	67053321	rs4225249	10	22906845	rs3665690	15	59162786	rs4230758
1	166321951	rs3707309	5	67053321	rs4225249	10	34297659	rs13480578	15	74316084	rs3724474
1	179305169	rs3668273	5	79046996	rs3678094	10	42421803	rs3716113	15	90278319	rs3724956
1	192267912	rs3699344	5	82943584	rs3705373	10	53462955	rs3696307	15	101641254	rs3023429
1	193617817	rs3715125	5	92720835	rs3704889	10	70714406	rs13480646	16	5596485	rs4153115
2	3151175	rs3713997	5	108807704	rs3656524	10	72243080	rs13480647	16	12604654	rs4162874
2	11988388	rs4137557	5	108807704	rs3656524	10	82455611	rs3717445	16	19883172	rs4165081
2	20293400	rs4139548	5	120432371	rs3670250	10	92728249	rs4228405	16	38174909	rs4174474
2	30268356	rs3689602	5	127277828	rs3705399	10	102471129	rs3716716	16	49089580	rs4184376
2	40450275	rs3697051	5	137912435	rs3141573	10	116830927	rs3670118	16	57292597	rs4189277
2	45047811	rs13476470	5	141533535	rs3717290	10	127890188	rs3719409	16	63792299	rs4195412
2	60302386	rs3714030	5	150598041	rs3722801	11	4408733	rs3659787	16	75143255	rs4205499
2	60302386	rs3714030	5	150598041	rs3722801	11	5684650	rs4222040	16	90383864	rs4217372
2	75946661	rs3699089	6	3416870	rs3661828	11	14903307	rs3703198	16	95329654	rs4221067
2	77028245	rs3670874	6	15441783	rs3658616	11	24386229	rs3673413	17	5885430	rs3694565
2	94918939	rs13476645	6	17673652	rs3023064	11	39780701	rs3717967	17	5079178	rs3667161
2	99962752	rs3686727	6	28731469	rs3706286	11	46666864	rs3686921	17	14468498	rs3664721
2	103824484	rs3697882	6	44823195	rs3706944	11	55679273	rs3671065	17	24105207	rs3673763
2	118811005	rs3691456	6	62010344	rs3706318	11	69560965	rs3668244	17	27244878	rs3684506
2	121850773	rs3726142	6	75345544	rs3671401	11	82677260	rs3663879	17	44300074	rs3677240
2	134586818	rs13476785	6	82284691	rs3707989	11	89314273	rs3682081	17	58335285	rs3710084
2	138397679	rs3726475	6	89242512	rs3708822	11	99441451	rs4229088	17	67755219	rs3023456
2	150727187	rs3704224	6	105174947	rs3665833	11	110246168	rs3712384	17	79284189	rs4231670
2	150727187	rs3704224	6	121990121	rs3727110	11	121116553	rs3675603	17	84394009	rs3707550
2	160792944	rs3693259	6	135557845	rs3684061	12	3701820	rs3675632	17	93598958	rs3023460
2	164979405	rs3661349	6	148260469	rs3711088	12	15131892	rs3709592	18	5207638	rs3706767
2	180489599	rs3680965	7	4796809	rs4226386	12	28835162	rs3712523	18	22098944	rs3707236
3	11297853	rs3680834	7	16621522	rs3675839	12	30739722	rs3091105	18	22098944	rs3707236
3	26231610	rs3698991	7	30566471	rs4226520	12	46426114	rs3701242	18	34759922	rs3701931
3	32477107	rs3659585	7	31508107	rs3662246	12	48020093	rs3665793	18	43083464	rs3676196
3	37166987	rs3141019	7	47576838	rs3675009	12	59053677	rs3706319	18	44777584	rs3675819
3	52508729	rs3685081	7	51751706	rs3710949	12	67818222	rs3677704	18	54721426	rs3715080
3	65133735	rs3022960	7	62576551	rs3671564	12	74706281	rs3683927	18	56780585	rs3721446
3	72409948	rs3681493	7	75671284	rs3710266	12	75826388	rs3655558	18	67794075	rs3657976
3	80234955	rs3672565	7	81780013	rs3672773	12	90384551	rs3711162	18	77973654	rs3725940
3	87174449	rs4224040	7	88680105	rs3656205	12	99535606	rs3719660	18	78443851	rs3686065
3	95750438	rs13459185	7	102503409	rs3670440	12	106091063	rs3663596	18	89629192	rs3663208
3	109572245	rs3712218	7	104479593	rs3710857	12	114496728	rs4229611	19	003490564	0
3	109572245	rs3712218	7	120464651	rs3680026	12	119290434	rs3686631	19	18669375	rs3691881
3	118532449	rs3721089	7	123671703	rs3654689	13	4160601	rs3695486	19	21510766	rs3692864
3	130432706	rs3089257	7	134811064	rs3697227	13	14446330	rs3680731	19	31481029	rs3681148
3	135357403	rs4136498	7	151765715	rs3664224	13	23788316	rs3679575	19	38517304	rs3695591
3	150231659	rs3725806	8	3189168	rs3701395	13	31508761	rs3654710	19	45627210	rs3160376
3	150231659	rs3725806	8	15191287	rs3709624	13	44496918	rs3023382	19	48212356	rs3023496
3	159329523	rs3665134	8	27414184	rs3684251	13	60682856	rs3713287	19	60842385	rs3023498
3	159329523	rs3665134	8	31235216	rs3691295	13	67941214	rs3023384	X	17889948	rs13483721
4	3649668	rs3694594	8	47006288	rs4137370	13	74990455	rs3667493	X	36252886	rs13483729
4	15072175	rs3090919	8	55938034	rs3661085	13	87813907	rs3666540	X	68674333	rs3161045
4	23212481	rs4138316	8	70607462	rs3089230	13	105301661	rs3687254	X	82748657	rs3664154
4	30384672	rs3707198	8	83509096	rs4227271	13	120254901	rs3710370	X	100102202	rs13483918
4	30384672	rs3707198	8	89791885	rs3706660	14	8613747	rs3701221	X	114022081	rs3690903
4	47160354	rs3654185	8	95465749	rs3089148	14	10592844	rs3689508	X	131483758	rs3702256
4	59942679	rs3654495	8	109771826	rs3683511	14	18484813	rs3678171	X	150081739	rs13484074
4	63785765	rs3656076	8	125471593	rs3693295	14	29772395	rs3719262	X	162753251	rs3698078
4	75302622	rs3655623	9	4020321	rs3694533	14	47715833	rs3661783			

organs were collected. For tissue lysates, pre-weighed 5 mL tubes with 500 µL of sterile PBS were prepared for each organ. Organ hemisections were dissected and place into each tube, which were then stored on ice until further processing. Each tube was then weighed again, to determine the mass of organ contained within. At this point each organ sample was homogenized using the Qiagen TissueRuptor (qiagen.com). The homogenates were then clarified by transferring to a 1.5 mL microcentrifuge tube, and centrifuged at 12,000 rpm for 10 minutes at 4°C. The supernatant was then removed to a clean microcentrifuge tube, and stored at -80°C for future analyses.

For RNA sample collection, a 5 mL tube with 500 µL of Trizol reagent (Thermo Fisher Scientific Inc; thermofisher.com; cat: 15596018) was prepared for each organ sample. Organ hemisections were placed into 500 µL of Trizol reagent on ice. (Thermo Fisher Scientific Inc; thermofisher.com; cat: 15596018). The tissue samples were then lysed in Trizol and homogenized using a Qiagen TissueRuptor. Total RNA extraction proceeded according to the manufacturers instructions, with the final RNA pellet being resuspended in 50 µL of RNase-free H_2O.

2.2.8 ELISA

IFN-β ELISA was done using the Mouse IFN Beta ELISA Kit from PBL Inc (pblassaysci.com; Piscataway, NJ; cat: 42400-2). Serum samples were diluted either 1:5 or 1:10 in the provided dilution buffer, and the assay was conducted at half the recommended volume. Otherwise the assay was performed as instructed by the manufacturer.

ELISA tests for murine IL-6 were purchased as BD OptEIA kits from BD Biosciences (bdbiosciences.com; cat: 555240), and performed as per manufacturer's instructions. ELISA tests for murine RANTES (CCL5) were purchased from R&D as the Mouse CCL5/RANTES DuoSet ELISA (rndsystems.com; cat: DY478) and performed as per the manufacturer's instructions.

2.2.9 qRT-PCR

Quantitative reverse-transcriptase PCR (qRT-PCR) was performed on total RNA samples collected from organ samples.

Complementary DNA was generated using the Quantitect Reverse Transcription Kit (Qiagen; qiagen.com; cat: 205310). 1 µg of total RNA was processed for removal of genomic DNA, and then reverse transcribed using random hexamer primers. The resulting cDNA, was then assayed for several genes using SYBR® Green PCR Master Mix (Qiagen; qiagen.com; cat: 4309155).

PCR primers specific for the *M. musculus* genes Il6, Ifnb1, Isg15, and Gusb were purchased from Qiagen (qiagen.com; cat: QT00098168, QT00249662, QT00322749, QT00322749). PCR primers for the EMCV genome and mRNA have been previously validated by Carrocci et al. [115] and ordered as custom DNA oligos from Eurofins Genomics (eurofinsgenomics.com). The sequence for the forward EMCV primer is `GGGATCAGCTTTTACGGCTTT` , and the sequence of the reverse EMCV primer is `TGCATCCGATAGAGAACTTAATGTCT`.

Reaction mixtures were run on Eppendorf MasterCycle RealPlex qRT-PCR machines, according to the SYBR Green protocol.

2.2.10 Western blotting

To blot for phosphorylated proteins, stimulated cells ready for lysis were first washed with PBS. Cells were then lysed with RIPA buffer (10 mM Na_2HPO_4 pH=8, 150 mM NaCl, 1% NP-40 (v/v), 0.5% sodium deoxycholate (w/v), 0.1% SDS (w/v)) containing fresh protease inhibitor cocktail (Sigma Aldrich; sigmaaldrich.com; 11697498001) and fresh phosphatase inhibitor cocktail (Sigma Aldrich; sigmaaldrich.com; P0044). Cells were lysed for 5 mins at 4°C, and lysates were collected by pipetting into microcentrifuge tubes. Lysates were clarified by spinning for 5 minutes at 12,000 rpm in a microcentrifuge. The supernatant was removed and stored at -20°C prior to blotting.

Protein levels in lysates were determined by microBCA assay (ThermoFisher; thermofisher.com; cat: 23235), to ensure that a consistent amount of protein was loaded for each sample. 8 to 10 µg of protein was loaded into each well of a freshly made 10% SDS-PAGE gel, using a mini-gel casting system.

Preparing polyacrylamide gels

To prepare a 10% PAGE gel, a polymerization solution was made: 3.3 mL of Protogel (30% (w/v) acrylamide: 0.8% (w/v) bis-acrylamide stock solution (35:5:1) National Diagnostics; nationaldiagnostics.com; cat: EC-890), 4 mL of H_2O, 2.5 mL of 1.5 M Tris solution (pH 8.8), 200 µL 10% (w/v) SDS, 83 µL ammonium persulfate (BioRad; biorad.com; cat: 161-0700), and 10 µL of TEMED (BioRad; biorad.com; cat: 161-0800). Prior to polymerization this solution was poured into 2 assembled mini-gel cassette casts. Once the polymerization solution was added to each cast, approximately 300 µL of butanol was added as an overlay at the top of each. The gel casts were then incubated for an hour at room temperature to allow for complete polymerization.

Running a loaded gel

Samples were prepared by mixing normalized samples with 2× Laemmli Sample Buffer (BioRad; biorad.com; cat: 161-0737) at a 1:1 ratio. Samples were then heated at 95°C for 5 minutes. Samples were then placed in wells, and the gel was run at 90 V until the loading dye reached near the bottom of the gel. The running buffer was: 3 g Tris-Base, 14.4 g glycine, and 1.0 g SDS in 1.0 L of ddH_2O.

Gel transfer

After the gel is done running, proteins were transferred onto a membrane for immunoblotting. A transfer sandwich of blotting pad, blotting paper, membrane, blotting paper, and blotting pad was prepared. All but the membrane was submerged in transfer

buffer, while the membrane was submerged in 100% methanol. The polyacrylamide gel was then place on top of the membrane at the center of the sandwich, and all bubbles were removed from between each layer. The transfer was then run on a semi-dry transfer machine at 25 V (maximum of 300 mA) for 45 to 60 minutes. The transfer buffer consisted of: 3 g Tris-Base, 14.4 g glycine, and 100 mL of 100% methanol in 1.0 L with ddH_2O.

Immunoblotting

After transfer, the membrane was blocked with 3% (w/v) bovine serum albumin (BSA) in TBS with 0.1% Tween 20 (TBS-T) overnight at 4°C. Blocking buffer was removed, and primary antibody diluted in blocking buffer was added. Membranes were incubated with primary antibodies overnight at 4°C. Membranes were then rinsed three times with TBS-T, and then incubated with secondary antibody diluted in blocking buffer for 2 hours at room temperature. Primary antibodies against phosphorylated proteins were used at a dilution of 1:1000, and primary antibodies against non-phosphorylated proteins were used at a dilution of 1:2000. The secondary antibody used as an anti-rabbit IgG-HRP conjugate used at a dilution of 1:30,000. Each of the primary antibodies were purchased from Cell Signaling (cellsignal.com): phospho-IRF3 cat: 4947S, IRF3 cat: 4302S, phospho-STAT1 cat: 9167S, STAT1 cat: 9172S. The secondary antibody was from Vector Laboratories (vectorlabs.com) cat: PI-1000.

2.2.11 Confocal microscopy

Cells were plated into an 8-well chambered slide (Lab-Tek 8-chambered slide; Thermo Fischer; thermofisher.com; cat: 70411) at a concentration of 6×10^4 cells/chamber. After incubation overnight, growth media was removed and replaced with media containing the stimulant or media alone. After the indicated time, the stimulation media was removed, cell were washed with PBS, and then fixed with 4% paraformaldehyde (w/v) for 20 minutes at room temperature. Cells were washed again with PBS, and permeabilized with 0.1% Triton

X-100 in PBS (v/v) for 10 minutes at room temperature. Cell were once again washed with PBS, then blocked with 3% BSA in PBS (w/v) for 1 hour at room temperature. After washing with PBS, cells were incubated with primary antibody diluted in 1% BSA in PBS (w/v) overnight at 4°C. The next day, the cells were washed with PBS, and then incubated with secondary antibody diluted in 3% BSA in PBS (w/v) for 1 hour at 4°C. Cells were washed a final time, overlayed with ProLong® Gold Antifade Mountant with DAPI (Thermo Fisher; thermofisher.com; cat: P36931). A glass coverslip was place on top of each slide, and sealed on the edges with clear nail polish, at which point the slides were ready for confocal imaging on a Leica SP8 scanning confocal microscope.

2.2.12 miRNA nanostring

miRNA expression by Nanostring was conducted using the off-the-shelf miRNA code-set (Nanostring; https://nanostring.com; cat: 150406, GXA-MMIR-24), according the the manufacturers specifications. 100 ng of RNA was used for each sample, as measured by UV/Vis absorbance.

2.3 Results and Discussion

2.3.1 Generating a PIR1-deficient mouse

In order to generate a PIR1 knockout mouse model, embryonic cells containing a putative null allele containing a gene-trap insertion within the Dusp11 locus were purchased from the International Gene Trap Consortium (genetrap.org). The strain purchased was identified as Dusp11$^{Gt(BB0198)Wtsi}$. The 129P2/OlaHsd-derived cells carrying a gene trap insertion in the Dusp11 locus on chromosome 6. This allele is called the PIR1KO allele going forward. The insertion is the linearized pGT0lxr plasmid, which contains a splice-acceptor site, a stop codon, and a LacZ reporter.

These embryonic stem cells were used to generate transgenic pups that were then crossed with C57BL6/J mice. Initially, to follow the PIR1 KO allele, a reverse-transcription cDNA amplification protocol was used. Backbreeding of the PIR1KO-allele onto a C57BL6/J background was carried out for 5 generations, at which point tail DNA from several candidate offspring were analyzed to determine what percentage of the original 129 background strain persisted. The pup with the highest percentage of C57BL6/J-derived SNPs was chosen to continue backbreeding. This was carried forward until generation 11. During this time a genomic DNA genotyping protocol was established, allowing more reliable and faster turnaround of genotyping results. At the 11th generation backbreeding, several pups were once again chosen for SNP testing, by the same procedure. The panel of SNPs tested were distributed across all 19 chromosomes, and were compared to the 129 and C57BL6/J genomes.

The results of this analysis, as seen in Figure 2.5, show that at generation 5 (N=5) there remained several background-derived loci scattered across several chromosomes. One region of note is on chromosome 4, near the mouse type I IFN cluster, which overlaps with one of these loci of parental-origin [126]. Additional loci of 129P2/OlaHsd-derived polymorphisms were present on chromosome 16 and chromosome 19. By generation 11, all but one SNP

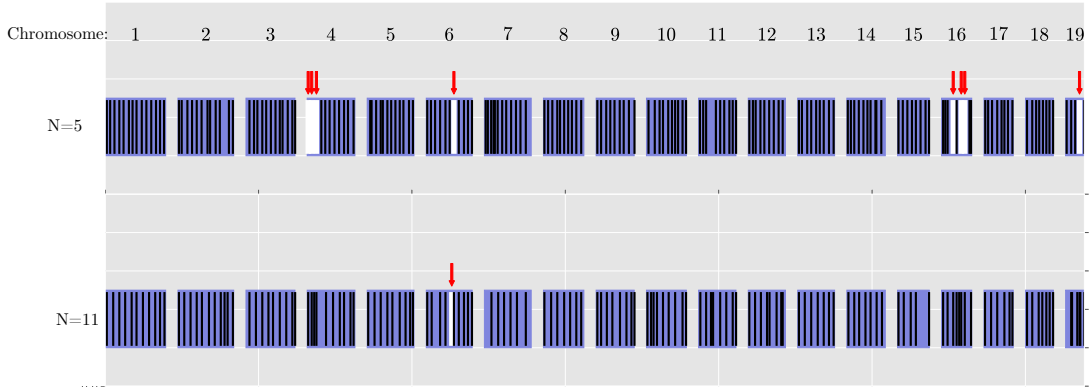

Figure 2.5: PIR1 KO mice nucleotide polymorphism analysis. Mice heterozygous for the PIR1-gene-trap allele were brackbred to C57BL6/J mice for 5 (N=5) and then 11 (N=11) generations. At these generations, DNA samples were collected and analyzed by polymorphism analysts. Each blue box represents a mouse chromosome. Each black line represents a SNP that was sequenced and identified to be derived from C57BL6/J. Each white line represents a SNP that was sequenced and identified as being derived from the background strain of the original embryonic cells (129P2/OlaHsd). SNPs found to have been derived from the background strain are also highlighted with red arrows.

locus was C57BL6/J-derived. The remaining 129P2/OlaHsd-derived locus was present on chromosome 6, and is adjacent to the Dusp11 gene. Taking into account the location of the nearest flanking C57BL6/J-derived loci, I can conclude that the N=11 mice have a C57BL6/J-derived genome, with the exception of a region surrounding the Dusp11 gene that can be no larger than 6 Mbp.

As female mice were bred to male C57BL6/J mice at several points during backbreeding the Y chromosome was assumed to be be completely C57BL6/J-derived. The X chromosome, while not pictured, was also tested, and showed no 129P2/OlaHsd-derived SNPs at N=5 or N=11.

2.3.2 Characterizing the gene-trap allele

Information provided along with the ES cells from the International Gene Trap Consortium included the sequence for the interrupted transcript generated by the gene-trap-containing allele which encodes a truncated *Dusp11* transcript consisting of most of Exon 1. From the sequence of this transcript provided, it was possible to surmise that the location of the gene-trap insertion was somewhere upstream of Exon 2; however, this was not enough information to develop a gDNA-based genotyping assay.

In order to pinpoint the location of the 5'-end of the gene-trap insertion, I designed a series of PCR primers that would amplify adjacent, overlapping regions of Intron 1. These primers were designed to amplify regions no larger than 800bp, since the inherent complexity of this exon made amplification of longer sequences difficult. The results of this experiment can be seen in Figure 2.6. Of the 20 primer pairs that were used, only four failed to amplify a segment of the genome in PIR1KO gDNA. These 4 pairs targeted the final 400 bps of Intron 1, narrowing down the insertion to this small region just upstream of Exon 2.

In order to sequence the intron:gene-trap junction, I PCR amplified this region using the forward primer from primer pair 4, and a reverse primer targeting the LacZ gene present in the gene trap insertion. Sequencing this product gave the exact position of the 5'-end of

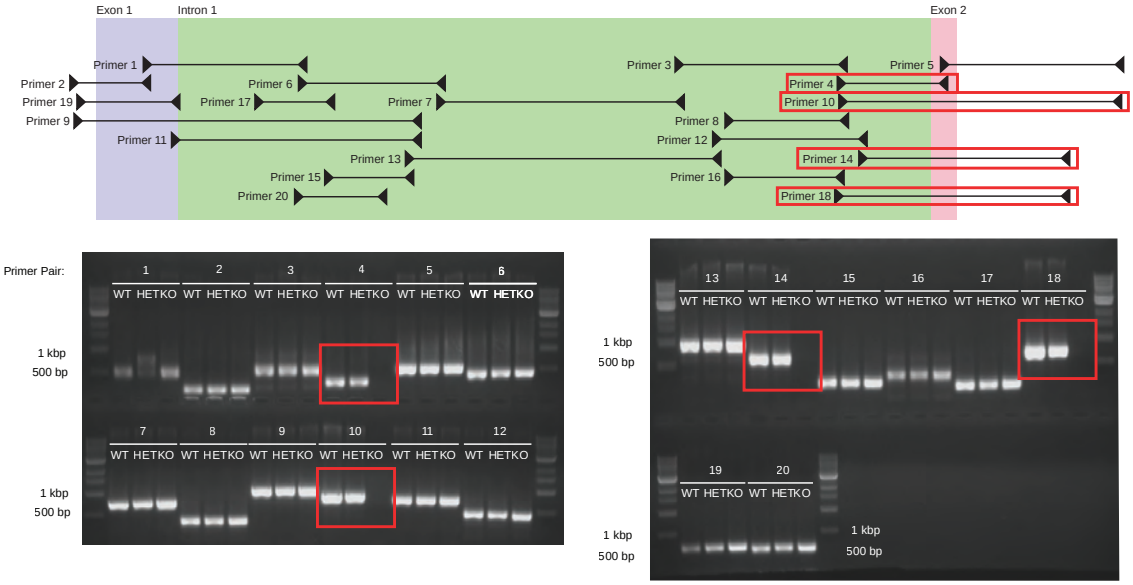

Figure 2.6: PCR analysis of intron 1 of the Dusp11. 20 PCR primer pairs were designed along the length of intron 1 to amplify in an overlapping manner the entirety of the intron and its flanking exons while ensuring that no single amplicon was larger than 1kb. Using this method, I was able to identify exactly where the gene-trap insertion is located within intron 1 in the PIR1KO allele. Primer pairs 4, 10, 14, and 18 produced no PCR products when incubated with genomic DNA derived from a Dusp11-KO mouse. This pinpointed the gene trap to within last last 400 bp of intron 1. Further analysis allowed for the sequencing of the point of insertion.

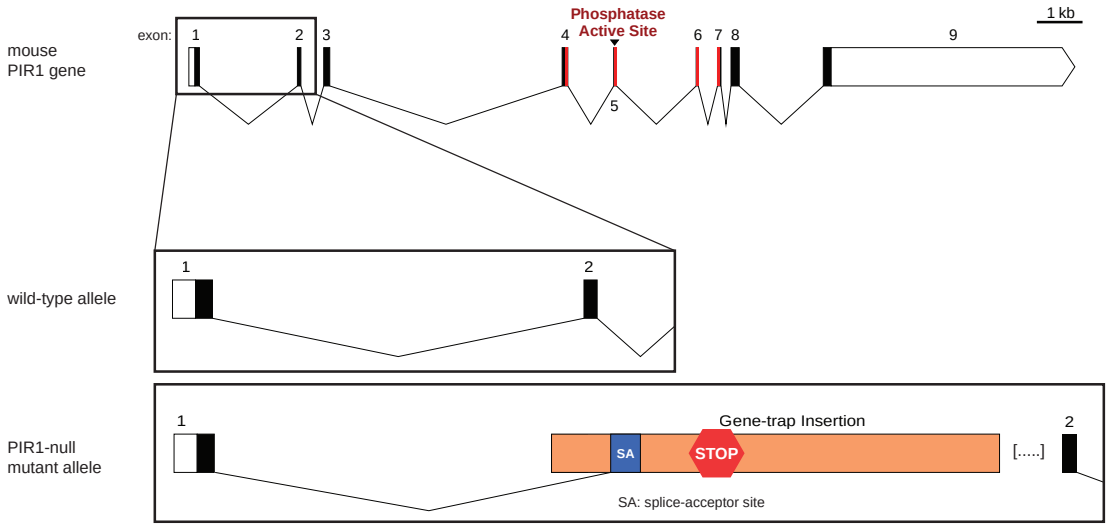

Figure 2.7: A exon schematic of the wild-type and null alleles of the murine *Dusp11* gene. The gene-trap insertion containing a splice-acceptor site (SA) and stop codon is positioned toward the end of intron 1. Splicing of exon 1 to the gene-trap insertion results in a null allele, producing truncated mRNA transcripts.

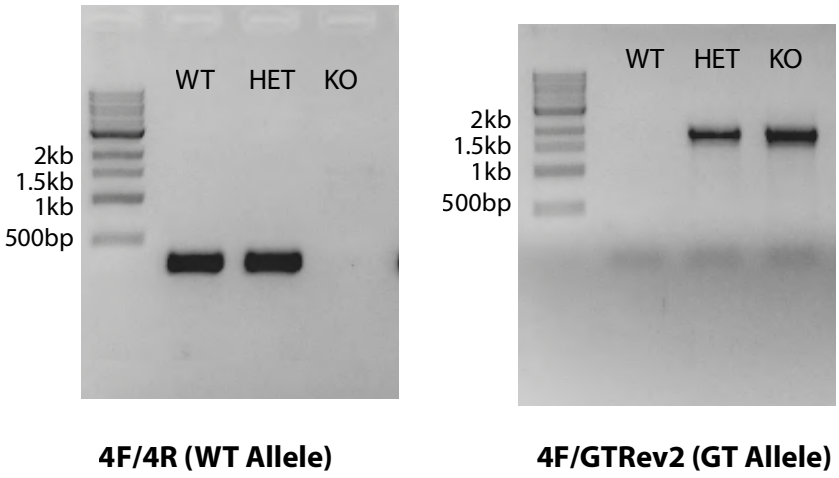

Figure 2.8: A robust genomic DNA PCR protocol was developed, which allowed for easy and reliably genotyping of the Dusp11-KO allele. Primers amplifying the upstream junction of intron 1 and the gene-trap insertion are used to identify the presence of the gene-trap allele.

the gene trap insertion. With this information, I was able to develop a robust and reliable gDNA-based genotyping protocol, the results of which can be seen in Figure 2.8.

2.3.3 EMCV infection *in vivo*

To test whether PIR1 plays a role in the pathogenesis of EMCV in mice, I infected wild-type C57BL6/J mice and PIR1KO mice (backbred to N=11) with 1×10^5 pfu of EMCV by intraperitoneal injection, and collected tissues at various time points.

EMCV titers from heart and brain samples

EMCV was recovered from heart and brain homogenates at 6, 24, and 48 hours post infection. Tissue homogenates were serially diluted onto monolayers of BHK-21 cells to measure the concentration of plaque-forming units per mL of organ lysate. The results of these studies are shown in Figure 2.9. The progression of EMCV infection in wild-type and PIR1KO mice is demonstrated by steadily increasing levels of infectious EMCV virions in the heart and brain as the infection progresses from 6 hours to 48 hours.

EMCV infection of heart tissue was detectable at 6 hours post infection. Of the wild-type mice infected with EMCV three of five had detectable levels of virus ranging from 15 to 250 pfu/mL. Of the PIR1KO mice infected for 6 hours, 3 of the 4 mice had detectable levels of virus, which averaged 40 pfu mL/mL. By 24 hours all of the infected mice had detectable levels of virus in their heart, and by 48 hours these titers reached an average of approximately 250 pfu/mL. Infection of brain tissue was not detectable until 24 hours post infection, when 3 out 5 wild-type and 4 out of 6 PIR1KO mice had detectable levels of virus. In these mice the titers ranged from 80 to 300 pfu/mL. By 48 hours, all the mice tested had detectable levels of EMCV in their brain, with values ranging from 200 pfu/mL to 2000 pfu/mL with an average around 950 pfu/mL for each genotype.

In this model of EMCV infection, EMCV was seen to infect the heart and reproduce to detectable levels much more quickly in the heart than in the brain. However the rate

of change of viral titers from 6 hours to 48 hours shows that viral replication in the brain might be faster. With respect to the comparison of wild-type and PIR1KO mice, these data show that PIR1 does not affect EMCV replication to a significant extent during the first two days post-infection.

Inflammatory and viral RNA expression levels in heart and brain samples

In order to test whether PIR1 affected viral RNA production or the transcription of type I IFN and inflammatory cytokine genes, I isolated RNA from the heart and brain of infected mice. cDNA was prepared for qRT-PCR analysis of mRNA expression levels of IL-6, ISG15, IFN-β, and EMCV genome/transcript RNA.

In the heart (Figure 2.10), several RNA expression patterns can be seen. First, the amount of viral RNA increases between 6 hours post infection and 24 hours post infection. At 24 hours post infection PIR1KO heart tissue had a higher concentration of viral RNA than the heart tissue of wild-type mice. Interestingly, organ homogenates did not show a significant difference in viral titers (as shown in Figure 2.9) in the heart at 24 hours post infection, suggesting that PIR1KO hearts had more viral RNA per infectious particle when compared to wild-type hearts. Between 24 to 48 hours, the amount of viral RNA in PIR1KO mice remains high and relatively constant, while the wild-type mice show an increase in viral RNA such that there is no longer a significant difference between the knockout and wild-type.

In infected hearts, mRNA levels of the cytokines IL-6 and ISG15 are upregulated from 6 hours to 24 hours post infection in both mouse genotypes. However, again, at 24 hours PIR1KO mice exhibit higher levels of both IL-6 and ISG15 in the hearts when compared to wild-type mice. These differences are gone by 48 hours in the case of IL-6, and diminished in the case of ISG15, with both cytokines not showing much more upregulation between 24 to 48 hours post infection.

In contrast, IFN-β expression in the heart follows a unique kinetic pattern from 6 hours to

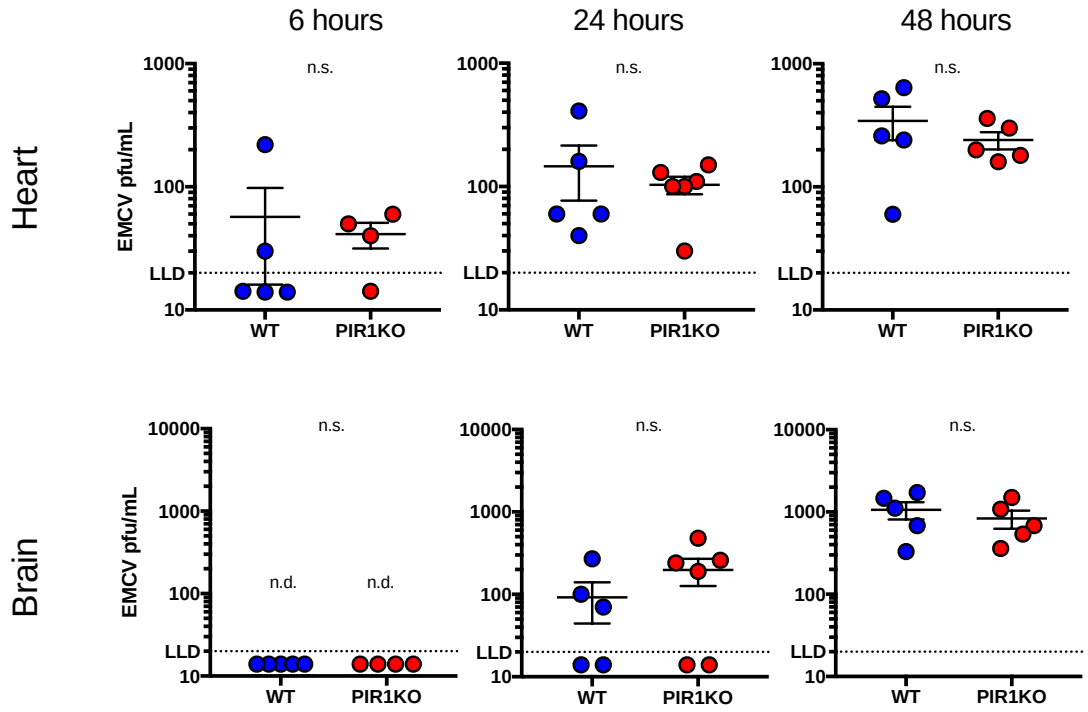

Figure 2.9: Measurement of EMCV titers in the heart and brain of wild-type and PIR1KO mice. EMCV titers of brain and heart homogenates form wild-type and PIR1KO mice. Mice were infected with 1×10^5 pfu by intraperitoneal injection. Bisections of whole brain and whole heart were isolated at the designated time points post infection, lysed, and supernatants collected by centrifugation. EMCV was titered on BHK-21 cells. Each ● represents a wild-type mouse, and each ● represents a PIR1KO mouse. Wild-type and PIR1KO groups were compared using the Mann-Whitney U test. No significance was detectable in any of the comparisons.

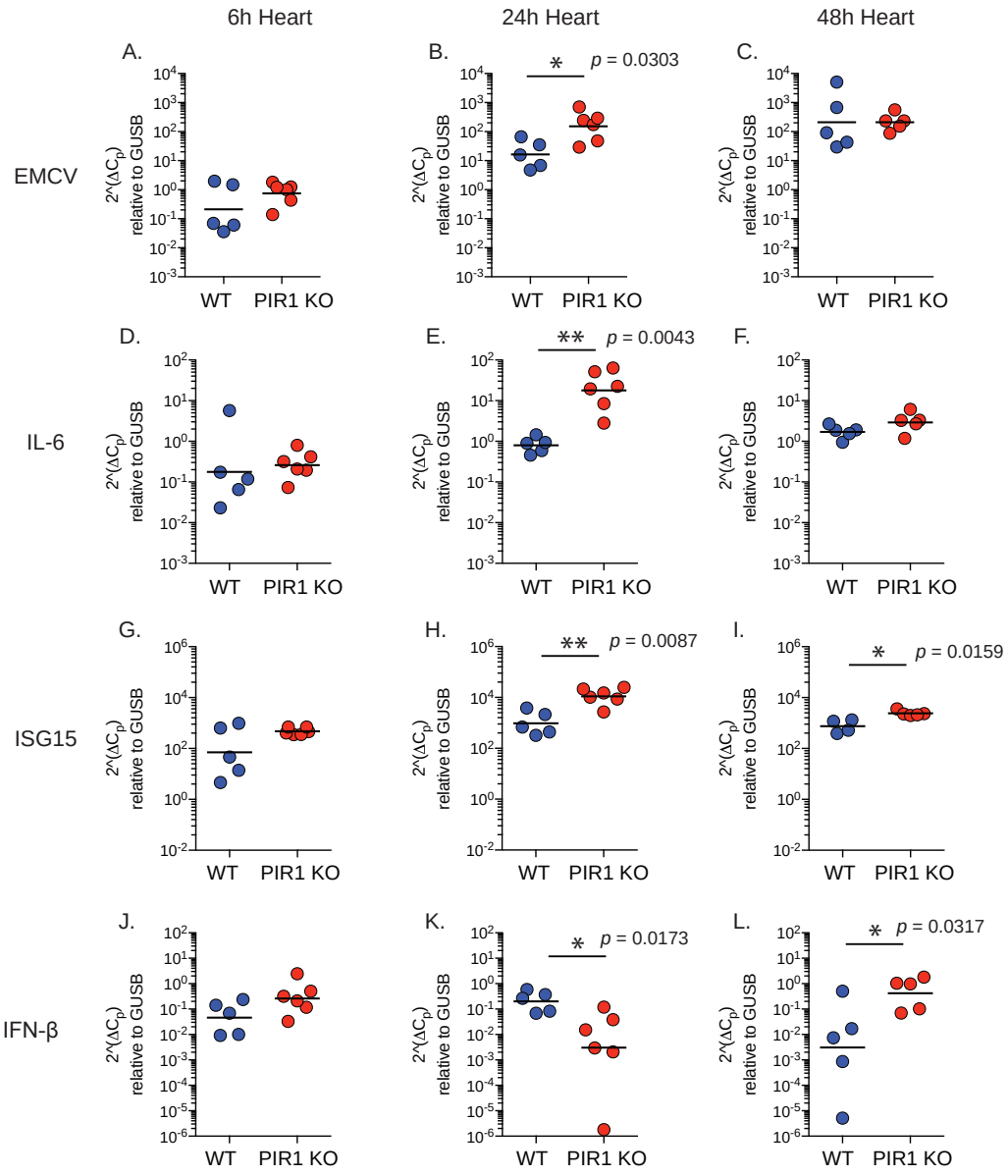

Figure 2.10: Gene expression in the heart following infection with EMCV. qRT-PCR was used to measure gene expression from total RNA isolated from heart lysates. Mice were infected with 1×10^5 pfu of EMCV by intraperitoneal injection, and organs were collected at 6 hours (A, D, G, J), 24 hours (B, E, H, K), and 48 hours (C, F, I, L) after infection. The expression of the EMCV 3dPol gene (A, B, C), IL-6 (D, E, F), ISG15 (G, H, I), and IFN-β (J, K, L) were normalized to the housekeeping gene GUSB. WT and KO groups were compared using the Mann-Whitney U-test. Each ● represents a wild-type mouse, and each ● represents a PIR1KO mouse. * $p \leq 0.05$, ** $p \leq 0.01$, *** $p \leq 0.001$

48 hours post infection. In wild-type mice IFN-β gene expression remains fairly unchanged until 48 hours at which point it decreases, presumably because of downregulation. The PIR1KO mice, however, show an early decrease in IFN-β expression at 24 hours, and then a subsequent increase at 48 hours post infection. On account of these opposing changes, the PIR1KO mice have significantly less IFN-β gene expression at 24 hours and significantly higher levels of IFN-β gene expression by 48 hours.

In the brain, the same genes were analyzed at 6, 24 and 48 hours post infection (Figure 2.11). In the brain homogenates, the amount of EMCV RNA is seen to increase dramatically at each time point, but no differences between mouse genotypes are observed. Additionally, IL-6 and IFN-β levels can be seen increasing up to 48 hours post infection, but I did not observe any significant difference between the wild-type and PIR1KO mice. In contrast, ISG15 mRNA expression levels appear to drop between 6 and 24 hours post infection in the PIR1KO mice. ISG15 expression levels in wild-type mice were equivalent at 6 hours and 24 hours post infection and decreased between 24 and 48 hours post infection.

Together, this data from heart homogenates (Figure 2.10) and brain homogenates (Figure 2.11) show that PIR1 may play a dynamic and tissue-specific role in modulating components of the immune response. EMCV is known to have different pathological effects depending on the tissue that is infected. This is consistent with my findings from RNA expression analysis of brain and heart homogenates which show different patterns of gene expression. Furthermore these data show that PIR1 appears to affect the progression of the EMCV infection in the heart, between 6 hours and 24 hours, by partially controlling viral RNA production, but the difference between wild-type and PIR1KO animals disappears by 48 hours post infection. In the brain, PIR1 appears to not affect viral replication, with only ISG15 expression at 24 hours showing a difference between the two genotypes.

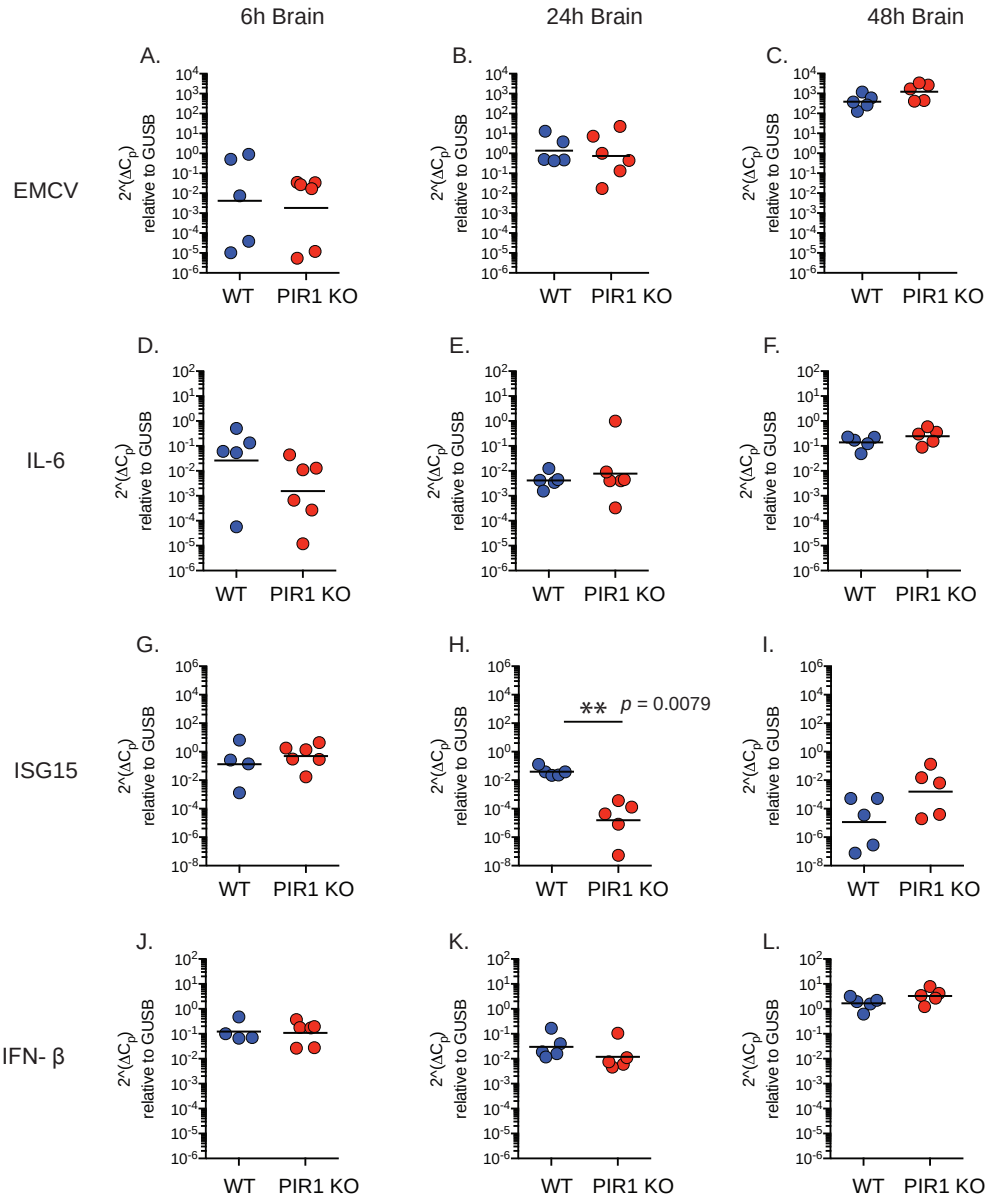

Figure 2.11: Gene expression in the brain following infection with EMCV. qRT-PCR analysis of gene expression from total RNA isolated from brain lysates. Mice were infected with 1×10^5 pfu of EMCV by intraperitoneal injection, and organs were collected at 6 hours (A, D, G, J), 24 hours (B, E, H, K), and 48 hours (C, F, I, L) after infection. The expression of the EMCV 3dPol gene (A, B, C), IL-6 (D, E, F), ISG15 (G, H, I), and IFN-β (J, K, L) were normalized to the housekeeping gene GUSB. WT and KO groups were compared using the Mann-Whitney U-test. Each ● represents a wild-type mouse, and each ● represents a PIR1KO mouse. * $p \leq 0.05$, ** $p \leq 0.01$, *** $p \leq 0.001$

IFN-β expression in sera samples

In order to test whether PIR1 has an effect on the global expression of IFN-β protein in EMCV-infected animals, I collected sera from each mouse at 24 and 48 hours post infection with EMCV. I then measured the amount of IFN-β protein expression by ELISA analysis. As seen in Figure 2.12, there is was no significant difference in the circulating levels of IFN-β in the wild-type and PIR1KO mice at 24 hours and 48 hours post infection.

PIR1KO mice do not have a difference in survival rates following infection with EMCV.

Finally, I wanted to investigate whether PIR1 plays a role in protecting mice from lethal disease following infection with EMCV. Previous work had demonstrated a role for MDA5 and LGP2 in protecting mice from EMCV [53,54]. In these studies, loss of MDA5 or LGP2 resulted in a dramatic acceleration of death following infection with EMCV. I hypothesized that PIR1 might play a role in this response due to its interaction with LGP2 (Figure 2.3). I hypothesized that PIR1KO mice would succumb to infection much faster than wild-type mice.

As can be seen in Figure 2.13, there was no observable difference in the rate of death when comparing wild-type to PIR1KO mice. Both genotypes showed 100% mortality by 100 hours post infection, with the majority of mice from each group succumbing to infection by 75 hours post infection.

2.3.4 Investigating the role of PIR1 *in vitro*

In an effort to better elucidate the role PIR1 plays in type I IFN signaling *in vitro*, I generated bone-marrow-derived dendritic cells from wild-type and PIR1KO mice and stimulated them with viral stimulants. After overnight incubation (18 hrs), supernatants were assayed by ELISA for IFN-β levels. The combined data from three independent experiments can be seen in Figure 2.14. The results from these replicated experiments do show a

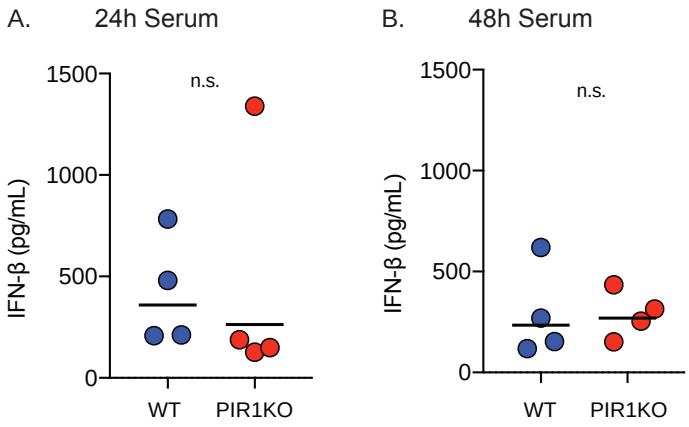

Figure 2.12: Measurement of IFN-β from the serum of EMCV-infected mice. Serum was collected from wild-type and PIR1KO mice infected with 1×10^5 pfu of EMCV by intraperitoneal injection at 24 and 48 hours post infection. The concentration of IFN-β was then measured by ELISA. Wild-type and PIR1KO samples were compared using the Mann U-test.

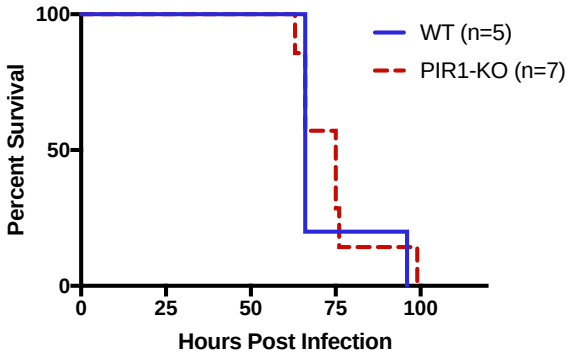

Figure 2.13: Mortality of mice to EMCV. Wild-type and PIR1 KO mice were infected with 1×10^5 pfu of EMCV by intraperitoneal injection, and monitored for death. PIR1KO mice show no survival advantage following infection with EMCV.

difference in IFN-β production between the two cell types. The wild-type BMDCs induce a 15-fold change in the amount of IFN-β in the culture supernatant when compared to background. In contrast, the PIR1KO BMDCs only yield a 7-fold increase in IFN-β production following overnight stimulation with EMCV. While both cell types produced substantial amounts of IFN-β in response to EMCV, the PIR1KO cells produce less. Both cell types responded to Sendai virus, suggesting that the IFN-β defect seen in the PIR1KO cells is EMCV-specific.

PIR1-deficient cells show diminished RLR pathway activation

As the 18-hour stimulation of BMDCs showed that PIR1KO cells have a modest defect in their ability to produce IFN-β, I sought to investigate whether PIR1 was playing a role at earlier time points post stimulation. I transfected wild-type and PIR1KO BMDCs with the synthetic MDA5/LGP2 ligand and viral RNA mimetic polyIC. In order to monitor MDA5/LGP2:MAVS pathway activation, I looked at IRF3 phosphorylation by western blot. Following RLR activation and the initiation of RLR:IFN signaling, the transcription factor IRF3 undergoes phosphorylation, dimerization, and then translocation into the nucleus where it can turn on the expression of the type I IFN genes (Figure 1.2 on page 10). I also assessed the phosphorylation status of the type I IFN receptor signaling molecule STAT1. Phosphorylated STAT1 serves as a marker for how much type I IFN cytokine has been released and subsequently bound to its receptor on the cell surface.

Using lysates collected from BMDCs stimulated for 2 and 4 hours with transfected polyIC, I looked for phosphorylated IRF3 and phosphorylated STAT1 by western blot (Figure 2.15). I found that at 2 hours post stimulation the PIR1KO cells had substantially more phospho-IRF3 and phospho-STAT1, when compared to the wild-type cells. This difference was gone, however, by four hours, with both cell lines showing equivalent levels of phospho-IRF3. At 4 hours post stimulation phospho-STAT1 appears to be absent in both cells lines (while total STAT1 is consistently present). It is possible that by 4 hours post

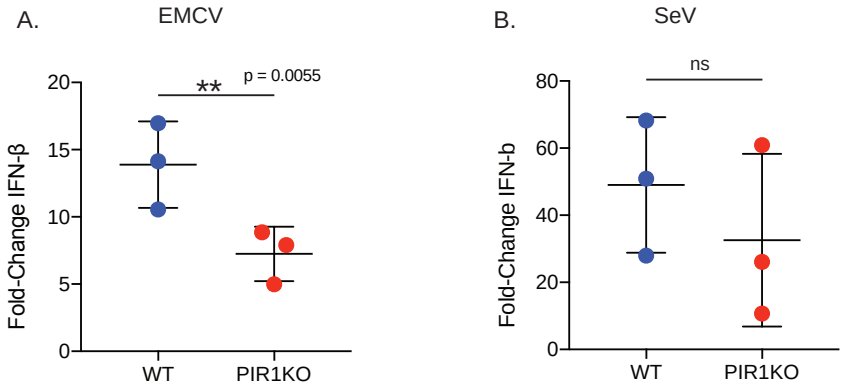

Figure 2.14: IFN-β ELISA on BMDC cell supernatants. The data shown are mean ± SD of duplicate determination of IFN-β from three independent replicates of BMDC differentiation and stimulation. Cells were stimulated for 18 hours, supernatant collection, and measurement of IFN-β by ELISA. EMCV was used at an MOI=10, Sendai Virus was used at 80 HA/mL. Significance was tested using a ratio paired t-test testing wild-type to PIR1KO. ns = not significant.

stimulation STAT1 has become inactivated and dephosphorylated. This is consistent with previous findings that STAT1 inactivation is a fairly rapid process with active, phosphorylated STAT1 being absent from the nucleus by 4 hours in human fibroblasts stimulated with IFN-γ [127].

2.3.5 The effect of PIR1 on small RNA pathways

Since PIR1 plays a prominent role in facilitating the production of antiviral small RNAs in *C. elegans* [94], I sought to investigate whether PIR1 affects small RNA processing or expression.

PIR1KO cells appear to have increased baseline expression of many miRNAs

As PIR1 is known to interact with the dicer molecule Dcr-1 in *C. elegans*, I wanted to see if PIR1 plays any role in global miRNA regulation. Using a miRNA Nanostring codeset, I measured the expression of the annotated miRNAs relative to housekeeping genes. Figure 2.16 shows that in wild-type mice, following stimulation with EMCV, several miRNAs increase in expression level. However, this stimulation-induced increase in miRNA expression is absent in PIR1KO cells. Instead, as can be seen in Figure 2.16-C, at baseline—without any stimulation—the PIR1KO cells have a global upregulation of many miRNAs.

This is an intriguing result, and suggests that PIR1 might be having global regulatory effects on the miRNA expression pathway. PIR1 has been shown to promote the stability of certain non-canonical miRNAs and other small RNAs [96]. It is possible that I observed a similar effect. With a loss of PIR1, as other small RNAs are destabilized, canonical miRNAs, which are detected by the Nanostring-miRNA assay, could be upregulated.

```
<div class="added" remark="add-generation"">
```

It should be noted that this experiment was conducted with not yet full backbred PIR1KO mice (N=6) and littermate wild-type mice as controls. While polymorphisms

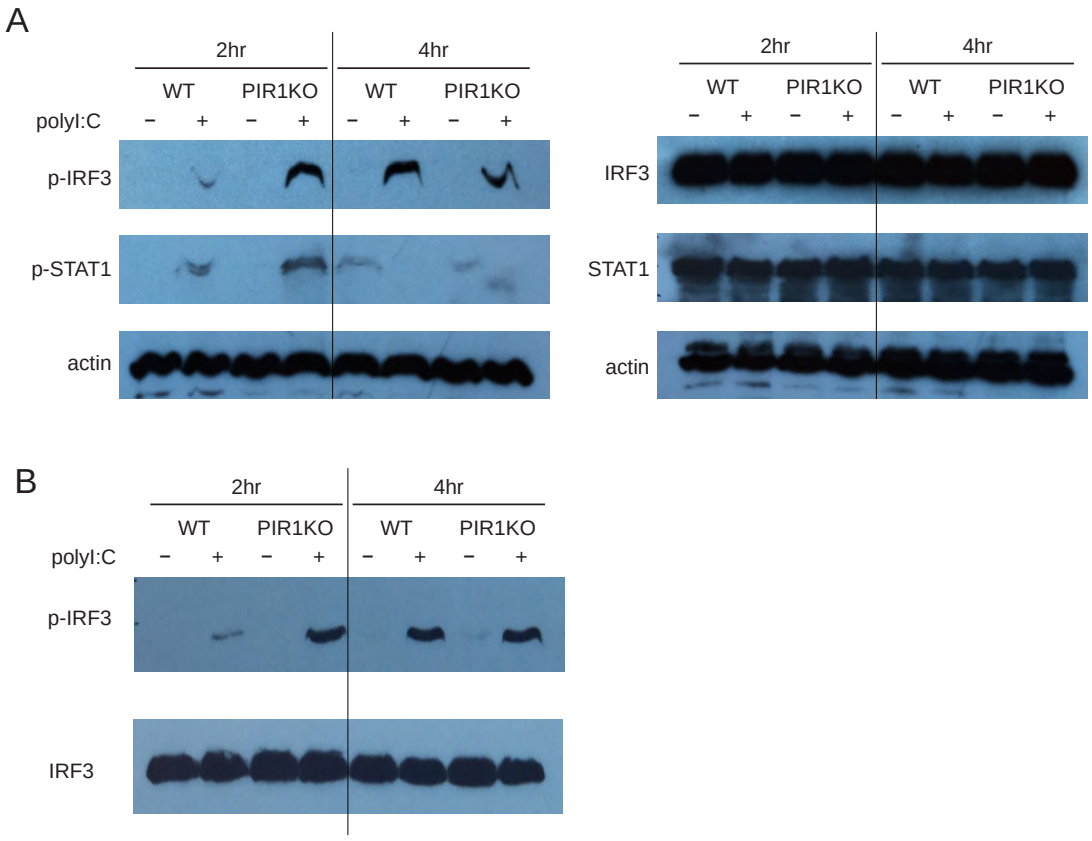

Figure 2.15: PIR1 appears to play a role in the earliest stages of RLR signaling. (A) Whole cell lysates from WT and PIR1KO BMDCs show that PIR1KO BMDCS have greater accumulation of phospho-IRF3 2 hours after transfection with polyIC. However, this difference is gone by 4 hours, as the wild-type and PIR1KO cells appear to have equally high levels if phospho-IRF3 at this time point. Additionally, the PIR1KO cells appear to have increased levels of phosphorylated STAT1 at 2 hours. A difference that once again is absent by 4 hours. (B) Biological replicate, showing decreased IRF3 phosphorylation at 2 hours post transfection with polyIC.

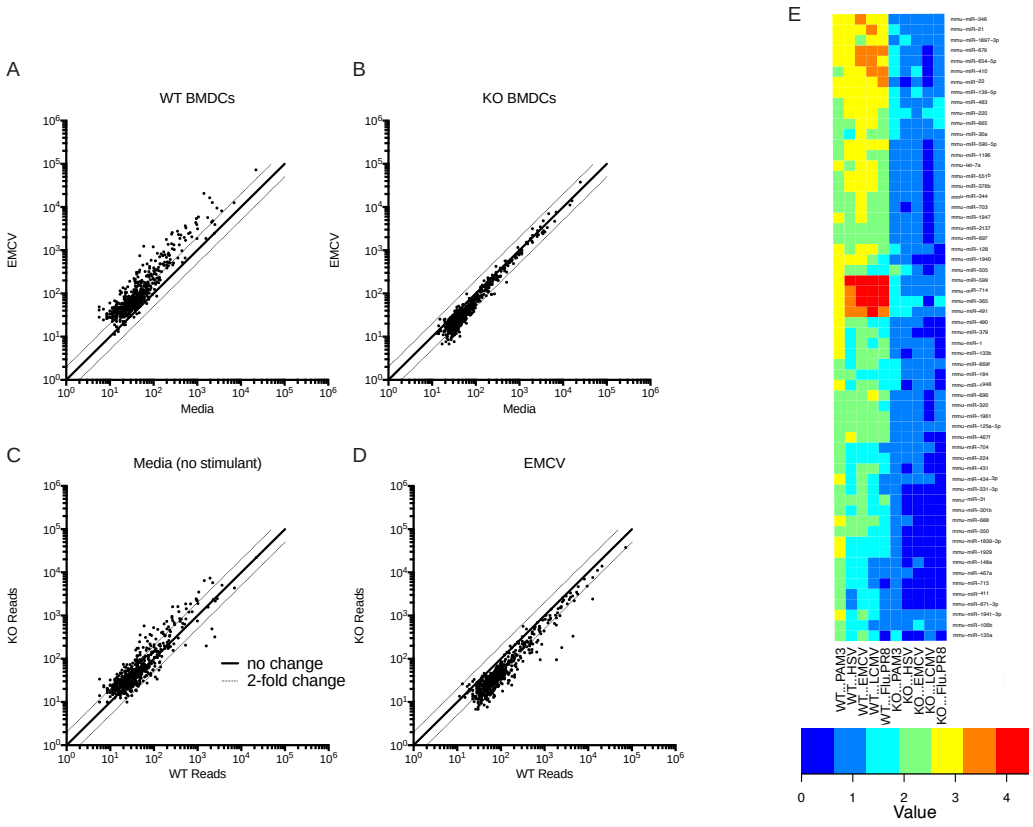

Figure 2.16: PIR1KO-derived BMDCs appear to have higher expression of certain miRNAs in an unstimulated state. This results in a failure to properly upregulate these miRNAs following infection with EMCV. Cells were stimulated for 6 hours with EMCV or media control, and total RNA was assayed via the Nanostring miRNA reporters. (A-D) Dot plots showing the expression level of each miRNA. (A) Wild-type cells before and after infection with EMCV. (B) PIR1KO cells before and after infection with EMCV. (C) A comparison of miRNA expression levels in unstimulated wild-type and PIR1KO cells. (D) A comparison of miRNA expression wild-type and PIR1KO cells following infection with EMCV. (E) A heat map showing the log transformed fold induction of the 50 most differentially induced miRNAs, following stimulation with several stimuli. Mice used in this study were N=6 backbred PIR1KO mice and littermate wild-type controls.

in the genetic background could account for the observed differences here, the findings by Burke et al. [96] point to PIR1 playing a role in the production or stability of certain classes of miRNAs. More rigorous study of a global miRNA effect or PIR1 is needed to better understand if PIR1 is playing such a role and what consequence it might have following stimulation.

2.4 Conclusions

While PIR1 plays a critical, albeit not fully characterized, role in the antiviral small RNA response in *C. elegans*, the role of PIR1 in mice is not nearly as dramatic, at least not in the context of an EMCV infection. However, data presented here hints at a potential role for PIR1 in the earliest steps of RLR signaling, and in early EMCV infection.

2.4.1 Role of PIR1 in RLR signal transduction and/or ligand production

PIR1 appears to have a subtle role in the kinetics of type I IFN signaling at the earliest moments of infection with EMCV or stimulation with polyIC. Generally, following viral infection in an immuno-competent mammalian host, the type I IFN response is considered the dominant antiviral response. While studies looking at the effect of type I IFN genes and the type I IFN receptor (IFNAR) have demonstrated this, the feedforward and self-enhancing nature of the response have made it difficult to evaluate whether other intracellular antiviral mechanisms exist.

I have shown here that PIR1 has tissue-specific effects on the innate immune response to infection with EMCV, with IL6 and IFN cytokine production being altered in the hearts of PIR1KO mice at 24 hours post infection, when compared to wild-type. The effects of the knockout were less pronounced in the brain. Furthermore this effect did not seem to alter the global progression of the infection, with EMCV viral titers and mortality being unaffected by a loss of PIR1.

My *in vitro* studies show that PIR1 antagonizes MDA5:LGP2 ligand recognition in BMDCs stimulated with transfected polyIC, limiting IRF3 phosphorylation and STAT1 phosphorylation 2 hours after stimulation. This phenotype is notable at 2 hours, but is gone by 4 hours, once again suggesting PIR1 is most critical in the early innate immune recognition of viral RNA, but ultimately has minimal consequence upon the downstream manifestations of innate immune signaling. This could be explained by the feed-forward

nature of type I IFN signaling. The stimulation of the RLR:MAVS:IRF3 pathway results in the secretion of IFN-β which can then bind to the IFNAR receptor on the secreting cell to further activate IRF genes. As a result, once this process it set in motion it is difficult to discern how much stimulant was responsible for starting the whole process. Consequently, if PIR1KO cells are delayed by a hour or so in activating RLR:MAVS:IRF3 signaling, it could be possible for these cells to appear equivalently stimulated several hours later.

PIR1 might be antagonizing early dsRNA recognition events by processing RNA molecules to render them non-stimulatory. As a 5' RNA phosphatase, it is possible that the mechanism by which PIR1 antagonizes RLR signaling is via the dephosphorylation of stimulatory RNA rendering it inert. However, this mechanism would need to be minimal or short-lived, since I did not notice any major difference in type I IFN signaling between wild-type and PIR1KO cells. Furthermore, the work by Daniel Chaves in *C. elegans* suggests that PIR1 might be doing more than simply deactivating immunostimulatory RNA. It is possible that PIR1 is processing stimulatory RNAs as part of a small RNA antiviral immune response. In the worm, Chaves showed that PIR1 is required for effective processing of viral RNA molecules into antiviral 22G molecules. In the mammalian system, PIR1 might be promoting a similar processing of viral RNA molecules. When PIR1 is absent, as is the case in the PIR1KO BMDCs in Figure 2.15 (Page 67), this might result in a higher initial concentration of immunostimulatory RNA resulting in a faster initiation of the IFN signaling cascade, resulting in the noticeable surge in phospho-IRFs at 2 hours post stimulation.

The role of PIR1 with respect to its RNA phosphatase activity, and its antiviral role in C. elegans

Recent work by Burke et al. has demonstrated that PIR1 is important for dephosphorylating special subclasses of non-coding RNAs and certain RNA-polymerase-III-derived miRNAs expressed by the host, as well as DNA viruses human adenovirus and bovine leukemia virus [96]. Burke et al. have also shown that, when left phosphorylated, the 5p

arm of these miRNAs are less stable and less efficiently loaded and used by Argonaute complexes.

I hypothesize that PIR1 promotes the small RNA processing of polyIC. Commercially available polyIC exists in a bi-phosphorylated state (there are β and α phosphates present on the 5' of many molecules as a consequence of the synthetic process) [128]. It is possible that the presence of these phosphates promotes PIR1 recognition and the initial processing of polyIC following transfection. However, over time, the amount of polyIC introduced directly into the cytoplasm may overwhelm PIR1 processing in favor of RLR signaling. One can imagine that if this small RNA processing pathway were less efficient in the absence of PIR1—as is the case in the *C. elegans* model—then transfected polyIC would activate RLR signaling more rapidly.

2.4.2 Combining the small RNA and IFN pathway phenotypes: a proposed model

My findings for a limited and transient role for PIR1 in the earliest moments after intracellular stimulation with dsRNA, when combined with Daniel Chaves' findings for the antiviral role of PIR1 in *C. elegans*, along with the growing body evidence that mammalian cells are capable of responding to viral RNA via both a type I IFN and avRNAi response, suggests that PIR1 plays a role promoting the avRNAi response over the RLR:IFN response.

I propose a model where, after an initial infection with a virus, in the earliest moments of replication, a limited pool of immunostimulatory RNA is sorted into one of two competing pathways. This RNA can either be processed by Dicer and directed into an avRNAi pathway, or recognized by MDA5:LGP2 to trigger a type I IFN response. Once the type I IFN response is triggered, any the avRNAi pathway is antagonized by the poly(ADP-ribosylation) of argonaute proteins.

In this model, PIR1 may have the effect of shunting immunostimulatory dsRNA toward the avRNAi pathway, and away from RLR:IFN pathway. During the initial moments of

infection this might slow down the activation of RLR signaling (as seen in Figure 2.15), but would not necessarily increase viral susceptibility since the avRNAi pathway is itself an antiviral pathway.

It should be noted, however, that the functional role of this pathway and PIR1 in the course of a viral infection is likely to be limited. Pathogenic viruses have evolved alongside their hosts for millennia, and as result are capable of subverting antiviral processes, especially when those process are themselves ancient—as the avRNAi pathway is. This combined with the fact that the avRNAi pathway appears to have been superseded by the type I IFN response in mammals, suggests that the global consequence of PIR1 on mammalian viral infections is likely to be limited.

Should the model put forward in Figure 4.1 prove to be correct, PIR1 and the avRNAi pathway it promotes would be an antiviral innate immune response that every RNA virus would encounter immediately after infecting a cell. Furthermore, continued investigation into the interaction between these two antiviral pathways and the role of PIR1 in antagonizing one and promoting the other would allow for a better understanding of how viruses interact with infected cells and their small RNA machinery following infection, furthering our understanding of the intricate interactions between virus and host.

CHAPTER III: CD200R1 supports HSV-1 viral replication and licenses pro-inflammatory signaling functions of TLR2.

The majority of this work has been peer-reviewed and published in the journal *PLOS One* [129]. This chapter discusses the rationale for this work, and presents the results. It also introduces additional pieces of data that were generated after this publication which elucidate further the role of CD200R1 in HSV infections. Both the published data and unpublished data are included, and both are considered in the discussion and conclusions.

In addition to contributing to the design, analysis, and interpretation of the experiments herein, I was assisted in processing experimental samples and carrying out certain assays. Michael King helped perform the plaque assays on samples generated from *in vivo* and *in vitro* experiments. Anna Cerny assisted me in conducting the intracranial infections. Glennice Ryan helped in the stimulation of peritoneal exudate cells and the transduction and stimulation of PECs and BMDMs.

I trained in brain histopathology with Thomas Smith M.D. and developed the novel histological scoring system described in Figure 3.4, processed the tissue samples for histological analysis, and served as the blinded scorer on the histology scoring data presented in part B of Figure 3.5. I also generated the data presented in Figure 3.7, parts A and B of Figure 3.8. I generated the cells and produced the lysates for the western blots in Figure 3.13 and titers in Figure 3.11. I generated the cells, developed the assay, and produced and analyzed the data in Figure 3.15. I assisted in the mouse infections, tissue harvesting, and processing for the samples used in Figures 3.2, 3.6, and 3.5. Finally I assisted in the mouse husbandry of the CD200R1KO mouse used in this work.

[129] Soberman RJ, MacKay CR, Vaine CA, Ryan GB, Cerny AM, Thompson MR, Nikolic B, Primo V, Christmas P, Sheiffele P, Aronov L, Knipe DM, Kurt-Jones EA. CD200R1 supports HSV-1 viral replication and licenses pro-inflammatory signaling functions of TLR2. PloS one. 2012;7(10):e47740. PMCID: PMC3474780 DOI: 10.1371/journal.pone.0047740

3.1 Introduction

3.1.1 Herpes Simplex Encephalitis

Herpes Simplex 1 (HSV-1) is an enveloped, double-stranded DNA virus that is a very common human pathogen worldwide. In developing countries greater than 95% of the population tests positive for HSV-specific antibodies by adulthood [130], with developed countries reaching a seroprevalence of 40% to 60% by 30 years of age [131]. Clinically, HSV-1 infection most often manifests as perioral lesions, known as *herpes labialis*, more colloquially known as cold sores. These lesions are generally self limited, and resolve within a few days to a few weeks. Despite the outward resolution of the cold sore, the HSV-1 infection is not over; the virus will persist in a latent state within the nuclei of sensory neurons of the face, most commonly in the ganglia of the trigeminal nerve (cranial nerve V). As a result of local injury, stimuli, or other stressors [132], HSV-1 can sporadically emerge from its state of latency and begin self-replicating, emerging from the axonal termini of the latently-infected sensory neurons to form new perioral lesions.

However, the cosmetic concerns of these outward lesions are small when compared to a greater and more deadly risk of HSV-1 latency and reactivation. When HSV-1 enters the CNS, it can result in encephalitis, an infection and inflammation of the brain parenchyma associated with acute focal brain deficits [133] and a high fever [134]. Herpes simplex encephalitis (HSE), while rare, is the most common cause of sporadic encephalitis in the United States (10 to 20 percent of the 20,000 viral encephalitis cases annually), and if left untreated has a 70% mortality rate [135]. Because of the wide prevalence of HSV-1, the rapid progression of disease once encephalitis is present, and the high risk of mortality, HSE must always be considered during the treatment of patients presenting with the signs and symptoms of meningitis or encephalitis [134]. PCR testing of CSF samples can rule out HSV-1 infection, but frequently empiric treatment with the antiviral acyclovir is initiated before test results are available [134].

While this antiviral treatment can be effective in limiting the progression and consequences of HSE when initiated early enough in the course of the infection, the mechanisms by which HSV-1 causes its damage are not fully understood. There appears to be a complicated interplay between the pathogenic replication of virus in host neurons and the host antiviral immune response. The CNS typically exists in a highly anti-inflammatory state, but the HSV-1 infection is able to trigger a robust immune response. This inflammation and the subsequent infiltration of immune cells into the otherwise immune-privileged space of the CNS can itself be detrimental, often leading to substantial cell damage and neuron loss. Yet, at the same time, HSV-1—if left unchecked—will damage and kill host neurons via repeated lytic infections. The combination of these two opposing, yet equally damaging mechanisms likely lead to the life-threatening CNS pathology seen in HSE [136].

The HSV Replication Lifecycle

Upon entering a cell, the HSV replication lifecycle begins, as the vhs protein starts to degrade host mRNA molecules [137]. The viral capsid is then transported to the nucleus where gene expression commences. HSV gene expression is triphasic, with each of the three rounds of gene expression relying upon the previous. First α genes are expressed, which lead to the expression of β genes, which then turn on γ genes. The expression of γ genes, many of which encode for virion structural proteins, leads to virion assembly and viral egress [132].

The lifecycle depicted in Figure 3.1 only describes the lytic lifecycle of HSV-1. Under certain circumstances, instead of initiating a lytic infection, the virus will enter into a latent infection (reviewed in [138]). During a latent infection, the viral DNA associates with nucleosomes and forms a circular episome within the nucleus of the infected cell [139,140]. During this time, viral protein expression in repressed, while several noncoding latency-associated transcripts (LATs) are produced [141].

At some point, by a mechanism that is not well understood, HSV can transition from a latent infection into a lytic infection, produce virions, and egress. Usually this will manifest

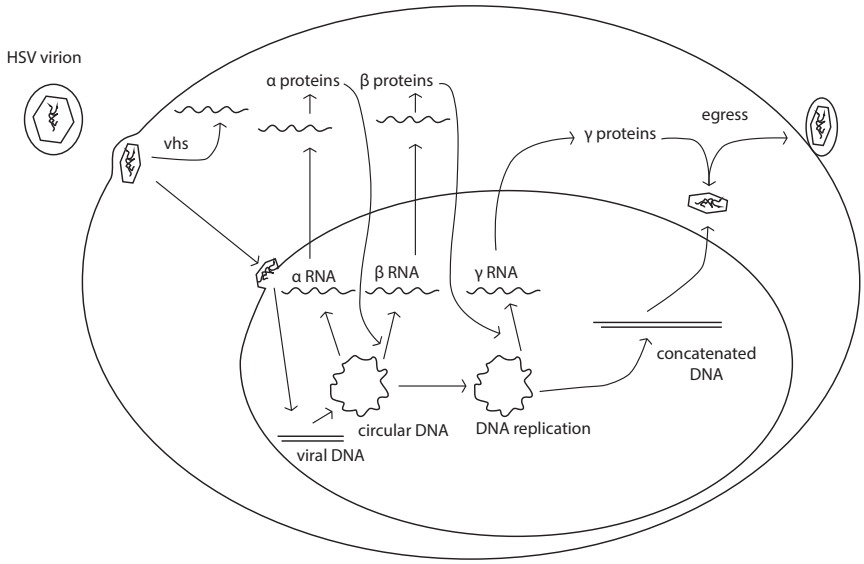

Figure 3.1: A schematic representation of the HSV replication cycle during a lytic infection. Upon entering a cell, the HSV vhs protein will begin inhibiting a number of host processes. The viral capsid will then be transported to the nucleus where gene expression begins. While simplified, HSV gene expression can be considered triphasic, with each of the three rounds of gene expression relying upon the previous. First α genes are expressed, which in turn turn on β genes, which ultimately turn on γ genes. The expression of γ genes, which encode for many structural proteins, then leads to virion assembly and viral egress. Adapted from Field's Virology [132].

as new cold sore lesions, as virions travels via anterograde transport along the axon of sensory neurons to emerge in the skin, leading to a localized infection and inflammatory reaction. However, it could manifest as a life-threatening encephalitis.

There are three potential opportunities for HSV-1 to enter the central nervous system (CNS). First, during a primary infection, the virus is able to travel via retrograde transport into the CNS via sensory neurons in the trigeminal nerve, from the skin around the mouth, or in the olfactory nerve, from the nasal mucosa. Second, during recurrent outbreaks, as latent virus is reactivated and replicating, the virus again has the opportunity to move via retrograde transport into the CNS. Finally, around one–third of cases of HSE are seen in patients without a known primary or recurrent infection, suggesting that the virus was latent, and was able to reactivate and spread inward either from a latently infected peripheral ganglion or previously infected CNS neurons [134].

HSV and the Innate Immune System

In the case of latent HSV-1, we know there are interactions with the host's adaptive immune system, as both HSV-1 specific T-cells and antibodies can be detected following an initial infection. This adaptive immune response appears to be important for controlling recurrent infections and maintaining latency [142,143]. However, we also know that HSV interacts extensively with the innate immune system, including during CNS infection, and it is this interaction that our laboratory has studied.

HSV-1 virions first interact with host cells at their cell membrane, where virions bind to cell surface receptors to initiate entry into the cell. However, glycoproteins present on the viral envelope (gH/gL and gB), can also be recognized by the pattern recognition receptor TLR2 [8]. This interaction may also involve an association with the αvβ3 integrin [9–11]. HSV-1 recognition by TLR2 then leads to the activation of NF-κB, in a MyD88-dependent manner [144], and a strong inflammatory response. This TLR2-driven response is problematic within the CNS in the case of HSE [145]. In fact, TLR2-/- mice exhibit

improved survival as compared to wild-type mice following HSV infection, likely due to decreased levels of intracranial inflammation [145].

Within the endosome, TLR3 can recognize and respond to dsRNA produced during the HSV infection to induce inflammatory and antiviral responses. Double-stranded RNA has been found in HSV-1 infected cells [146], and specifically within the CNS, TLR3 is activated by HSV-1 infection, triggering an important defense against encephalitis [147,148]. Yet, how HSV-1 induces this TLR3 activation is unclear, as we do not know how the stimulatory dsRNA ends up within the endosome to engage TLR3.

TLR9 is also activated during an HSV-1 infection, as it recognizes and responds to dsDNA [149], within the endosome. HSV-1 activation of TLR9 appears to be cell-type specific, with plasmacytoid dendritic cells responding to HSV-1 DNA [150]. TLR9-/- mice are still able to control infection, and other cell types such as macrophages and conventional dendritic cells are still able to produce type I IFN in response to HSV-1, suggesting that TLR9 signaling might be redundant to other defense pathways in these cells [151].

Within the cytoplasm, several pattern recognition receptors are activated by viral DNA, to stimulate innate immune processes. The DNA sensor DAI was found to recognize HSV-1 DNA and inhibit infection [152–154]. HSV-1 DNA has also been found to activate RIG-I signaling via RNApolIII transcription of DNA into triphosphorylated RNA [155]. Viral DNA in the nucleus or cytoplasm can activate the DNA-binding protein IFI16, which leads to the activation of the type 1 IFN signaling and ASC inflammasome activation [156]. HSV-1 DNA has also been shown to activate cGAS, leading to the production of the second messenger cGAMP and type I IFN activation via STING [157].

Despite these varied methods for host sensing of the virus, HSV-1 has evolved many mechanisms to antagonize these processes (well reviewed by Su el al. [158]). The HSV protein ICP0 is a well-studied virulence factor responsible for negatively regulating many antiviral responses within an infected cell. ICP0 inhibits MyD88 signaling following TLR2 activation [159], inhibits NF-$\varkappa$B translocation to the nucleus [159], interferes with DNA

recognition by inhibiting the signal mediator STING [160], and interferes with the the ability of IFI16 to induce a response to viral DNA [161].

Other HSV-1 viral factors interfere with innate immune signaling by directly modifying or interacting with host defense proteins, reducing their ability to mount a response. U_L36 deubiquitinates TRAF6, inhibiting the activation of TBK1 and ultimately blocking type I IFN stimulation [161]. U_S11 interferes with formation of RIG-I and and MDA5 signaling complexes, limiting the ability of infected cells to respond to foreign RNA [162]. U_S3 down-regulates TLR3 expression, while also inhibiting the polyubiquitination of TLR2, leading to deceased signaling capacity for both of these TLR pathways [163,164]. U_S3 has also been found to hyperphosphorylate IRF3 and the p65 component of NF-$\varkappa$B, preventing both from properly activating and translocating to the nucleus to activate the expression of type 1 IFN genes [165,166]. ICP34.5 appears to bind and sequester the kinase TBK1, thus preventing it from activating IRF3 and inducing a type I IFN response [167,168]. Viral tegument protein VP16 blocks IRF3-mediated gene activation, preventing IRF3 from interacting with its coactivator CREP-binding protein [169]. U_L41 (aka vhs) actively degrades many host mRNA transcripts including those that encode for the antiviral proteins vipirin [170], ZAP [171], and tetherin [172].

In the immune-privileged environment of the CNS, HSV-1 infection can evade some innate defenses to progress quite rapidly, but such an infection will trigger a significant host inflammatory response. It is thought that the clinicopathologic features of HSE are a result of these combined damaging effects. As mentioned previously, the current standard of treatment for HSE is antiviral therapy with acyclovir alone, which is effective in reducing both the morbidity and mortality of the infection [173]. However, co-therapy with an anti-inflammatory agent in addition to acyclovir has been shown in small cohort and case studies to improve treatment outcomes [174,175]. Current studies are underway investigating whether steroidal anti-inflammatory agents are useful in treating HSE inflammation. Yet, more specific treatment options will only come with a better understanding of the

factors that drive the balance toward inflammatory and/or antiviral processes during HSE.

Mouse models of Herpes Simplex Encephalitis

Since HSV is able to latently infect a host, and infection of the CNS typically follows reactivation at some undefined time point, studying the natural course of HSE is difficult. However, several mouse models exist that attempt to approximate a natural HSE infection, such as the intranasal administration of virus [176], or direct inoculation via corneal scarring [177], and dental pulp injection [178]. Each of these models approximate the PNS to CNS course of HSE, but each has their own limitations and confounders. Most importantly, peripheral inoculation of HSV at the mucosa, such that there is a natural progression of HSV from the PNS into the CNS, affords the adaptive immune response ample opportunity to develop a CD4 and CD8 T-cell response, complicating any study of the direct innate immune response within the brain.

Therefore, in order to study the innate immune response of the CNS to HSV-1 in isolation, without this added complexity of an adaptive immune response, the Kurt-Jones lab established a model of HSE that involves the direct inoculation of HSV-1 into the CNS, via an intracranial injection at the lambda point on the back of the mouse skull. HSV-1 virions are delivered intrathecally, allowing for immediate primary infection of the cells within the CNS and the induction of an inflammatory response [179].

3.1.2 CD200:CD200R Signaling

Due to the tight junctions that constitute the blood-brain barrier, monocytes and lymphocytes very rarely enter the central nervous system. Yet, during infection significant inflammation does occur, with chemokines and chemoattractants recruiting neutrophils, macrophages, and other effector cells through the blood-brain barrier to the site of infection. However, it is not just this barrier to entry that renders the CNS immune-privileged. Upon entering the CNS, immune cells encounter various anti-inflammatory signals, which

reduce or limit their inflammatory response.

A significant component of this anti-inflammatory signaling milieu is the CD200 signaling pathway. CD200 is a cell-surface protein that is expressed on neurons, astrocytes, and other glial cells within the CNS [180]. It has been shown to be an important mediator of microglial and macrophage inactivity within the CNS, helping to prevent spurious activation of these cells that might lead to neuronal loss [24]. However, CD200 is not itself anti-inflammatory, but instead functions as a ligand for the anti-inflammatory CD200 Receptor 1 (CD200R1) [181]. CD200R1, also a cell-surface protein, is expressed on many different myeloid-derived cells including macrophages and neutrophils, but especially microglia within the CNS. Upon engagement with its ligand, CD200R activates an intracellular signaling pathway that ultimately limits the inflammatory capacity of myeloid-derived immune cells.

CD200R1, the most well-studied receptor for CD200, has a cytoplasmic tail responsible for signaling after the binding of the receptor with its ligand CD200. Upon binding CD200 on the cell surface, the cytoplasmic tail of CD200R1 on myeloid-derived cells undergoes tyrosine phosphorylation, leading to the recruitment of the signal mediators Dok1, Dok2, and SHP-1 [19,20]. Phosphorylation of Dok1 and/or Dok2 and the activation of SHP-1 subsequently activates RasGAP [21]. RasGAP then antagonize inflammatory processing by several mechanisms. In macrophages it has been shown that RasGAP negatively regulated ERK signaling, leading to a reduction in TNFα and NO production following TLR stimulation [22]. RasGAP has also been shown to interfere with the activation and translocation of NF-ϰB to the nucleus [23].

CD200:CD200R1 Signaling in CNS Infections

The majority of the evidence supporting CD200R1 as a negative regulator of inflammation derives from the findings that CD200-/- or CD200R1-/- mice have worsened inflammation compared to wild-type in several mouse models of inflammatory diseases. For example,

models of autoimmune arthritis and autoimmune encephalitis are both worsened in CD200-/- mice compared to wild-type [24]. Similarly, the pathologic inflammation of Dextran Sodium Sulfate Induced Colitis is exacerbated when CD200 or CD200R1 are knocked out [25]. Conversely, in one study of allograft survival in transplanted mice, the upregulation of CD200 was protective, showing increased rates of tissue survival [182].

In the context of an infection, the effect of an the anti-inflammatory pathway driven by CD200:CD200R1 signaling is pathogen and disease specific. For example, following infection with influenza (IAV), CD200-/- mice have increased levels of inflammation and infiltration within their lungs, resulting in a more severe illness [183]. A similar result in seen in CD200-/- mice infected with meningococcus, with CD200 signaling being required to limit inflammation following *N. meningitidis* septicemia [27]. In a mouse model of *Toxoplasma* encephalitis, CD200-/- mice again have a worsened disease progression due to unregulated inflammation within the CNS [28]. However, by contrast in the case of *L. amazonensis*, CD200-/- mice have improved disease outcomes and are better able to combat the infection, due to a stronger oxidative response against this typically indolent pathogen [26].

CD200R1$^{-/-}$ mice are protected from HSV-1 encephalitis

In our direct inoculation model of HSE, HSV in the CNS induces a strong inflammatory response, contributing to the observed mortality of infected mice [179]. For this reason we sought to investigate the role of CD200R1 anti-inflammatory signaling in HSE. The first experiment conducted was a survival study, where wild-type and CD200R1-/- mice were infected via intracranial injection with 1×10^5 pfu of HSV-1. The results of this experiment (Figure 3.2) showed that CD200R1-/- mice had a significantly higher rate of survival when compared to wild-type mice. Wild-type mice began dying as early as 3 days post infection and continued to die until day 9, at which point approximately 25% of the mice survived the duration of the study. The CD200R1-/- mice, however, were much more resistant to the disease process, with only approximately 25% of the mice dying around day 5 or 6, and

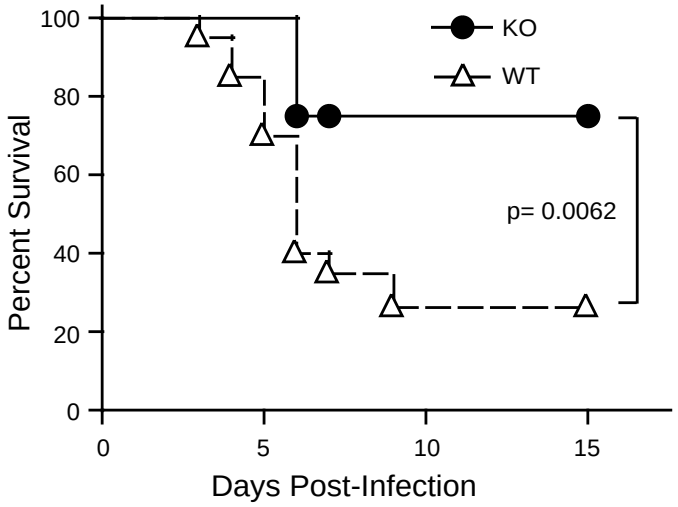

Figure 3.2: CD200R1$^{-/-}$ mice are protected from HSV-1 encephalitis. CD200R1$^{+/+}$ (WT) and CD200R1$^{-/-}$ (KO) mice were administered 1×10^5 pfu HSV-1 by intracranial injection. Survival was monitored for 15 days. Data includes a total of 3 separate experiments (n=20, WT; n=16, KO). An unpaired, two-tailed Student's t-test was used to determine statistical significance.

75% surviving the duration of the experiment.

Knowing a significant portion of the lethal damage to the CNS during HSE derives from the inflammatory response, and understanding CD200R signaling as an important anti-inflammatory pathway within the CNS, I hypothesized that CD200R1-/- mice have reduced levels of inflammation in brain leading to a less severe disease, and ultimately greater survival. Surprisingly, however, my investigation revealed instead that CD200R1-/- mice have less death following infection because of a reduced capacity of HSV-1 to replicate within the CNS in CD200R1-/- mice. Here, I will present my work demonstrating that CD200R1 is an important host factor that promotes HSV-1 replication.

3.2 Methods

3.2.1 *In vivo* intracranial infection

Virus was diluted to the appropriate concentration in sterile saline. 6 to 8 week old mice were anesthetized with isoflurane, and the head was sprayed with isopropanol. Using surface landmarks, a 30G needle was inserted into the lambda point (intersection of the lambdoid suture and the sagittal suture). A spacer was placed on the syringe to assure that the needle was inserted only about 5 mm deep into the skull. The spacer allowed for consistent intrathecal injection in pilot studies using dextran blue as a marker. For each inoculation 20 μL of solution was injected.

3.2.2 Immunohistochemistry staining for HSV

Whole brains were extracted from euthanized mice by dissection. The entire brain was then either processed whole or bisected along the sagittal plan and then processed. Brains were then placed in cassettes and submerged in Bouin's fixative (5% acetic acid, 9% formaldehyde, and 0.9% picric acid 0.9) for 18 hours. Brains were then transferred to 1× PBS pH 7.4, and then delivered to the DERC facility (University of Massachusetts Medical School, University Campus) for cutting, paraffin embedding, microtome slicing, and placement on glass slides. Before being embedded in paraffin, the brains were cut along a coronal plane into 5 segments, and oriented so that each slice of the parrafin block contained a section from each segment.

The paraffin sections were then either stained in the traditional manner with hematoxylin and eosin, or processed further for immunohistochemistry.

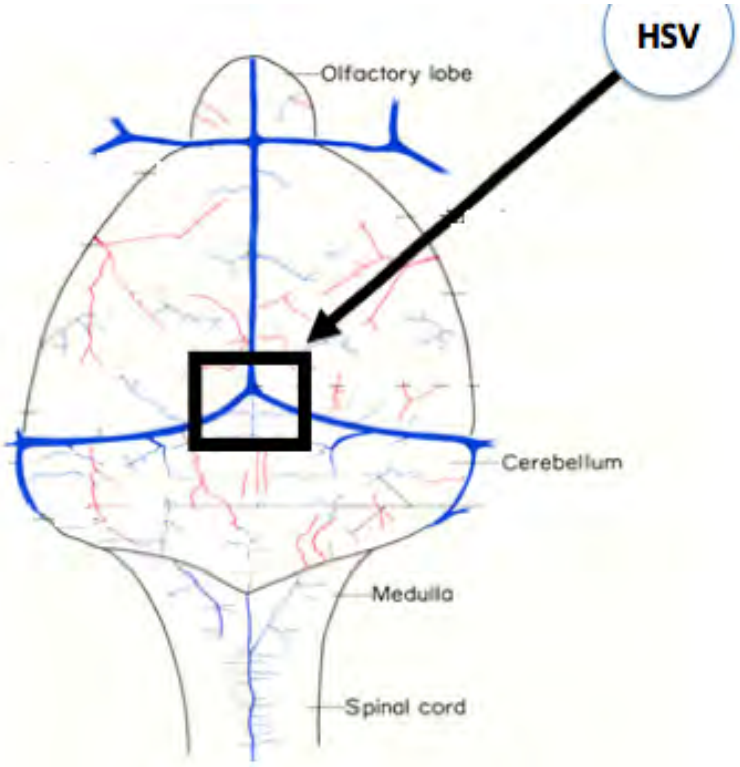

Figure 3.3: Intracranial infection method. A schematic of the location of infection, including surface landmarks used. Using a 30G needle, 20 μL of diluted virus was infected at the lambda point, where the sagittal suture and lambdoid suture meet.

3.2.3 Culturing Mouse Embryonic Fibroblast

Isolation of Mouse Embryonic Fibroblasts

Pregnant mice were euthanized at 14 to 16 days postcoital using CO_2 or isoflurane followed by cervical dislocation. The uterus was dissected out and placed into a 100 mm tissue-grade dish filled with sterile PBS on ice for 5 minutes. Each embryo was separated from its placenta and surrounding membranes. For each embryo, the head was separated for genotyping, and the internal organs were removed to avoid non-fibroblast contamination. The embryos were then moved to a second 100 mm dish and swirled to remove small loose pieces of debris and as much blood as possible. The embryos were then transferred to a 15 mL conical tube containing 5 mL of 0.25% trypsin (GIBCO, contains EDTA), and incubated at 4°C overnight to allow diffusion of trypsin into the embryo.

After overnight incubation the tubes were incubated at 37°C to activate the trypsin. After 15 minutes, the excess trypsin was poured off, and 4 mL DMEM/FCS (DMEM with 10% Hyclone FCS, 1% L-glutamine, 1% Pen-Strep) were added. The embryos were then dispersed by pipetting up and down using a large-bore pipette, until only small clumps remained. Any debris and connective tissue was allowed to settle out of solution.

The cell suspension for each embryo was then plated into a 100 mm dish—with this plating being referred to as passage zero—and an additional 4 mL of complete DMEM was added. Cells were then incubated overnight at 37°C and 10% CO_2 to allow cells to adhere. The next day, the media was changed and the cells were split if confluent.

Splitting MEFs Whenever the cells were confluent, they were promptly split. To split MEFs for passage 1, the growth media was removed from the monolayer, and the monolayer was then washed twice with PBS, ensuring that any remaining clumps and debris from MEF isolation were also washed away. After washing, 2 mL of trypsin were added to each plate and incubated for at 37°C in a 10% CO_2 incubator. After 5 minutes, the trypsin was neutralizes with an equivalent amount of DMEM medium supplemented with 10% FCS

(DMEM complete), and the cells were dislodged by pipetting. The cell suspension was then transferred to a conical tube and centrifuged for 4 min at 300×g. The cells pellet was resuspended in fresh DMEM complete and plated at a 1:4 or 1:5 ratio into a new dish with 8 ml of DMEM complete. This is equivalent to splitting the cells at an approximate density of 1×10^4 cells/cm^2 every 3 days.

Freezing MEFs At each passage, aliquots of MEFs were cryogenically preserved. After collecting cells and pelleting, cells to be frozen were resuspended in 1 mL of freezing medium (90% HyClone FCS, 10% DMSO (v/v)) and transferred into a cryovial. Cells were placed in an insulating container and stored at -80°C for 2 weeks, at which point they were transferred to liquid nitrogen.

Thawing MEFs To thaw MEFs previously stored in liquid nitrogen, the cryovial was removed from refrigeration and placed directly into a 37°C water bath. While swirling the tube continuously, the cell suspension was allowed to melt half way (meaning half the volume of the vial was liquid and half was still frozen solid). At this point the vial was removed from the water bath, and 1 mL of DMEM/10% FCS was added to the cryovial and mixed well by pipetting to finishing thawing the cells. The cells suspension was then transferred to a 25 cm^2 tissue-culture flask along with 5 mL of additional DMEM complete and incubated at 37°C with 10%CO_2.

If cells did not appear to grow well the next day following thawing, half the media was discarded and replaced with DMEM supplemented with the following: 15% FCS, 1% of nonessential amino acid, 1% HEPES buffer, 1% sodium pyruvate.

3.2.4 Infection with GFP-expressing viruses, and measurement of infection by flow-cytometry

Cells were plated in a 24-well plate at a concentration of 1×10^5 cells/well, and incubated for 4 hours at 37°C. The growth media was then removed and replaced with serum-free media. The cells were inoculated with GFP-expressing HSV at the specified MOI. The

virus was allowed to adsorb for 1 hour at 37°C with intermittent swirling. After the hour, the media and virus were removed, the cells were washed once with sterile PBS, and then incubated with 500 µL of DMEM complete supplemented with 165 µg/mL of pooled human IgG (Sigma; https://sigmaalrich.com; cat: I2511) to neutralize extracellular virions.

At the specified time point post infection the cells were collected for flow-cytometric analysis of GFP expression as a measure of virus replication. The growth media was removed, and 200 µL of trypsin 0.25% was added to each well. After incubation at 37°C for 3 minutes the cells were lifted out of each well by pipette and placed into a microcentrifuge tube. The cells were pelleted by centrifuge for 5 minutes at 300×g and 4°C, and the cell pellet was washed once with sterile PBS. The cells were pelleted a final time, and resuspended in 100 µL of sterile PBS. Once resuspended, 100 µL of 8% formalin in PBS was added to each samples. Cells were then stored in the dark at 4°C until they could be analyzed by flow cytometry.

3.2.5 Analysis of HSV protein expression by western blot

Cells were infected with HSV-1 for 24 hours, at which point the cells were washed and lysed with 1× Laemmli Sample Buffer (BioRad; biorad.com; cat: 161-0737). Once lysed samples were stored at -20°C until thy could be processed. Samples were heated to 95°C for 5 minutes, the loaded in a SDS-PAGE gel. The gel was run at 90 V until the loading dye reached near the bottom of the gel. The running buffer was: 3 g Tris-Base, 14.4 g glycine, and 1.0 g SDS in 1.0 L of ddH_2O.

After the gel was done running, proteins were transferred onto a membrane for immunoblotting. A transfer sandwich of blotting pad, blotting paper, membrane, blotting paper, and blotting pad was prepared. All but the membrane was submerged in transfer buffer, while the membrane was submerged in 100% methanol. The polyacrylamide gel was then place on top of the membrane at the center of the sandwich, and all bubbles were removed from between each layer. The transfer was then run on a semi-dry transfer machine

at 25 V (maximum of 300 mA) for 45 to 60 minutes. The transfer buffer consisted of: 3 g Tris-Base, 14.4 g glycine, and 100 mL of 100% methanol in 1.0 L with ddH2O

After transfer, the membrane was blocked with 3% (w/v) bovine serum albumin in TBS with 0.1% Tween 20 (TBS-T) overnight at 4°C. Blocking buffer was removed, and primary antibody diluted in blocking buffer was added. Membranes were incubated with primary antibodies overnight at 4°C. Membranes were then rinsed three times with TBS-T, and then incubated with secondary antibody diluted in blocking buffer for 2 hours at room temperature. Primary antibodies were used at a dilution of 1:2000. The primary antibodies were all purchased from Abcam (abcam.com): ICP4 cat: ab6514, ICP8 cat: ab20194, ICP27 cat: ab31631, VP16 cat: ab110226.

3.2.6 Antibodies

Anti-CD200R1 and anti-CD200 for cell surface staining were purchased from AbD Serotec. Goat anti-CD200R1 intracellular domain-specific antibody was from Santa Cruz. Anti-IL-1β was goat polyclonal anti–mouse IL-1β (AF-401-NA; R&D Systems). The primary antibody used in immunohistochemical studies was rabbit polyclonal anti-HSV2 (B0116; Dako) and the secondary antibody used was biotin-conjugated goat anti-rabbit (H+L) IgG (656140; Invitrogen). The secondary anti-rabbit antibody used in blotting studies was rabbit anti-goat (H+L) IgG HRP conjugate (172–1034; Bio-Rad).

3.2.7 PCR Primers and Screening for CD200R1 Gene Targeting

CD200R1-/- mice used had been backcrossed to generation N9 or N10 on the C57BL/6 background. To identify the knockout allele in genomic DNA, tail vein DNA was purified using the DNeasy kit (Qiagen). PCR was then performed using the forward primer Neo1, located in the 5'-promoter region of the neo gene cassette (5'-`TGCGAGGCCAGGCCACTTGTGTAGC`-3') combined with the reverse primer CD200R1-rev, located outside the short arm of the knockout construct (5'-`GGGATGCAGAACATAGGAGGCAG`-3') corresponding to a sequence within

the first third of intron 1 of the CD200R1 gene. The PCR product yields a 1.5 kbp product. To identify the wild-type allele primer WT1 (5'-CAGTAGTTTTGGAGAATGTGACAG-3') was combined with WT-rev (5'-GATAGCCCTTGCTCCTATGACTGAG-3') to yield a 1.4 kbp product corresponding to a region of intron 1 that is present in WT DNA but is deleted by insertion of the targeting construct. The PCR conditions for both sets of primers were: (95°C, 15 min; 94°C, 30 sec; 62°C, 1 min; 72°C 2 min; 35 cycles using Thermo Start ReddyMix PCR master mix (Thermo Scientific).

3.2.8 Exon-Specific screening.

The following forward and reverse primers were combined to probe the expression of CD200R1 exons in peritoneal macrophages: exon 1F (5'-ATGTTTTGCTTTTGGAGAACT-3') and exon 7R (5'-CTAGATTCCAATGGCCGACAA-3') to amplify the full length cDNA; exon 1F (above) and exon 5R (5'-CACCTCTACTCAGTTCTATGG-3') to amplify exons 1–5; exon 5F (5'-TGAAGTAACCTACTTTCCAGA-3') and exon 7R (above) to amplify exons 5–7. RNA was prepared using RNeasy (Qiagen) and RT-PCR was performed using 1 unit Taq polymerase, and Q solution (Qiagen). The PCR conditions for all pairs of primers were: (94°C, 20 sec; 62°C, 20 sec; 72°C 2 min; 35 cycles).

3.2.9 Preparation and Stimulation of Peritoneal Macrophages

Mice were injected with 4% thioglycollate and peritoneal exudate cells were routinely harvested 3–4 days later [6]. Peritoneal exudate cells (> 90% macrophages) were plated at 1×10^6 cells per well in 24-well plates in DMEM containing 10% FCS. Lipopolysaccharide (LPS) was obtained from Sigma and phenol extracted as previously described [184]. Pam2CSK4 was obtained from EMC Microcollections (Tubingen, Germany).

3.2.10 Immunohistochemistry and Viral Particle Detection

For immunohistochemistry, fixed brain sections from CD200R1$^{+/+}$ and CD200R1$^{-/-}$ mice were deparaffinized by rinsing three times in xylene for 5 minutes each, and then for 5 minutes each in 100% ethanol, 90% ethanol, and 70% ethanol. The slides were then gently rinsed with tap water.

To permeabilize the sections the slides were submerged in 0.2% Triton X 100 in PBS at room temperature for 10 minutes. Antigen retrieval was carried out using a pH 5.7 sodium citrate solution. The retrieval solution was pre-heated to just below boiling, and then slides were added. The slides in retrieval solution were then heated by microwaving for 50% power for 5 minutes, and allowed to cool to room temperature on the bench top.

Slides were then blocked. To block endogenous peroxidase activity slides were incubated in 2% H_2O_2 93.3% methanol in H_2O for 20 minutes at room temperature. Slides were then washed twice with PBST, and then blocked 90 µL of avidin blocking per slide (Vector; https://vectorlabs.com/; cat: SP-2001). A paraffin film coverslip was added to each slide and they were then incubated in a humid container at room temperature for 15 minutes. Slides were once again washed twice with PBST. 90 µL of biotin blocking solution was then added to each slide, followed by a paraffin film cover slip, and 15 minutes of incubation in a humid container at room temperature. Slides were washed twice again with PBST, and then blocked with blocking solution solution (1% dehydrated milk, 1% BSA, and 5% goat serum in PBST). 80 µL of this serum blocking solution was added to each slide, followed by a paraffin film coverslip, and a 1 hour incubation in a humid container at room temperature.

After blocking, slides were washed twice with PBST, and incubated with primary antibody diluted 1:100 in the blocking solution without serum. Antibody was added to each slide, followed by a paraffin film coverslip. The slides were then incubated in a humid container at 4C overnight. At this point, the slides were washed twice with PBST, and then stained with secondary antibody. The secondary antibody was diluted 1:100 and added

to the slides in the same manner as the primary antibody. The slides were then incubated in a humid container at 4C for 1 hour. The slides were washed twice with PBST, and then incubated with avidin-biotin complexes (Vector; https://vectorlabs.com; cat: PK-4005). Complexes were formed by mixing avidin-DH with biotinylated-HRP in PBST at a ratio of 1:1:50 and incubating them for 30 minutes at room temperature. 100 μL of this avidin:biotin-HRP complex was added to each slide and allowed to sit for 30 minutes at room temperature.

The slides were washed twice with PBST, and developed with 3,3'-diaminobenzidine (DAB Vector; https://vectorlabs.com; cat: SK-4100). DAB developing solution was added drop-wise to each slide, which were then allowed to react for 2 to 10 minutes, until staining was clearly visible in positive control samples. At this point the reaction was stopped by rinsing the slides with tap water. Slides were then counterstained by submerging in hematoxylin for 45 seconds. Slides were then rinsed thoroughly with tap water. Slides were then dipped 4 times in a blueing solution, and then washed again with tap water. The slides were dehydrated by reversing the rehydration procedure from above. Finally slides were mounted using Permount (Fisher; https://fishersci.com; cat: SP15-100) and a glass coverslip.

3.2.11 Histological Scoring of Brains

48 hours post-infection, mice were anesthetized with isoflurane and euthanized by exsanguination. Brains were dissected and stored in Bouin's Fixative Formula (Fisher Scientific, Pittsburgh, PA) for 24 h. Each brain was cut into 4 coronal sections, paraffin embedded, sectioned, mounted and stained with hematoxylin and eosin (H&E) by the histology core at University of Massachusetts Medical School, Worcester, MA. To quantify the severity and the extent of pathologic inflammation in the brains of HSV-1 infected mice, a histologic inflammation scoring system was used. Each of seven regions of the brain was assigned an inflammation score of 0 (no apparent inflammation), 1 (minimal inflammation), or 2 (moder-

ate to severe inflammation). Inflammation was judged on the presence and extent of cellular infiltrate and reactive gliosis. The regions of the brain that were scored were: frontal cerebral cortex, posterior cerebral cortex, hippocampus, diencephalon/mesencephalon (which includes the thalamus, hypothalamus and brainstem), cerebellum, the caudal paraventricular structures (defined as those areas adjacent to the lateral ventricles), and the rostral paraventricular structures (defined as those areas adjacent to the 3rd ventricle, the cerebral aqueduct, and the 4th ventricle). Each brain was scored blindly by two observers. The scores for each of the seven regions were summed to arrive at a total brain inflammation score for each mouse with a maximum possible score of 14.

3.2.12 Preparation of Viruses

HSV-1 strains including viruses expressing ICP8-GFP [185] were generated in the laboratory of Dr. David Knipe. Viruses were added to MEFs and peritoneal macrophages at an MOI of 10.

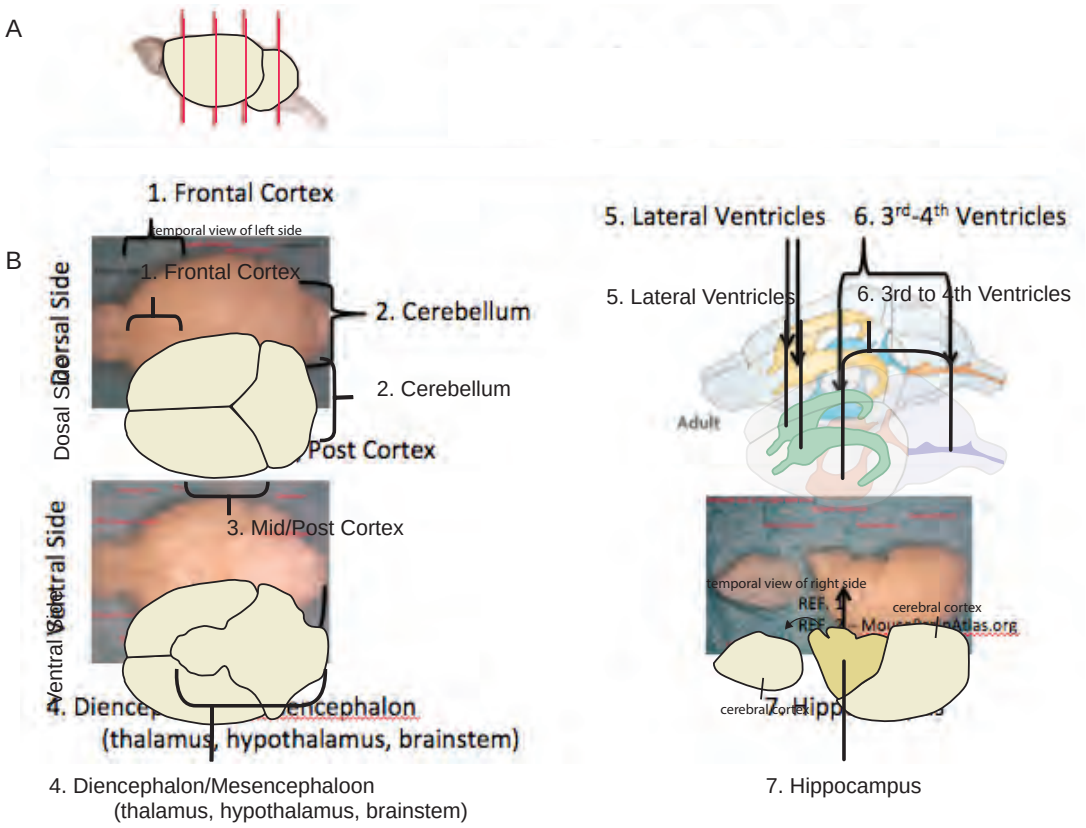

Figure 3.4: Histology scoring system to measure extent and degree of inflammation in the brain. In order to evaluate the extent and severity of inflammation within the brain following *intrathecal* inoculation with HSV-1, I developed a novel histology scoring system. I identified seven regions of the brain that are well dispersed throughout the superficial and deep regions of the brain, and are themselves well removed from the initial site of inoculation (labelled 1 to 7). Each region was examined on H&E stained sections, and the level of inflammation was blindly rated on 3-point scale: 0 is no noticeable inflammation, 1 is mild or minimal inflammation, and 2 is any amount of inflammation above minimal (i.e. moderate to severe). These scores were then added together to get a score that ranges from 0 to 14.

3.3 Results and Discussion

3.3.1 CD200R1 -/- mice show similar levels of inflammation early in infection

In order to assess levels of inflammation following infection with HSV-1 via intracranial injection, brains were collected from infected CD200R1-/- and wild-type mice. These brains were first assessed by H&E staining for histopathological signs of inflammation. Both wild-type and CD200R1-/- mice showed viral inclusions, gliosis, and perivascular infiltration and inflammation following infection with HSV-1. In order to quantify the degree and extent of inflammation, I developed a histopathological scoring system that assessed inflammation on a scale of 0 (no inflammation), 1 (minimal inflammation), or 2 (moderate to severe inflammation). Using this scoring system, 7 different superficial and deep regions of the brain were analyzed. As seen in Figure 3.5, the amount and extent of inflammation in the brain at 3 days post infection, were not noticeably different.

While histological analysis of brain inflammation revealed no apparent differences, cytokine expression was analyzed to assess for any inflammatory phenotype which could contribute to the HSE protection seen in the CD200R1-/- mice. Inflammatory cytokines IL-6, MCP-1 (CCL2), and RANTES (CCL5) were measured by ELISA from homogenates of brain samples collected at one day and four days post infection. As shown in Figure 3.6A-C, the levels of inflammatory cytokines IL-6, MCP-1, and RANTES were not significantly different between genotypes at either time point. However, IFN-β, measured by ELISA, was found to be dramatically lower in the CD200R1-/- mice, when compared to wild type mice, at both 1 and 4 days infection in brain homogenates(Figure 3.6DC), and at 4 days post infection in the serum(Figure 3.6E).

Despite a lack of clear differences in brain inflammation as assessed both by histology and by inflammatory cytokine production, on histological examination I noticed what appeared to be a difference in the size and extent of viral inclusions, with wild-type brain sections having larger and more numerous nuclear ground-glass inclusions when compared

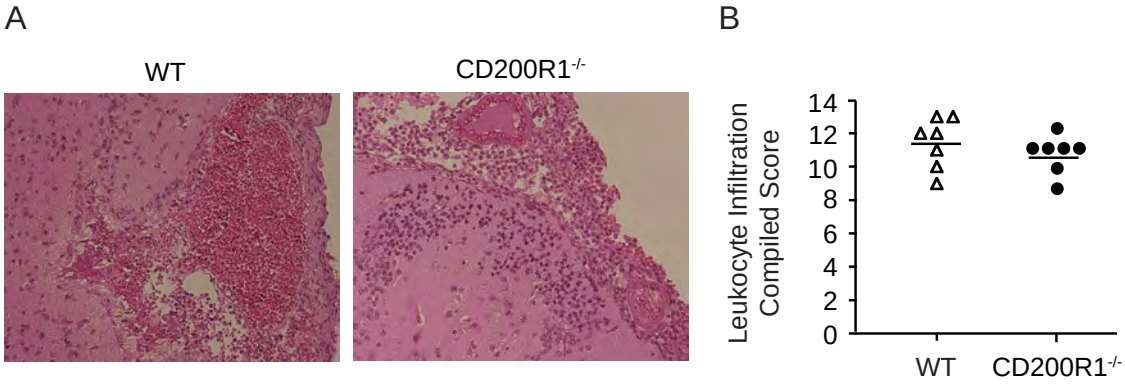

Figure 3.5: (A) H&E staining of CD200R1$^{+/+}$ (WT) and CD200R1$^{-/-}$ (KO)- brain sections prepared on day 3 post-intracranial infection (100×). Data is representative of 2 separate experiments each with 3–5 mice per genotype (n=7 WT and n=8 KO). (B) Total leukocyte infiltration scores from 7 regions of the brain on day 3 post-intracranial infection.

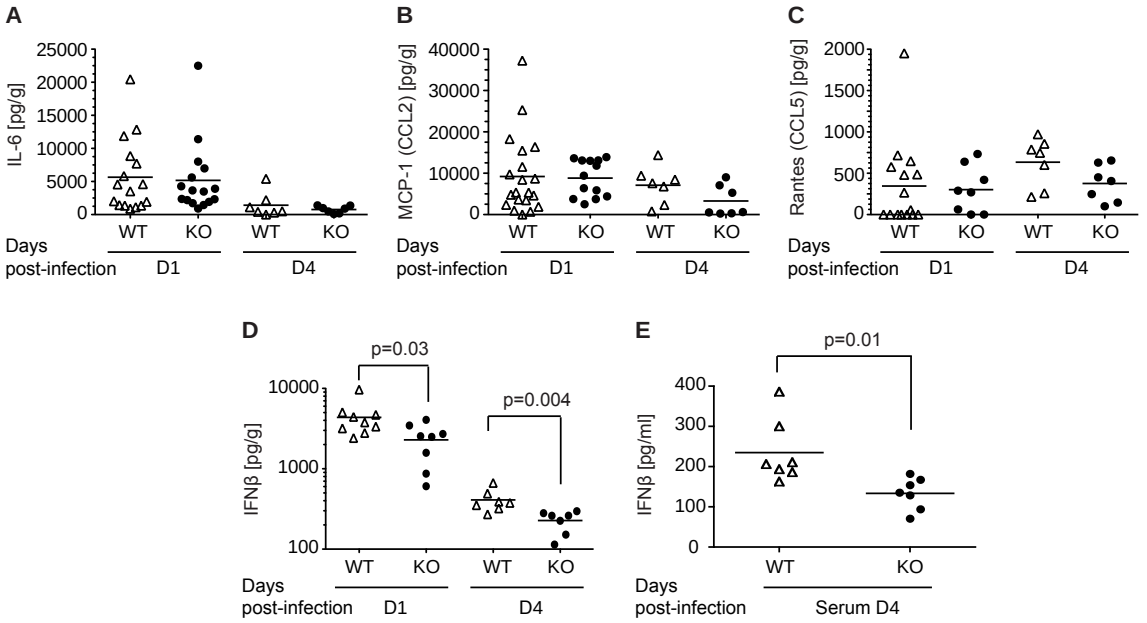

Figure 3.6: CD200R1$^{+/+}$ CD200R1$^{-/-}$ and brains have distinct cytokine response profiles. (A-D) Cytokine levels were measured in CD200R1$^{+/+}$ (WT, open triangles) and CD200R1$^{-/-}$ (KO, closed circles) brains on days 1 and 4 (D1 and D4) post-cranial injection of 105 PFU HSV-1. (A) IL-6; (B) CCL2/MCP-1; (C) CCL5/Rantes; (D) IFN-β. The mean of each group is indicated by a horizontal bar. The statistically significant groups, as determined by Kruksal Wallis test, are linked by bars and have p-values listed. (E) IFN-β levels were measured in the serum of CD200R1$^{+/+}$ (WT, open triangles) and CD200R1$^{-/-}$ (KO, closed circles). Statistical analysis was performed as above. Data includes a total of 5 experiments each with 3–7 mice per genotype (n = 20 WT and n = 13 KO day 1; n = 7, WT and KO day 4).

to CD200R1-/- brain sections. These nuclear inclusions (Cowdry type A inclusions) are histological signs of viral infection, and here suggested that while the overall inflammation was not altered in the CD200R1-/- mice, the overall amount of virus might have been. In order to properly assay this finding, I performed immunohistochemistry for HSV-1 in the brain. Using a polyclonal antibody against HSV structural proteins, I was able to detect HSV in the brain sections of wild-type and CD200R1-/- animals 3 days post infection with HSV-1. As shown in Figure 3.5, the wild-type mice had more infected neurons, spread further throughout several regions of the brain, when compared to the knockout mice. While HSV-infected cells are clearly visible in the CD200R1-/- brain sections as well, the extent of infection is clearly less. As can be seen in the rightmost panel (400×), many of the HSV-1-positive cells are neurons, identifiable based on their long axonal projections that are positive for HSV proteins.

In order to assess whether the reduced inclusions correlated with decreased amounts of viral replication, brain homogenates from mice infected with HSV-1 via intracranial injection were collected at 1, 3, or 4 days post infection. These homogenates were then assayed for viral titer by serial dilution on Vero cell monolayers for plaque analysis. As can be seen in Figure 3.8, at one day post infection, both wild-type and CD200R1-/- mice have roughly 10^3 to 10^4 pfu/mL of HSV-1 in brain homogenates. By day 3, however, a clear difference can be seen, with CD200R1-/- mice having lower levels of HSV-1 virus than wild-type mice. Many of the CD200R1-/- mice at this point were found to have no detectable HSV in their brains, meaning the infection had been cleared. The same pattern is seen again at 4 days post-infection, with CD200R1-/- mice having lower levels of HSV-1 in their brains, as compared to wild-type.

3.3.2 CD200R1 is important in TLR2 mediated innate immune responses

In order to assess the effect of CD200R1 on cytokine production following stimulation with HSV-1, peritoneal exudate cells (PECs) were collected and peritoneal macrophages

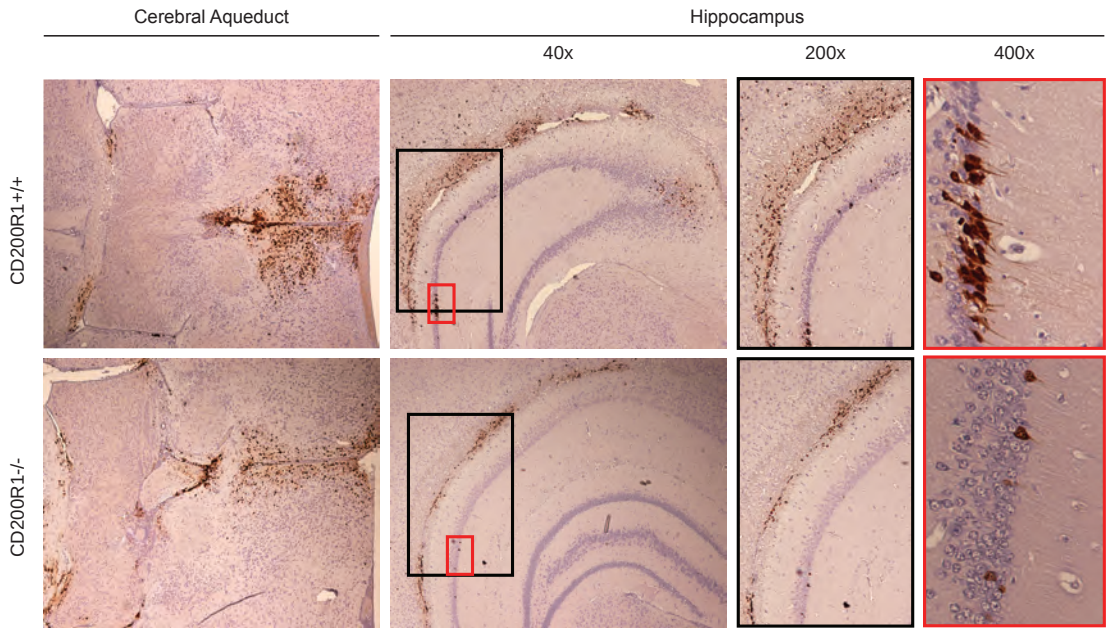

Figure 3.7: CD200R1$^{-/-}$ mice show a more diffuse spread of HSV-1 infection 3 days post-infection when compared to CD200R1$^{+/+}$ mice. Immunohistochemical analysis on paraffin-embedded brain sections using an anti-HSV-1 antibody and counterstained with hematoxylin. Brown regions are positive for HSV-antigen. These images are representative of 2 experiments (n=6 WT and KO).

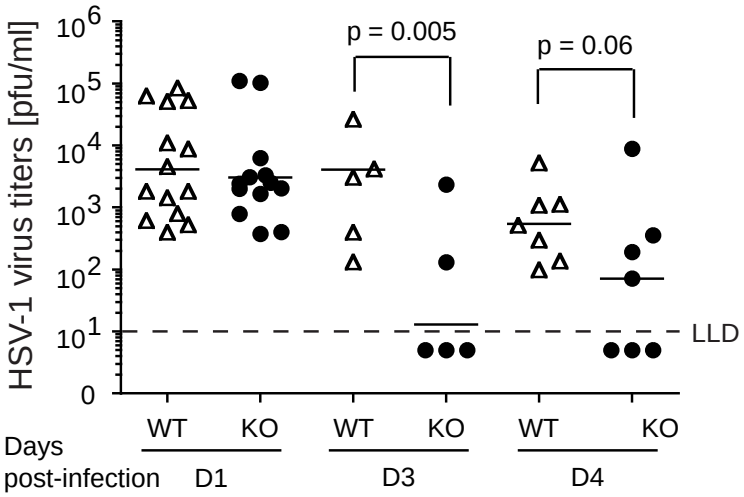

Figure 3.8: HSV-1 titers in WT (open triangles) and KO (closed circles) brain homogenates on days 1, 3, and 4 post-intracranial infection with 10^5 pfu of HSV-1 as measured by plaque assay. Limit of detection (LLD) indicated by dashed line. Data includes a total of 4 experiments. Each symbol represents an individual mouse. The mean of each group is indicated by a horizontal bar. Statistically significant groups (as determined by an unpaired, two-tailed Student's t-test analysis) are linked by bars, or indicated by asterisks and have p-values listed.

were then elicited from wild-type and CD2OOR1-/- mice. The cells were stimulated with either HSV-1, the TLR2 ligand Pam2CSK4, or the TLR4 ligand LPS. After 24, 48, or 72 hours supernatants were collected and assayed for the cytokines IL-6, RANTES, and MCP-1 by ELISA (Figure 3.9A). Following HSV-1 infection, wild-type cells secreted roughly 30,000 ng/mL of IL-6 by 24 hours, which increased to 50,000 ng/mL at 48 and 72 hours. In contrast CD200R1-/- cells produced around 20,000 ng/mL of IL-6, with no apparent increase as time progressed. With respect to RANTES production, the CD200R1-/- cells produced about half as much as the wild-type cells at 24 hours post infection. By 48 hours however, both wild-type and CD200R1-/- cell types appear to reach equivalent levels of RANTES production. When looking at MCP-1 production following HSV-1 stimulation, no apparent differences were observed between wild-type and CD200R1-/- cells at any time point.

A similar, but earlier pattern is observed when the TLR2 ligand Pam2CSK4 was used to stimulate PECs. In this case, CD200R1-/- PECs produced around 15,000 pg/mL of IL-6 at each of the three time points, while wild-type cells generated five-fold higher levels of IL-6 (around 80,000 pg/mL). The same is true with RANTES production, with the CD200R1-/- cells producing a significantly lower amount at each of the time points tested, as compared to wild-type. MCP-1 production was not affected in the same way following Pam2CSK4 stimulation, with wild-type and CD200R1-/- PECs generating equivalent amounts of MCP-1 at 24 and 48 hours post stimulation. However, at 72 hours after stimulation with Pam2CSK4, the CD200R1-/- cells produced significantly more MCP-1 than wild-type.

Here, the TLR4 agonist LPS served as a positive control for the inflammatory response, and it demonstrated that both cell types are capable of generating an inflammatory response via the activation of a different TLR molecule. Unlike following TLR2 activation, LPS stimulation showed similar patterns between the wild-type and CD200R1-/- PECs, demonstrating that both cell types have active TLR signaling pathway. It should be noted that at 48 and 72 hours post stimulation with LPS the CD200R1-/- PECs appear to have a

elevated MCP-1 response, suggesting that CD200R1-/- might be a critical negative regulator of MCP-1 expression at later points in an infection.

In order to assess whether the defects in IL-6 production seen in CD200R1-/- signaling affected inflammasome activation and IL-1β production we assayed IL-1β secretion following infection with HSV-1, with a dual stimulation of LPS and ATP as a control (Figure 3.9B). Wild-type and CD200R1-/- PECs and BMDMs were tested, and in both cell types the absence of CD200R1 resulted in significantly lower levels of secreted IL-1β. All of the cells tested were capable of wild-type levels of inflammasome activation following LPS+ATP stimulation, suggesting that HSV-1 requires CD200R1 to efficiently activate inflammasome signaling and IL-1β secretion. This result was further verified by assessing the amount of cleaved and active IL-1β secreted and retained in PECs (Figure 3.9C). The CD200R1-/- PECs had significantly less IL-1β including active IL-β in the culture media, while retaining a substantial amount of unsecreted pro-IL-β. Together this suggests that CD200R1 is an important mediator of inflammasome activation following HSV-1 infection.

One of the early effects of innate immune activation is the upregulation of TLR2 on the cell surface. This upregulation is detectable following stimulation of many TLR molecules including TLR2 itself [186,187] and is thought to result from activation of the NF-ϰB pathway [188]. In order to assess whether this TLR2-upregulation reaction is affected by CD200R1, PECs from wild-type, CD200R1-/-, and TLR2-/- mice were stimulated with HSV-1. The macrophages were then assessed for surface expression of both CD200R1 and TLR2 by flow cytometry (Figure 3.10). As can be seen in Figure 3.10A, in wild-type cells following infection with HSV-1, CD200R1 is removed from the cell surface. At baseline roughly 12% of the PECs are positive for CD200R1, with this number decreasing to about 5% following infection with HSV-1. This downregulation reaction is TLR2-independent, as TLR2KO PECs still show this downregulation. The amount of TLR2 on the cell surface was also measured (Figure 3.10B). At baseline, around 1% of both wild-type and CD200R1-/- PECs were positive for TLR2 on the cell surface. Following infection with HSV-1, the number

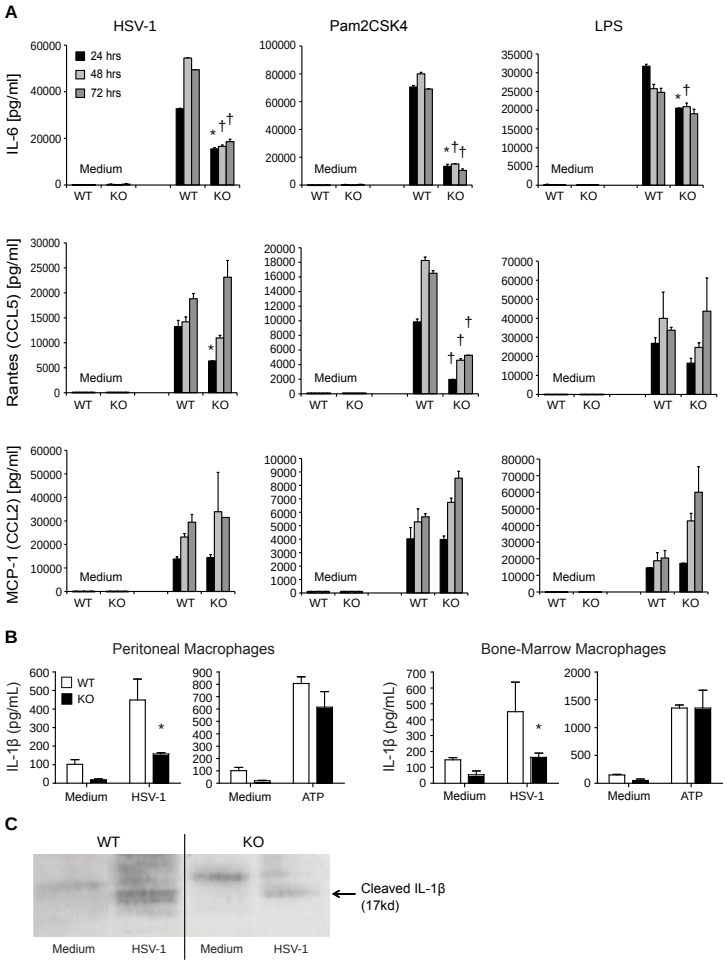

Figure 3.9: (A) CD200R1$^{+/+}$ (WT) or CD200R1$^{-/-}$ (KO) elicited peritoneal macrophages were stimulated with either HSV-1 (MOI 10, left column), Pam2CSK4 (100 ng/ml, center column), LPS (100 ng/ml, right column), or medium for 24, 48, or 72 hours. Levels of IL-6 (upper row, pg/ml), CCL5/Rantes (middle row, pg/ml), and CCL2/MCP1 (lower row, pg/ml) were measured by ELISA. Data shown are mean and SD of representative experiment (total of 3 experiments, n=4, WT and KO). An unpaired, two-tailed Student's t-test was used to determine statistical significance of independent experiments, p values: * $p < 0.05$, † $p < 0.01$. (B) Supernatant IL-1β levels from WT and KO elicited peritoneal macrophages (left panels) or bone marrow macrophages (right panels) 16 hours after infection with HSV-1 (MOI 10) or after a 3 hour stimulation with LPS (100 ng/ml) followed by ATP (1 mM) for 1 h. ELISA results are representative of 3 experiments. (C) WT and KO elicited peritoneal macrophages were cultured for 20 hours with HSV-1 (MOI 10). Media (left lanes) and cells (right lanes) were analyzed by SDS-PAGE followed by Western blot for cleavage of pro-IL-1β to IL-1β. Data representative of 3 experiments (n=4, WT; n=5, KO).

of TLR2-positive cells increased to 12% among wild-type cells, but remained unchanged in CD200R1-/- cells. This demonstrates that in CD200R1-/- cells, inflammatory signaling and TLR2 expression in response to HSV-1 infection is significantly limited.

Based on the *in vivo* phenotype of decreased viral replication, and the apparent lack of inflammatory signaling present in CD200R1-/- cells following infection with HSV-1, I wanted to further probe how well HSV replicated in CD200R1-/- cells. Mouse embryonic fibroblasts (MEFs) were infected with HSV-1, and viral replication was assessed by measuring the amount of virus present in the culture supernatant 24 hours after infection (Figure 3.11). The amount of HSV-1 was measured by plaque formation on Vero cells (Figure 3.11A), and by quantitative PCR of genomic DNA (Figure 3.11B). By both of these measurements, wild-type MEFs produced five-fold more virus then CD200R1-/- MEFs. This result once again demonstrated that HSV-1 replication is severely impaired in CD200R1-/- cells.

The viral replication studies in Figure 3.11 measured total virus production. However, there are a number of sequential gene expression events that take place during HSV-1 replication (Figure 3.1), with α genes turning on β gene expression, and β genes turning on γ gene expression. In order to further probe whether CD200R1-/- was affecting viral entry, viral gene expression, or viral egress, I infected MEFs and PECs with a strain of HSV-1 that expresses an ICP8-GFP fusion protein. ICP8 is a β (early) viral gene that functions as an important regulator of viral DNA replication [132]. As this gene is highly expressed midway through the HSV-1 replication cycle, the CD200R1 effect on HSV-1 replication can be identified as being upstream or downstream of ICP8 gene expression. I measured the percentage of ICP8-GFP-positive cells in cultures at various time points post infection. The replication cycle of HSV-1 in culture is roughly 6-12 hours. I added pooled human IgG to the culture supernatants after virus adsorption in order to neutralize released HSV virions and prevent secondary infection (cells infected by virions generated from previously infected cells). ICP8-GFP expression was measure by flow cytometry at 1 to 144 hours post-infection. The results, as seen in Figure 3.12 shows that CD200R1-/- cells are much

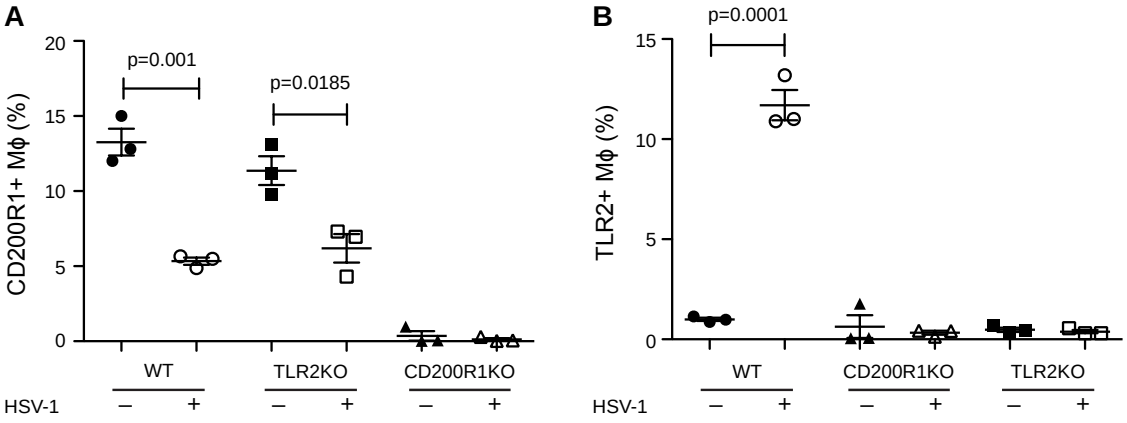

Figure 3.10: CD200R1 controls expression of TLR2 in macrophages.(A, B) The expression of CD200R1 (A) or TLR2 (B) on the surface of WT (circles), TLR2KO (squares), or CD200R1KO (triangles) elicited peritoneal macrophages (MΦ) before (–, closed symbols) or after HSV-1 infection (+, open symbols) as determined by flow cytometry. The lack of expression of CD200R1 or TLR2 on the surface of CD200R1KO or TLR2KO macrophages, respectively, served as internal controls. Data representative of 3 experiments (preparations from individual mice n=3 WT and KO are shown). An unpaired, two-tailed Student's t-test was used to determine statistical significance of independent experiments.

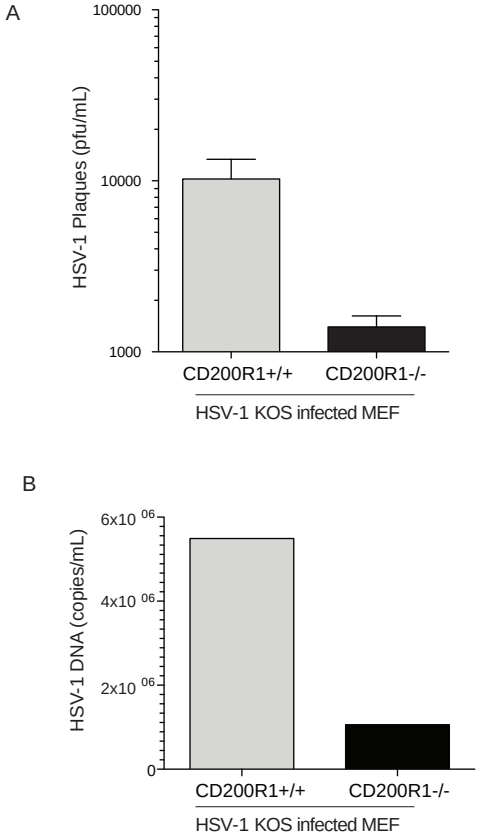

Figure 3.11: CD200R1 MEFs show several log decrease in viral titer, after a 24 hour incubation with HSV-1 virus. CD200R1$^{+/+}$ and CD200R1$^{-/-}$ MEFs were infected with HSV-1 at an MOI of 10 and incubated for 24 hours. Viral replication was measure by assessing (A) the amount of live virus present in the culture supernatant by plaque assay on Vero cells, and by (B) quantitative PCR analysis of HSV DNA present within the culture supernatant. Mean ± SEM is shown.

less permissive with respect to HSV-1 infection and ICP8 gene expression, compared to wild-type cells. Wild-type MEFs reached a peak infection rate of over 40% by 12 hours post infection with ICP8-HSV, but CD200R1-/- MEFs, only reached a peak infection rate of around 20%. Macrophages, in general, are much less permissive to HSV infection than MEFs, and I observed that the GFP-positive rates in these cells are much lower than in MEFs. Despite this, the CD200R1-/- macrophages also have a significantly lower percentage of positive cells by 24 hours post infection, compared to wild-type macrophages. At 24 hours post infection, over 10% of the wild-type macrophages were GFP-positive, but the percentage of GFP-positive CD200R1-/- macrophages was less than 5% of total cells.

ICP8 is a β (early) gene expressed during the middle of the HSV-1 lifecycle (Figure 3.1). Given that I observed a marked defect in ICP8-GFP expression in CD200R1-/- cells (Figure 3.12), this indicated that CD200R1 was affecting some point in the viral replication cycle at or upstream of ICP8 expression. In order to better understand whether CD200R1, a cell-surface protein, was affecting viral entry or viral gene expression, I examined the expression levels of several viral proteins by western blot (Figure 3.13). After infecting wild-type and CD200R1-/- MEFs with HSV-1, cell lysates were collected at 3 hours or 6 hours post infection and probed for the α (immediate-early) gene ICP4. Lamin and actin blotting was performed on the same membrane as loading controls. As seen in Figure 3.13 wild-type and CD200R1-/- MEFs express ICP4 to equivalent levels, with both cell types expressing substantial amounts by 6 hours post infection. Cell lysates were also probed for ICP27 (another α gene), the β (early) gene ICP8, and the γ (late) gene VP16. At 6 hours post infection I observed significant differences in protein expression, with CD200R1-/- MEFs showing decreased levels of each of these genes. These results point to CD200R1 affecting HSV-1 replication at a point early in the lifecycle, after virus entry and ICP4 expression but before ICP27 expression.

In order to verify these findings derived from the CD200R1-/- mice, I ectopically expressed and knocked down CD200R1 in U2OS cells and bone-marrow-derived dendritic cells

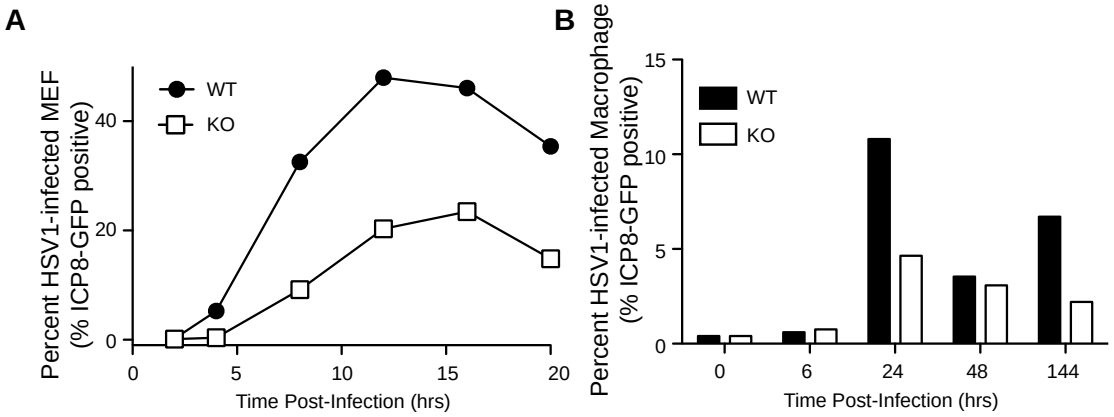

Figure 3.12: CD200R1 regulates replication of HSV-1 in cells. (A, B) Flow cytometry to assess GFP expression in CD200R1$^{+/+}$ (WT) and CD200R1$^{-/-}$ (KO) mouse embryonic fibroblasts (MEFs; A) and elicited peritoneal macrophages (B) at various time points following infection with ICP8-GFP virus (MOI). Histograms of each sample were generated. A gate was set on the uninfected control for each condition, which excluded 99% of the uninfected cells. This gate was then applied to the paired infected samples to calculate the percentage of GFP-positive cells. Data representative of 3 experiments.

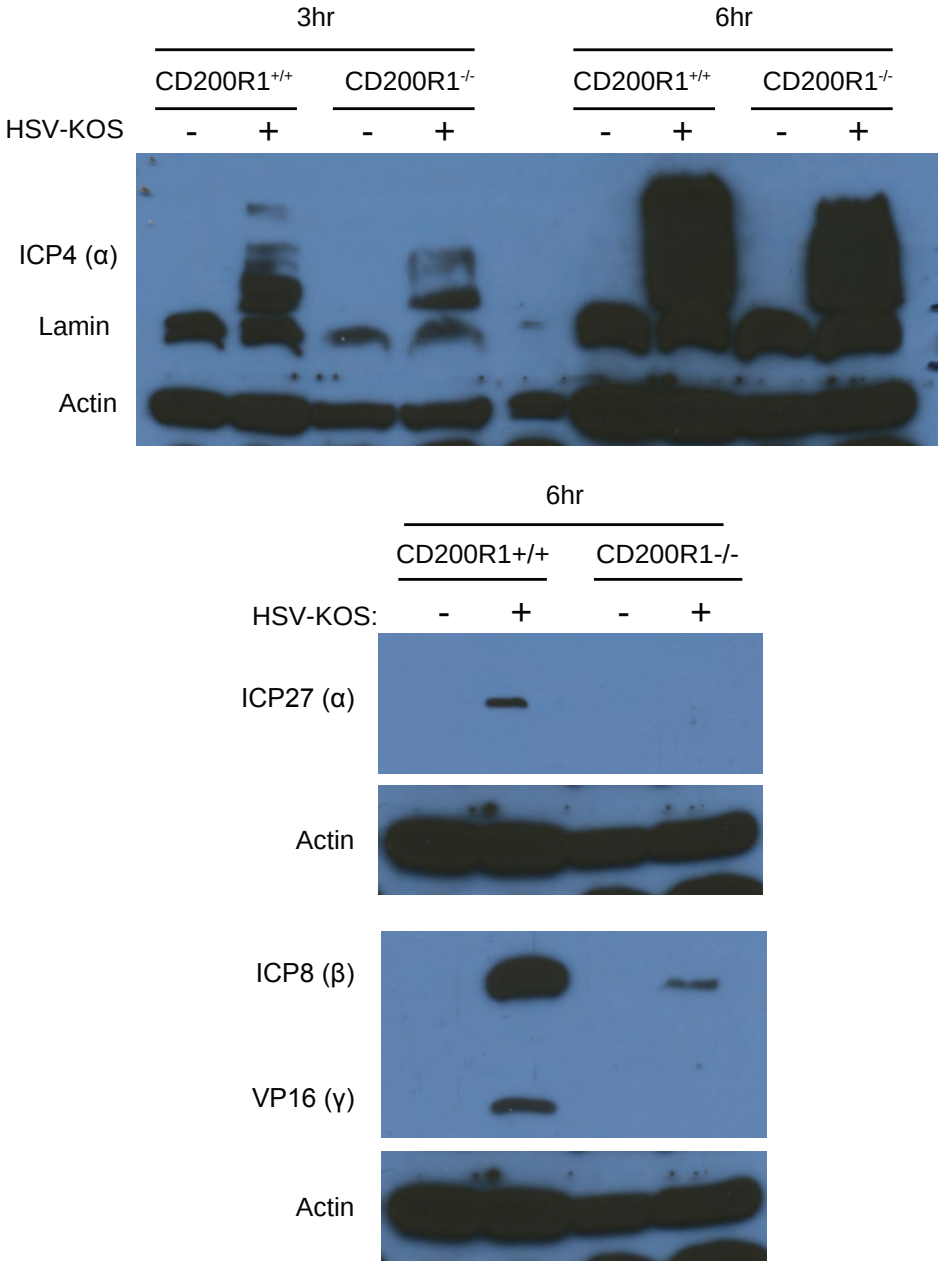

Figure 3.13: Western blot analysis of several HSV proteins expressed during the course of infection. CD200R1$^{-/-}$ cells show decreased expression of ICP4 and ICP8, with no noticeable expression of the proteins VP16 and ICP28. CD200R1$^{+/+}$ and CD200R1$^{-/-}$ MEFS were infected with HSV-1 KOS at an MOI of 20. After 3 hours or 6 hours, cell lysates were collected and analyzed by western blot for the expression of HSV proteins ICP4, ICP27, ICP8, and VP16. ICP4 and ICP27 are α genes, ICP8 is a β gene, and, VP16 is a γ gene. Blotting for actin and lamin served as loading controls.

(Figure 3.14). U2OS cells are a human osteosarcoma cell line that are known to be permissive to HSV-1 infection and replication. Lentiviral vectors were used to transduce these cells to express ectopic CD200R1, TLR2, or short-hairpin RNA constructs targeting endogenous CD200R1. As can be seen in Figure 3.14A, the overexpression of CD200R1 or TLR2 resulted in a near two-fold increase in HSV viral replication, as measured by plaques-forming units in the culture supernatant. Conversely, knockdown of CD200R1 by shRNA resulted in approximately two-fold decrease in virus production at 24 hours.

In BMDCs a similar result was observed for CD200R1 but not TLR2 expression (Figure 3.14B). Ectopic expression of CD200R1 in wild-type BMDCs once again resulted in significant increase in viral replication. However, unlike in the U2OS cells, ectopic expression of TLR2 did not result in higher levels of HSV-1 replication. CD200R1-/- BMDCs phenocopied CD200R1-/- MEFs and PECs by producing less HSV-1 than wild-type cells. This defect in HSV-1 replication could be rescued by the ectopic expression of CD200R1 in CD200R1-/- cells, which lead to a dramatic increase in HSV-1 replication to a level well above that of the wild-type control cells. Additionally TLR2 expression in CD200R1-/- also rescued the HSV-1 replication phenotype, returning CD200R1-/- cells to a level of HSV-1 replication equivalent to control wild-type cells. The fact that TLR2 was able to rescue CD200R1-/- BMDCs cells while also resulting in elevated levels of HSV-1 replication in U2OS cells points to a role for TLR2 downstream of CD200R1 in the HSV-1 replication cycle.

Since CD200R1-/- cells have a defect in HSV-1-induced and TLR2-induced IL-6 production (Figure 3.9), fail to upregulate TLR2 in response to HSV-1 stimulation (Figure 3.10), and are unable to support wild-type levels of HSV-1 replication following transduction with ectopic TLR2 (Figure 3.14), I asked whether TLR2 itself is an important mediator of HSV-1 replication *in vitro*. Using the ICP8-GFP strain of HSV-1, I infected wild-type and TLR2-/- MEFs for 6 hours and 8 hours, and measured the percentage of ICP8-GFP-positive cells by flow cytometry (Figure 3.15). Just like the CD200R1-/- MEFs, TLR2-/- MEFs showed

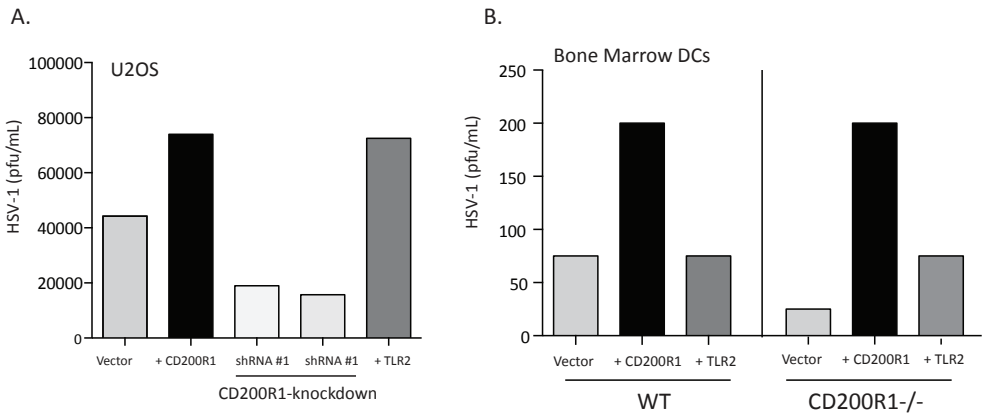

Figure 3.14: Ectopic expression of either CD200R1 or TLR2 promote HSV-1 replication. (A) U2OS were transduced with lentiviral vectors expressing CD200R1, TLR2, or a shRNA targeting CD200R1. After antibiotic selection, cells were plated and infected with HSV-1 for 24 hours. HSV replication was measured by plaque assay on culture supernatants. (B) WT or CD200R1$^{-/-}$ BMDCs were transformed during differentiation with lentiviral vectors expressing control (GFP), CD200R1, TLR2, of shRNA targeting CD200R1. Following differentiation and antibiotic selection, cells were plated and infected for 24 hours with HSV-1. HSV-1 titers in culture supernatants were measured by plaque assay.

significantly less ICP8 expression when compared to wild-type, further suggesting the defect in CD200R1-/- cells is related to TLR2.

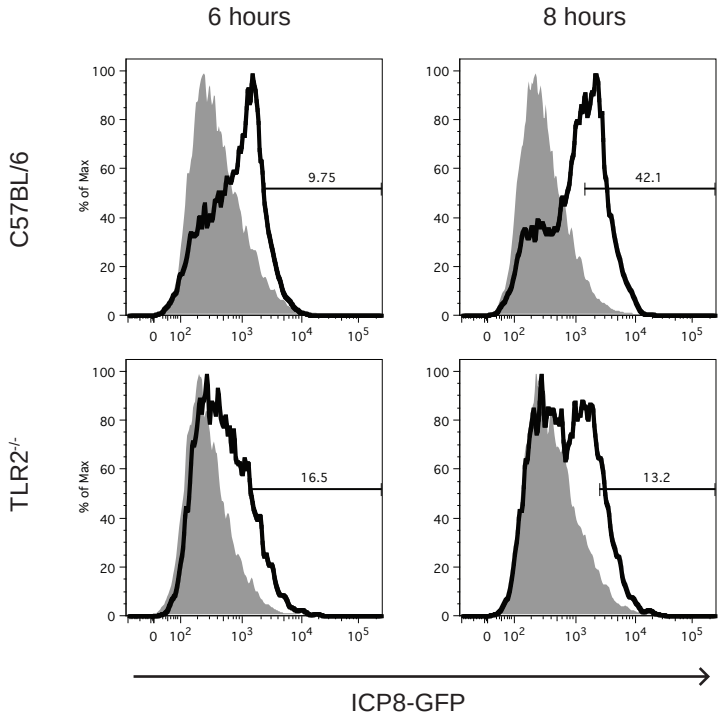

Figure 3.15: TLR2$^{-/-}$ MEFs, like CD200R1KO MEFs, do not support robust HSV-1 replication, as measured by GFP-expressing gene expression. C57BL/6 and TLR2$^{-/-}$ MEFS were infected with an ICP8-GFP-expressing strain of HSV-1 for 6 and 8 hours, then fixed and analyzed for GFP expression by flow cytometry. Grey background represent negative (uninfected control MEFs of each cell type). GFP-positive gates were set at the 99th percentile of GFP-positive cells in the uninfected control sample for each cell line. This gate was then applied to the HSV-infected sample for that cell line. Percent GFP-positive samples based on these gates are reported on each panel.

3.4 Conclusions

I have found that CD200R1 is an important host factor supporting HSV-1 replication early during infection. I also found CD200R1 is an important factor in TLR2 signaling and TLR2 upregulation in macrophages. Additionally I have found that the expression of TLR2 can rescue in CD200R1-/- cells the ability to support HSV-1 replication. *In vivo* the collective results of these findings are that CD200R1 is required for efficient viral replication and dissemination with in the CNS, and a lack of CD200R1 is protective in a mouse model of herpes simplex encephalitis.

Taken together, these results point to CD200R1 playing a role in promoting TLR2 upregulation and TLR2-mediated inflammatory signaling early in the replication cycle of HSV-1. HSV-1 depends on some amount of inflammatory signaling to turn on the expression of several host factors required for efficient replication. Our results suggest that this processes involves CD200R1- and TLR2-mediated gene expression. Without the activation of these signaling pathways during viral replication, the expression of certain early viral proteins are not able to proceed at sufficient levels, limiting replication.

This novel pro-inflammatory function for CD200R1 stands in contrast to its previously characterized role as an important anti-inflammatory signaling molecule. Future work investigating how CD200R1 carries out this function and how it interacts with and promulgates TLR2 signaling would allow for a better understanding of the intricate dynamic interactions between pro- and anti-inflammatory pathways.

CHAPTER IV: Discussion

4.1 On the role of PIR1 in antiviral responses in mammals

PIR1 plays a critical role in promoting an effective antiviral small RNA response in the model organism *C. elegans* by promoting the efficient production of antiviral RNAs early on in an infection, allowing the host to effectively restrain viral replication through RNA interference [94]. We have also known that human PIR1 selectively interacts with the RIG-I-like receptor LGP2 (Figure 2.3 on page 26), and that in mice infected with EMCV, type I IFN production is dependent on LGP2. Therefore, we originally hypothesized that mammalian PIR1 would play an important role in type I IFN signaling in response to EMCV. However, it is clear from my data that, at least in response to EMCV, this is not the case. Following infection with EMCV, PIR1KO mice upregulate type I IFN to wild-type levels and show no significant differences in overall survival or viral replication. As has been reported multiple times (and in my own unpublished experiments), loss of MDA5:LGP2:MAVS:IFN signaling in mice leads to a fulminant EMCV infection with rampant viral replication and accelerated mortality [53,54]. Such phenotypes are not observed in the PIR1KO mouse. These results, however, do not rule out a role for PIR1 in the IFN response to other viruses that engage MDA5:LGP2 signaling, and these other viruses should be investigated in the future using our PIR1KO model.

My results also do not rule out a role for PIR1 in a mammalian small RNA pathway. In fact several pieces of *in vitro* data, when combined with other published evidence, suggest that PIR1 might be functioning in this capacity. While controversial, a growing body of evidence appears to support the existence of a functional—albeit enigmatic—antiviral RNA interference (avRNAi) response in mammals [189]. While it appears that such a mammalian avRNAi pathway does exist, and that it is employed in certain situations in mammalian systems, it is also clear that the type I IFN pathway is the predominant antiviral response to pathogenic infections in mammals. Therefore, it seems mammals have two distinct antiviral pathways: the type I IFN pathways and the avRNAi pathway. While the importance of the

mammalian avRNAi pathway is still up for debate, it has been shown to interact with the type I IFN pathway, suggesting that these two disparate defense systems might coexist in some cells. How exactly they interact is not yet well understood, but PIR1 might play a role this interaction.

4.1.1 A potential role for PIR1 in the avRNAi anti-viral response

Since immunostimulatory RNA is encountered on a regular basis from endogenous sources or from non-pathogenic viruses, it would make sense that a certain threshold of immunostimulatory RNA would be required in order to trigger the broad and disruptive antiviral type I IFN response. I would hypothesize that an avRNAi pathway which exists in mammalian cells could process small amounts of foreign RNA on a regular basis. However, given that RLRs like MDA5 have a threshold of detection for RNA above which they oligomerize and initiate signaling [190], should the avRNAi pathway prove ineffective in preventing the build up of foreign RNA, this threshold concentration would be achieved, and type I IFN would be induced. It is also possible that activation of type I IFN would shut down or suppress any avRNAi pathway, given the fact that mammalian dsRNA-processing pathways are known to be negatively regulated following stimulation with type I IFN [84]. It could then follow that, as an RNA phosphatase known to interact with Dicer, PIR1 would affect this balance by promoting the avRNAi pathway when only small amounts of viral RNA are present. While there is adequate evidence to suggest this model, many questions remain unanswered, and much work remains to clearly elucidate these dynamic interactions and test these hypotheses.

Open questions on PIR1 and avRNAi in C. elegans

While the mechanism is not yet fully understood, PIR1 has been shown to be a critical mediator of the avRNAi response in *C. elegans* following infection with the worm virus Orsay Virus [94]. It has been suggested that PIR1 facilitates the efficient production of antiviral

RNAs early on in an infection, promoting host defense through RNA interference. During the processing of primary avRNA molecules, dsRNA molecules are cleaved by Dicer and the cleavage products are loaded into complexes with RDE-1 as primary avRNAs. These RDE-1 complexes then detect and target viral RNA molecules for RdRP. PIR1 mutant worms are able to produce primary avRNAs, but these molecules are less abundant and are not effective at inducing the synthesis of secondary avRNA molecules. This could be a symptom of inefficient loading of primary avRNAs into complexes with the argonaute protein RDE-1. Argonaute loading is a multi-protein process the occurs in concert with Dicing and involves Dicer as well as other dsRNA-binding proteins [191]. As PIR1 interacts with these proteins, and as it binds to the 5'-end of RNA molecules, one possibility could be that PIR1 promotes RDE-1 loading with primary avRNA molecules. Without PIR-1, primary avRNAs would get produced, but they would be less stable and as a result would not be able to carry out their antiviral effect. Another possibility could be that PIR1 affects the processing and maturation of secondary avRNAs. As these RNA molecules are 5'-triphosphorylated, they likely require dephosphorylation in order to be properly loaded into their respective effector argonuate complexes. Perhaps an inability to properly produce stable secondary avRNAs results in the ineffective activity of the whole avRNAi pathway. More work is needed to better understand the true mechanism of PIR1 in these critical processes, and to potentially reveal new insights and avenues of inquiry for the role of PIR1 in mammals.

Open questions on PIR1 and avRNAi in Drosphila

Recent work in the fly (as reported by Daniel Chaves [94]) has shown that the fly orthologue to PIR1 (CG13197) is required for inhibiting flock-house virus replication and promoting survival, a response that is known to require antiviral RNAi. At this point, however, as in the worms, a precise mechanism for this phenotype has not yet been uncovered. Whether PIR1 affects the production of antiviral siRNAs by Dicer-2 or somehow otherwise promotes the production of secondary avRNA molecules from complementary vDNA is yet

to be determined. It is possible that PIR1 could be involved in the loading of Dicer products into their appropriate Argonaute complexes as is hypothesized for the worm. It is also possible that the maturation of secondary avRNAs requires 5'-dephosphorylation, since these are *de novo* RNA transcripts that are missing a 5' cap. Again, further investigation will be needed to probe the relationship between PIR1 and the *Drosophila* avRNAi pathway.

A potential role of PIR1 in a mammalian avRNAi pathway

Two recent studies by Maillard et al. and Li et al. showed that under certain circumstances, avRNAi can be detected in human and mouse systems [82,192]. Pluripotent mouse stem cells were shown to produce significant levels of virus-derived small RNAs, which showed hallmarks of Dicer production, and were bound in Argonaute complexes. This was also true in very immature weanling mice, where viral replication was limited by the production of small RNAs. Interestingly, in stem cells and other progenitor cells—like oocytes [193]—the avRNAi pathway is readily detectable by deep sequencing [192]. However, upon differentiation, the avRNAi pathway appears to go away, and get replaced by type I IFN signaling. Together these data suggest that the mammalian antiviral RNAi response is prominent and important only in specific subsets of cell types or in specific contexts.

Many mammalian viruses express potent inhibitors to the small RNA pathway, suggesting that antagonizing RNAi is often beneficial for viral replication. In the case of Influenza A, when the potent RNAi antagonist NS1 is deleted, antiviral RNAs are readily detected by deep sequencing of the host cells. These RNA molecules are loaded into Ago complexes, and do in fact appear to function as antiviral RNA molecules [83].

Intriguingly, worms and flies are now both thought to employ an amplification step in their generation of antiviral RNA molecules. In *C. elegans* this amplification is accomplished by RdRP. As of yet, no bonafide mammalian RdRP enzyme has been found, and no notable evidence for RdRP-mediated small RNA amplification. However, in *D. melanogaster* this amplification is accomplished through a complimentary (cDNA) intermediate. Generation

of this cDNA is dependent on reverse transcription activity, apparently derived from endogenous reverse transcriptases associated with retrotransposons already present in the fly genome [79]. Mammalian genomes, including those of mice and humans, contain many active retrotransposons, which could play an analogous role in amplifying antiviral interfering RNA molecules. In fact, the presence of complementary DNA to several RNA viruses has been previously reported, further suggesting that such a mechanism might exist in mammals [194–196]. Future work should take care to characterize the nature of these cDNAs and their abundance during infection in both wild-type and PIR1KO mice.

However, even if mammals are not inherently capable of amplifying viral RNA molecules, this does not exclude the possibility for small RNA amplification via a viral RdRP. Many mammalian viruses encode for an RdRP enzyme, expressed during infection and required for viral replication. Ectopic expression of the poliovirus RdRP, for example, can lead to the production of immunostimulatory RNA in the absence of viral RNA [197]. The same is also true for the RdRP of Simliki Forest Virus [198] and Hepatitis C Virus [199]. Furthermore viral RdRPs, which usually require a primer to initiate RNA polymerization, are known to under certain circumstances synthesize RNA in a template-independent manner [200,201]. Together this means that small RNA amplification could still occur in infected hosts that do not themselves express an RdRP enzyme via a viral RdRP.

Taken together it seems reasonable to conclude that mammalian cells have a functional pathway by which viral RNA can be recognized and processed, in a Dicer-dependent manner, into small RNAs. However, it also appears that this pathway, which is actively inhibited by many viruses, and in some cases is co-opted by viruses to facilitate viral replication, will only be detectable in specific contexts (such as oocytes, stem cells, and suckling mice). In contrast, in fully-differentiated cells and mature animals, the avRNAi pathway becomes less important to the more robust IFN response.

A potential role of PIR1 in a mammalian miRNA pathway

Separate from the antiviral response, recent studies by Burke et al. have shown that human PIR1 plays a role in promoting the stability of certain non-canonical miRNAs [96]. Additionally, preliminary work by Darryl Conte has shown that PIR1 can interact with human Dicer (Figure 2.3 on page 26). Consistent with these observations, I have found that PIR1 affects Dicer-dependent miRNA levels (Figure 2.16 on page 68).

While the exact mechanism is not yet understood, it is suggested that the presence of a 5'-triphosphate on a pre-miRNA or small RNA molecule affects that ability of Dicer:Argonaute complexes to properly load the 5p-arm of these molecules into an effective silencing complex. The hypothesis that PIR1 promotes the stable loading of certain small RNA molecules into Argonaute complexes fits with the current model for PIR1 in the worm, as well as my findings on the role of PIR1 in the earliest stages of RLR induction (as shown in Figure 2.15 on page 67).

All together, mammals have all the components required to mount an RNAi-mediated response to a viral infection, and in specific circumstances do harbor small RNA molecules during viral infections. While several studies have tried and failed to find small RNAs derived from various viruses [202], certain other viruses can apparently produce small RNAs [203–206]. However, these small RNAs are not necessary antiviral. In the case of enterovirus-71, dicer-dependent virus-derived small RNAs were found to be proviral and thought to help regulate viral replication [207]. Future work characterizing the differences in small RNAs in wild-type versus knockout mice, at baseline and under infection, will allow for a more complete understanding of the role of mammalian PIR1 in small RNA biology.

4.1.2 Future work and limitations in studying the avRNAi response in mammals

It is well understood that the predominant innate antiviral response pathway in mammals is the type I IFN response. Upon infection with an RNA virus, type I IFN is induced by the cytosolic RNA sensors RIG-I and MDA5 (as discussed in Section 1.2.1 on page 8). It is well documented that mice lacking any of the components of the RNA-sensing and IFN signaling pathway genes are highly susceptible to RNA viruses, often dying rapidly with higher rates of viral replication and dissemination.

In contrast, many of the components of the avRNAi pathway are required for embryogenesis and early development, making them difficult to study by knock-out. To date, no *in vivo* studies using transgenic mice carry a knock-out mutation to a component of the avRNAi pathway have demonstrated an effect of the avRNAi pathway no survival to a viral infection. This might suggest that in a mature animal responding to a pathogenic infection, this pathway is not critical, but more work is need to confirm this.

In the context of the commonly studied pathogenic infections, type I IFN is the critical mediator of antiviral signaling and is responsible for hampering viral replication, while the avRNAi pathway is not considered an equivalent or redundant antiviral pathway. It is still possible that the avRNAi pathway plays a role in complementing the type I IFN response or responding to RNA that would not otherwise engage the type I IFN pathway.

The complex interaction between the type I IFN and avRNAi responses

The type I IFN pathway and the avRNAi pathway appear to interact with each other significantly during the course of an infection. Perhaps the best evidence that these pathways coexists, interact, and potentially complement each other is the fact that the former has been shown to negatively regulate the later. There is growing evidence that the type I IFN pathway, upon activation, negatively regulates many parts of the avRNAi response

by directly ribosylating the Argonaute proteins, reducing their activity [86]. Cells lacking in type I IFN signaling, show an enhanced ability to process dsRNA into functional siRNA. When type I IFN was added back to these cells, this elevated dsRNA-processing activity is lost [84], suggesting that upon activation type I IFN signaling shuts off the avRNAi pathway.

There also are a number of molecules that are directly involved in both pathways, affording an opportunity for cross-talk. The dicer-partner protein PACT, which is an important co-factor in miRNA processing, coordinates with the RLR RIG-I to facilitate IFN signaling in response to certain viral RNA ligands [208,209]. The other dicer-partner protein TRBP, which helps promote dsRNA processing, interacts with the RLR LGP2 to facilitate IFN induction following infection with EMCV [210].

Additionally, a number of recent studies have suggested that the RIG-I-like receptors do not simply function as sensors for viral RNA, but instead might help facilitate an antiviral response independent of IFN induction. RIG-I has been shown to inhibit viral protein and enzyme binding to to IAV and HBV viral RNA in an IFN-independent manner [211,212]. RIG-I and MDA5 also actively remove viral proteins from dsRNA in an ATP-dependent manner allowing the viral RNA to be bound to dsRNA-binding protein PKR [213]. Together these findings support the hypothesis that RLR-pathways are interacting with an alternative antiviral response, independent of IFN induction.

Given the feed-forward nature of the the type I IFN response—where small amounts of IFN-β or IFN-α signal in an autocrine or paracrine manner to further induce the production of more IFN cytokines—initial activation leads to an amplification and ramp up of the antiviral response until negative regulatory processes can kick in to shut it down hours to days later. Therefore, it would seem reasonable that there exists a threshold amount of foreign RNA beyond which IFN release is triggered. It is already understood that such a threshold exists, at least at the ligand-binding level. Certain mutations in the dsRNA-sensor MDA5 result in an increased affinity for dsRNA resulting in a greater tendency

for signaling complex association and signal initiation even when encountering endogenous dsRNA species that are otherwise non-stimulatory [190].

If mammalian cells have two functional antiviral pathways—the avRNAi pathway and the type I IFN pathway—foreign RNA could be detected by either. However, viral RNA that is shuttled into the the avRNAi pathways would get processed and cleaved into small RNA molecules, neutralizing this RNA and effectively decreasing the amount of foreign RNA available for IFN induction. If in certain circumstances this shuttling of viral RNA into the avRNAi pathway for cleavage is inhibited, then MDA5 signaling might get triggered sooner, as there would be more viral dsRNA available for MDA5:LGP2 complex formation.

I would hypothesize that in a naive cell, both antiviral pathways exists simultaneously. I would also hypothesize that during the earliest moments of a viral infection or following the introduction of dsRNA into the cytoplasm the avRNAi has precedence, being allowed to cleave the foreign RNA and to render it inactive. The cleaved molecules could then be loaded into Ago complexes as a temporary protection mechanism against subsequent viral RNA molecules. However, if the virus is able to replicate effectively despite this process, a dsRNA threshold is reached, at which point IFN signaling is initiated, cytokines are produced, and the ineffective avRNAi pathway is turned off.

Separating the overlapping pathways of avRNAi and miRNA synthesis

While complicated, the above mechanism allows for the coexistence of both antiviral pathways, at least early on, and fits much of the current literature. In order to test this hypothesis one could further investigate the dose-response of the type I IFN pathway, with and without an avRNAi response. Blocking the avRNAi response is difficult however, since so many of the components of this pathway also function in the miRNA pathway, helping to regulate countless other vital biological processes. As such, disruption of these pathway components would have countless secondary effects upon a given cell. Therefore, some way to distinguish and differentiate the miRNA pathway and the avRNAi response will be

required. Such a distinction has been found in *C. elegans* and *D. melanogaster*, and has allowed for better characterization of an antiviral-specific pathway. A proteomic analysis of Dicer-associated proteins following stimulation with viral RNA and synthetic dsRNA might provide a clue, as this was how DRH-1 was discovered to be an important cofactor to Dicer in worms [93].

Other techniques would include the use of labelled RNA, which could be followed by microcopy or co-IP as it gets shuttled into the different antiviral pathways and interacts with the specific RNA-binding proteins of each. A long synthetic or virus-derived RNA molecule could be multiply-labelled with radiation or high-quantum-yield fluorophores and transfected into the cells. These molecules could then be UV-crosslinked to whichever proteins they are bound, and then precipitated out. Mass spectrometric analysis or western blotting of the bound proteins could demonstrate which pathways are being engaged immediately after detection.

Alternatively, as has been shown previously, blocking type I IFN activity *in vitro* with a neutralizing antibody against the type I IFN receptor IFNAR is a possible solution. In the context of an inactive type I IFN response, I would expect that any avRNAi activity would persist longer, and perhaps allow for the small RNA hallmarks of this pathway to reach detectable levels.

Single-cell pathway analysis

As my proposed mechanism involves studying the binding and processing of a small number of RNA molecules within a given cell, other single molecule imaging techniques could be employed. For RNA ligands like polyIC or viral RNA being transfected into cells, the direct labeling of RNA molecules with high-quantum-yield fluorophores could allow for detection of single RNA molecules by confocal microscopy. If these RNA molecules are then processed, a decrease in signal would be evident. Another possibility is to use Click-It technology (dispersed ethynyl uridine) to label newly synthesized viral RNA during the

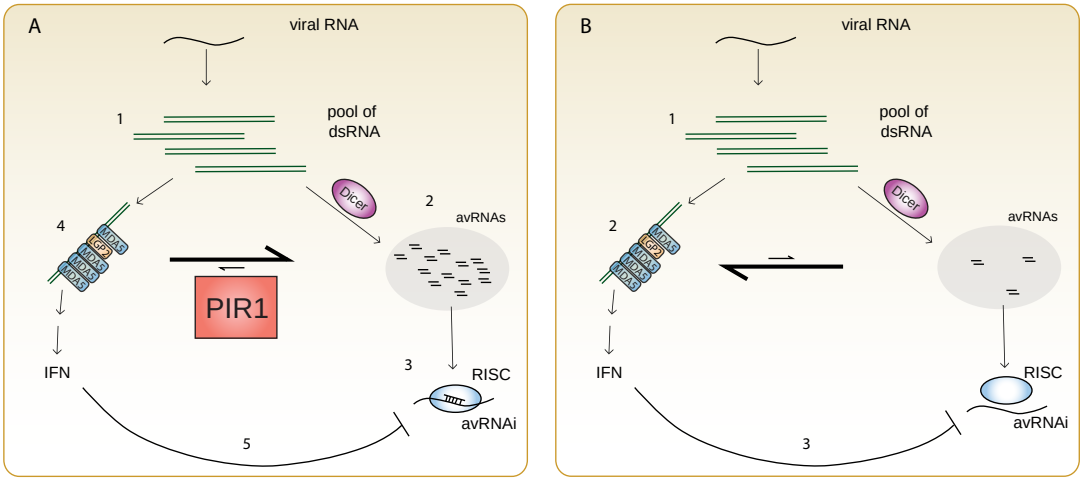

Figure 4.1: A proposed model for the role of PIR1 in the innate antiviral immune response. PIR1 affects the kinetics of dsRNA sensing via the RLR:MAVS signaling pathway. PIR1 antagonizes this pathway in the minutes to hours after the introduction of a stimulatory RNA molecule. At 2 hours, PIR1KO cells show increased IRF3 phosphorylation and increased type I IFN signaling. PIR1KO and wild-type cells appear equivalent by 4 hours. There are a number of mechanisms by which PIR1 could be affecting the several components of this pathway, and discovery of the exact mechanism will be the focus of future investigation. (A) Reconciling my results with current evidence of a complementary role for antiviral RNA interference (avRNAi) in mammalian cells, and the evidence put forward by Daniel Chaves that PIR1 is a critical component of an efficient and effective avRNAi response in *C. elegans*, my model hypothesizes that PIR1 promotes an avRNAi response at the earliest moments of infection. Upon the introduction of viral dsRNA into a cell (step 1), this RNA is first shuttled into the avRNAi pathway (step 2), where it gets processed and employed as antiviral molecules (step 3). If the avRNAi mechanism proves unsuccessful and enough dsRNA accumulates within the cell, the MDA5:LGP2:IFN pathway is activated (step 4). The type I IFN response, then negatively regulates the avRNAi response (step 5). (B) In the case of a PIR1KO cell, since PIR1 is not present to promote early avRNAi processing, the activation of MDA5:LGP2:IFN signaling (step 2) occurs earlier.

course of an infection. Watching the fate of these RNA molecules during infection and assessing their length based on signal intensity might allow for the detection of dsRNA cleavage in real-time.

Various deep sequencing techniques might also be used to shed light on this problem. Single-cell sequencing would allow for the identification and characterization of ligand and ligand-derived RNA molecules during the course of stimulation. When IFN is neutralized in culture, an immunostimulatory RNA could be transfected and then at specific time points post transfection, cells could be isolated and used to generate a single-cell-labelled library of small RNAs. Another approach might include targeting the sequencing of specific RNA motifs. CAP-Seq [214] would allow for the isolation of 5'-triphosphorylated RNA, and dsRNA-Seq could allow for the isolation of dsRNA molecules.

Furthermore, crosslinked-immunoprecipitation experiments, as have been done with various RNA-binding proteins in the past, could be carried out with a panel of RNA-binding proteins involved in both of these pathways. PACT, TRBP, Dicer, and LGP2, should each be investigated, and studied for which RNA molecules are bound to each, and where they are localized in relation to the RLR and avRNAi components. It might be that a high-throughput proteomics approach, as has been applied to the type I IFN pathway [215], could be employed to probe the RNA processing pathways as a network with and without IFN antagonism, in a more systematic manner.

4.1.3 Finding the relevance of avRNAi in mammals

A final question is why an alternative, less potent, suppressible, antiviral pathway would persist in mammalian systems. One reason could be to protect the cell from endogenous retroviruses—also known as retrotransposons—and other endogenous sources of dsRNA that if left unchecked could affect genome stability. Another possibility is that avRNAi may help respond to the multitudes of nonpathogenic viral RNA that we encounter daily. RNA phages present in the gut and on skin have been recovered in various organs including

the spleen, suggesting that while they are not able to trigger productive infections, phages can expose host cells to foreign nucleic acids [216]. Even plant viruses, which are regularly consumed along with their hosts, could present foreign RNA to our cells.

Additionally, it has been shown that some pathogenic viruses are recoverable from otherwise healthy people. Various rhinoviruses, coronaviruses, and adenoviruses are found in the nasopharnyx of children who exhibit no signs of an illness or infection [217], suggesting that we are constantly exposed to many viruses. Perhaps an avRNAi response could serve as a early defense in these situations where cellular processes do not need to be disrupted and cytokine signaling does not need to be induced.

Also worth considering is the phenomena of chronic or latent infections, in which a virus is able to withstand or shut down the host's defenses and persist for extended periods of time. A viruses might be able to utilize the antagonism between the avRNAi pathway and the type I IFN pathway to negatively regulate both, allowing it to remain in a cell undetected. Perhaps better understanding of the role of avRNAi here could lead to new treatments for chronic infections.

Finally, arboviruses are a group of arthropod-borne viruses that are able to productively infect both insects and mammals. These viruses include west-nile virus, chikungunya, and zika virus, all of which are transmitted by mosquito. As the mosquito is related to the fruit fly, it possesses many of the same antiviral mechanisms that are so well studied in *D. melanogaster*. As arboviruses have adapted a genome and set of proteins that are able to inhibit and circumvent insect avRNAi, they could be doing the same while infecting their human hosts.

Overall, a better understanding of how viruses interact with RNA-processing pathways will allow for a better understanding of virus:host interactions, and hopefully will uncover new mechanisms for antiviral therapies.

4.2 On the role of CD200R1 and TLR2 signaling in HSV replication

In the isolated and critically-sensitive environment of the central nervous system, there exists a delicate balance between the anti-inflammatory pathways protect the brain in case of aberrent inflammation and the pro-inflammatory pathways ready to defend against against pathogenic infections. In herpes simplex encephalitis, this balance is disrupted, leading to inflammation and viral replication, both of which lead to damage.

After infecting a cell, HSV-1 initiates an intricate series of signaling events that ultimately leads to viral replication. At the same time the infected host cell detects the viral pathogen and triggers antiviral and inflammatory responses. Here we have shown that in order for HSV-1 to replicate optimally, a certain amount of host detection and inflammation is required.

In studying the role of the anti-inflammatory signaling receptor CD200R1, I discovered that HSV-1 requires CD200R1 to properly replicate within the CNS. I further demonstrated that CD200R1 actively promotes TLR2 signaling, and in this way facilitates efficient viral gene expression during the viral replication cycle. My data show that CD200R1 is required for TLR2 upregulation in macrophages and for TLR2-dependent signaling leading to the production of specific inflammatory cytokines and chemokines. Without this signaling, HSV-1 replication appears to stall at the stage of α (immediate-early) gene expression. Finally, I showed that this HSV-1 replication phenotype in CD2001-/- cells can be rescued by either ectopic CD200R1 expression or TLR2 expression, suggesting that TLR2 functions downstream of CD200R1, and is required for efficient HSV-1 replication.

4.2.1 NF-κB signaling and HSV replication

During the course of infection, HSV-1 interacts extensively with innate immune signaling pathways. Frequently, HSV-1 proteins will actively antagonize defense pathways, but in the case of NF-κB signaling, HSV-1 actually promotes its activation. NF-κB signaling

during HSV-1 replication is known to increase levels of viral replication by delaying host cell apoptosis [218,219]. HSV-1 activates NF-κB signaling by engaging TLR2 on the cell surface [8]. Additionally HSV-1 can also activate NF-κB via the viral protein U_L37, which signals through TRAF6 to turn on NF-κB [220]. Several studies *in vivo* have found that inhibition of pro-inflammatory pathways actually limits disease and replication following infection with HSV-1 [221]. Additionally, a lack of TLR2 has also been shown to result in better disease outcomes following infection with HSV-1 in the brain [179].

With respect to CD200R1 and HSV, my data show that CD200R1 is required for HSV-1 induced production of IL-6 and IL-1β. In CD200R-/- mice, the defect in inflammatory signaling is likely the cause of defective HSV-1 replication via the decreased capacity for HSV-1 viral gene expression.

The mechanism by which CD200R1, an anti-inflammatory signal receptor, promotes this pro-viral inflammatory signal following infection with HSV-1 is still not know but the most promising explanation, based on my data, is through an effect on TLR2 expression.

4.2.2 TLR2 upregulation

TLR2 upregulation is a well documented phenomena observed following the activation of many TLR molecules, including TLR2 itself [186,187]. The exact mechanism of TLR2 upregulation is not fully characterized, and is likely cell-type and signaling pathway specific. It has been shown that TLR-mediated upregulation of TLR2 is dependent on MyD88 [186] and NF-κB [188], with the TLR2 promoter having two NF-κB sites, two CCAAT/enhancer binding protein sites, one cAMP response element-binding protein site, and one STAT consensus sequence site. The importance of each of these sites in the TLR2 promoter is cell-type specific, but frequently the two NF-κB binding sites are critical in turning on TLR2 gene expression [188].

CD200R1-/- cells are unable to upregulate TLR2 following infection with HSV-1, and produce significantly reduced levels of IL-6 following stimulation with HSV-1 or the TLR2

agonist Pam2CSK4. Since TLR2 upregulation is NF-κB driven, this TLR2 signaling phenotype present in CD200R1-/- cells possibly could be caused by reduced levels of NF-κB activation during early viral infection. Since we found that the induction of TLR2 fails in CD200R1-/- cells, but also that TLR2 over expression is sufficient to rescue the HSV-1 replication phenotype, it seems reasonable that might be that CD200R1 is a critical upstream factor for TLR2-mediated NF-κB activation and TLR2 upregulation. Further investigation of NF-κB activation in CD200R1-/- cells would allow us to better understand whether this is true. It is also possible that NF-κB activation during HSV-1 infection is a result of another innate immune pathway (TLR3 or an intracellular DNA receptor like cGAS), with that pathway leading to CD200R1-dependent upregulation of TLR2. However, the fact that CD200R1-/- PECs failed to generate IL-6 following stimulation with Pam2CSK4 indicates that CD200R1 is directly affecting some part of the TLR2 pathway. Taken together, it seems most plausible that CD200R1 facilitates TLR2-driven TLR2 upregulation.

As the TLR2 promoter contains binding sites for other transcription factors, it is possible that CD200R1 exerts its effect on TLR2 upregulation via one of these other transcription factors instead. Future investigation of TLR2 promoter region activity, during HSV infection could yield additional components involved in the C200R1:TLR2 pathway.

Finally, one limitation of my work is that I only measured TLR2 upregulation based on the surface expression of TLR2. It is possible that CD200R1 is affecting TLR2 protein localization instead of gene expression. TLR2 has been found in the endolysosome [222], and so the localization of TLR2 before and after stimulation in wild-type and CD200R1-/- cells should be studied to clarify this point. By using confocal microscopy, it might be possible to show if CD200R1 is responsible for shuttling TLR2 receptors to the cell surface following stimulation.

4.2.3 HSV signaling and TLR2

Certain strains of HSV-1 are known to be potent activators of TLR2. The glycoproteins on the viral envelope can be direct ligands that engage with and activate TLR2 [8]. Furthermore, TLR2 has been found in mouse models of HSE, to be a critical mediators of neuroinflammation. TLR2-/- mice were found to have a less severe disease, with less brain inflammation when compared to wild-type animals [179]. Here I have found that TLR2, like CD200R1, is an important host factor for viral replication *in vitro* (Figure 3.15 on page 115). TLR2-/- MEFs have reduced levels of ICP8 expression, suggesting a defect in the expression of certain viral genes, presumably due to a lack of TLR2-mediated activation of transcription factors, such as NF-κB, required for efficient viral gene expression.

More recently, TLR2 has been shown to activate type 1 IFN signaling in cooperation with the integrin αvβ3, following stimulation with HSV-1 or soluble HSV glycoproteins gH/gL [10,11]. These results suggest that TLR2 has a role in IFN signaling independent of its role in NF-κB activation. The engagement of TLR2 during an HSV-1 infection might have more wide-spread effects on inflammatory and antiviral signaling than previously thought. Investigations into whether integrin-associated TLR2-induction of type 1 IFN is also impaired in CD200R1-/- cells might help identify how CD200R1 is affecting TLR2 signaling.

4.2.4 How does CD200R1 affect TLR2 signaling and upregulation?

CD200R1 has been most studied for its anti-inflammatory activity. Binding of CD200R1 on macrophages with the ligand CD200 is well known to lead to suppressed production of pro-inflammatory cytokines [223]. How CD200R1 transmits this signal after binding it ligand is less clear. Upon engagement with it ligand, CD200R1 becomes phosphorylated on several tyrosine residues within its cytoplasmic tail. This phosphorylation event then leads to the recruitment and phosphorylation of the adaptor molecules Dok1 and/or Dok2 [20]. These Dok molecules subsequently recruit SH-2 domain protein SHP-1 [19]. SHP-

1 then activates RasGAP which functions as a negative regulator of Ras signaling. In macrophages Dok1 and RasGAP are critical mediators of CD200R1 signaling [19]. Independent of CD200R1 signaling, following LPS treatment of macrophages, Dok1 and Dok2 were found to be negative regulators of TNF-α and NO production through the negative regulation of the kinase ERK [22]. In fact Dok1-/- or Dok2-/- macrophages have increased levels of TNF-α and NO without stimulation, suggesting that these Dok proteins negatively regulate pro-inflammatory signals at baseline [224].

Ras and ERK are both MAP kinases that are thought to facilitate the activation of many pro-inflammatory processes in macrophages and other cell types by promoting the production of certain cytokines. Dok1 and/or Dok2 affect RAS and ERK signaling presumably via RasGAP activation, with RasGAP being a well-documented negative regulator of these kinases [225]. Interestingly, RasGAP has been found to directly regulate NF-ϰB activity as well. RasGAP has been shown to facilitate the retention of IϰBα and NF-ϰB complexes in the cytoplasm, affecting nuclear tranlocation and potentially NF-ϰB activation [23]. It is possible that CD200R1 is able to promote TLR2 signaling or TLR2 upregulation via Dok and RasGAP signaling,

Some evidence already exists linking the CD200R1 pathway with the TLR2 pathway specifically in the CNS. Astrocytes and microglia—two types of glial cells in the brain—express TLR2, and respond to TLR2 stimulation. Following TLR2 stimulation in these cells, Dok1 and Dok2 are phosphorylated. Additionally, knockdown of Dok1 or Dok2 in astrocytes cells leads to increased levels of IL-6 production following with the TLR2 ligand Pam2CSK4 stimulation. In microglia, a similar result was seen with Dok2 knockdown, while knockdown of Dok1 was found to be anti-inflammatory [226]. The fact that TLR2 stimulation leads to the activation of the Dok proteins, which themselves limit TLR2 signaling, again support the connection between CD200R1 and TLR2.

4.2.5 A general model for how CD200R1 affects TLR2 signaling and HSV-1 replication.

Synthesizing our results and the current literature on TLR2 and CD200:CD200R1 signaling, I have developed a model for how CD200R1 might affect TLR2 activation and HSV-1 replication (Figure 4.2). In this model, HSV-1 stimulates TLR2 activation during infection. This signaling activates NF-κB and other inflammatory processes which result in the production of inflammatory cytokines, the efficient expression of certain viral genes, and the upregulation of TLR2. CD200R1, via its intracellular domain and its signaling partners Dok1 and/or Dok2, presumably promotes this initial NF-κB activation. Without CD200R1, TLR2 mediated NF-κB activation is severally limited, resulting in lower levels of inflammation, and also lower levels of viral replication.

However, further work is required to precisely identify where in this process CD200R1 or CD200R1 signaling exerts its effect. It is possible that baseline activity of CD200R1 and its signaling partners directly affect NF-κB activity. This could be tested by assaying NF-κB activation following HSV-1 infection in wild-type and CD200R1-/- cells. IκB levels in the cytoplasm and NF-κB levels in the nucleus could be assayed to determine whether CD200R1-/- cells have more or less activation of this transcription factor. Additionally, since CD200R1 is implicated in the regulation of certain MAP kinases via its affect on RasGAP, and ERK signaling has been shown to be an important mediator of TLR2 signaling ([227–230]. The activity levels of Ras and ERK should be assayed in wild-type and CD200R1-/- cells to assess their requirement in this pro-viral process.

It is important to consider that baseline levels of CD200R1 activity do exist, as does baseline activity of Dok1 and Dok2 [224]. Therefore these molecules might be signaling to some degree without any pathogenic stimulus. As a result, the downstream signaling molecules Dok1 and Dok2 are excellent candidates for future studies. If ectopic expression of either or both of these molecules rescues the HSV-1 and TLR2 phenotypes of CD200R1-/-

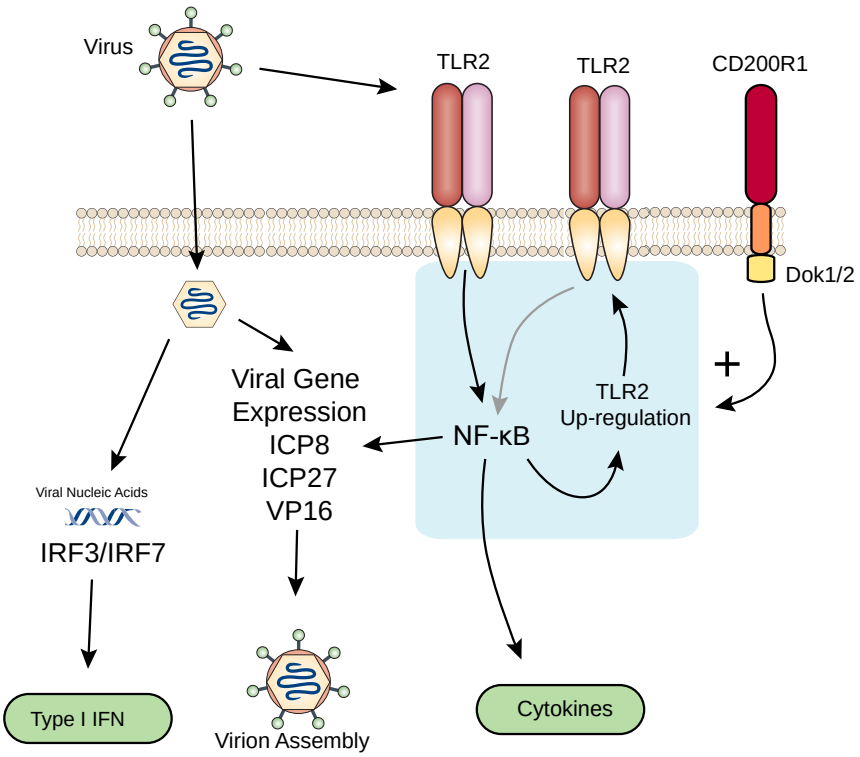

Figure 4.2: A model for the role of CD200R1 is TLR2 signaling and HSV-1 replication. HSV-1 is activates TLR2 on the cell surface early on in the infection. This signaling results in both an upregulation of TLR2 and the effective expression of various HSV-1 genes. CD200R1 facilitates this TLR2-mediated upregulation and inflammation process. The direct mechanism by which CD200R1 exerts this effect is open to further investigation.

cells, this would suggest that these proteins are part of the direct link between CD200R1 and HSV-1 replication.

Further studies could also pinpoint if the primary effect of CD200R1 signaling is on transcription, translation, or localization of TLR2 following stimulation. TLR2 is also know to localize to several different regions within the cell, including the outer membrane, phagocytic clefts, and the early and recycling endosome [231–233]. CD200R1 could affect TLR2 signaling by promoting its localization to a compartment where it will it will specifically be activated during HSV-1 infection. Investigating the distribution and location of TLR2 in wild-type and CD200R1-/- cells would allow a better understanding of the dynamics and importance of TLR2 localization during early infection.

4.2.6 The role of CD200R1 and TLR in herpes simplex encephalitis *in vivo*

It is clear from our studies that within the CNS, CD200R1 is a critical mediator of HSV-1 replication. While my *in vitro* studies suggest that the result of CD200R1 on HSV-1 replication is a result of TLR2 upregulation or signal amplification, we do not yet have clear evidence that this is also true *in vivo*. The functions of Dok1 and Dok2 are different between astrocytes and microglia, with Dok1 being pro-inflammatory in both, but Dok2 being anti-inflammatory in microglia and pro-inflammatory in astrocytes [226]. Subtle differences like these, and all of the other unique features of the CNS, demonstrate why further work is required to generalize our *in vitro* findings to the HSE model, and to conclude that TLR2 *in vivo*is responsible for decreased HSV-1 replication in the CNS of CD200R1-/- mice.

Finally, previous studies in our lab have shown the TLR2-/- mice survive better when compared to wild-type mice following intraperitoneal [145] or intracranial [179] infection with HSV-1, however, neither of these studies showed significant differences in viral titer in TLR2-/- mice when compared to wild-type mice. This discrepancy might be a result of differences in study design, but it might also suggest that the effect of CD200R1 on HSV-1 replication specifically within the CNS involves a mechanism separate from its effect

on TLR2 signaling. In order to better understand this apparent difference, CD200R1-/- mice could be injected intracranially with TLR2 ligands to test whether TLR2 is active in the CNS of these mice. Additional studies could include examining cultured neurons and microglia from CD200R1-/-, TLR2-/-, and wild-type mice for their ability to support and respond to HSV-1 replication. Lastly, the *ex vivo* infection of brain sections with HSV-1, a technique previously used to assess the regional tropism of HSV-1 within the CNS [234], could be valuable to tease out CNS-specific effects of CD200R1 and TLR2 on HSV-1 replication.

4.3 Conclusion

The work presented here ultimately demonstrates the role of two proteins on two disparate facets of the innate immune system. PIR1, being an ancient protein that is shared between humans and nematodes, potentially offers a key into better understanding how the evolutionarily conserved small RNA antiviral pathways interact with the newer type 1 IFN pathways found in vertebrates.

CD200R1, in contrast is a signaling molecule that plays an important role in modulating cellular immunity, however it appears to promote the replication of Herpes Simplex through the potentiation of TLR2 signaling.

Taken together, the cases of PIR1 and CD200R1, highlight how intricate and intertwined host pathways and viral replication are. This is not surprising given that we have evolved together for millennia. Common pathogenic viruses have evolved to replicate effective within the context of our immune systems, meaning that while our immune systems are generally good at clearing an infection in time, it is not good at preventing the virus from successfully replicated itself and spreading to our family and friends. What this does mean however is that perturbations to this delicate homeostasis can be fatal, either to the virus or to the host. It also means that perhaps some of the most worrisome pathogens are not those that are well known to infect humans like the flu, but are those that have not yet been discovered. New and emerging viruses are likely to surface with increasing frequency, as has already been seen with Ebola, SARS, MERS, Chikungunya, Zika, and others. These new viruses, which are not adapted to human hosts, are likely to interact with our immune systems in novel ways.

Appendix **I**: **Additional PIR1KO data**

A.1 Introduction

The following data are from experiments conducted with partially backbred mice (N=6). Any results herein should be verified in the fully backbred strain of PIR1KO mice. At N=6, the PIR1KO mice still carried many 129-derived SNPs in chromosome 4, which is the home if the type 1 IFN locus where many type 1 IFN genes include IFN-β and IFN-α are located. The use of littermate control whenever possible, should have mitigated much of the variability introduced by the mixed background, but as littermate are siblings they do not share their entire genome. It is likely that mixed background difference would still exists between littermate mice.

A.2 Materials and Methods

A.2.1 Influenza A virus infection of mice

The Influenza A strain used was the mouse-adapted strain PR8. For infection, an aliquot of virus was thawed on ice, and then diluted in sterile PBS. Mice were then inoculated at a dose of either 2000 pfu/mouse or 4000 pfu/mouse by an intrapharangyeal inoculation. Mice were infected in the morning. For the weight-loss study, mice were weighed prior to infected, and then weighed once a day at same time each morning for 10 days. For the survival study, mice were check for every 12 hours for death or moribundity.

A.2.2 *Listeria monocytogenes* infection and bacteria recovery from organs of infected mice

L. monocytogenes *stock preparation*

The streptomycin-resistant, wild-type 10403s strain of *L. monocytogenes* was generously donated by Kate Fitzgerald Ph.D. (University of Massachusetts Medical School; Worcester, MA, USA). A BALB/c mouse was inoculated intravenously with 400μL of 1×10^4 cfu of this bacteria. After 24 hours, this mouse was euthanized, the spleen was dissected out and place into 2 mL of H_20 with 0.02% Triton-X. The spleen was then lysed mechanically using the Qiagen TissueRuptor. This lysate was diluted and streaked onto a Tryptic Soy Broth (TSB) agar plate with 50 μg/mL of streptomycin, and growth overnight at 37°C.

A single colony was picked, and grown in 5mL of TSB overnight. The next day, this inoculum was added to 95mL of TSB and grown to an optical density (OD) at 600 nm was around 0.2-0.4 (generally an OD of 0.2 yields a titer around 5×10^7 cfu/mL). Once the target OD was achieved, the culture was spun down at 10,000×g for 15 minutes. Pelleted bacteria were resuspended in TSB with 15% glycerol, dispensed into 1mL aliquots in 2 mL cryogenic vials, and immediately placed into a -80°C freezer. After a day or two at -80°C, 2 to 3 aliquots were thawed for titer determination. Each aliquot was thawed on ice for 30

minutes, added to 9 mL of TSB, placed into a 125 mL Erlenmeyer flask, and grown at 37°C with shaking at 200 rpm for 1 hour. This culture was then centrifuged at 10,000×g for 10 minutes, the supernatant was removed, and the pellet was resuspended in 1 mL of sterile PBS.

Inoculation of mice with L. monocytogenes

A 1 mL aliquot of stock with a known concentration of bacteria was thawed on ice for 30 minutes, added to 9mL of TSB in a 125 mL Erlenmeyer flask, and incubated for 1 hour at 37°C with shaking at 200 rpm. This culture was centrifuged at 10,000×g for 10 minutes, the supernatant was removed, and the pellet was resuspended in 1mL of sterile PBS. The stock was diluted further with sterile PBS to a concentration of 1×10^5 cfu/mL.

Mice were then inoculated by tail-vein injection with 300 µL of the 1×10^5 cfu/mL, 3×10^4 cfu/mouse.

Recovery of L. monocytogenes *from infected animals*

At the specified time point post inoculation with *L. monocytogenes* tissue samples were collected in order to assay the bacterial burden. Organs were collected into pre-weighted 5 mL round-bottom polystyrene tubes containing 1.5 mL of sterile H_2O with 0.02% Triton-X and kept on ice.

The mice were euthanized and liver and spleen were collected and placed into the 5mL tubes on ice. These tubes were weighed once again to determine the mass of tissue collected.

The tissues were then mechanically lysed using the Qiagen TissueRuptor. The TissueRuptor probe was washed and equilibrated by submerging and running it in 80% ethanol, H_2O, then H_20 with 0.02% Triton-X between each sample.

Measuring L. monocytogenes *concentration*

To determine the concentration of *L. monocytogenes* in tissue lysates or bacterial stocks, samples were serially diluted 1:5 in H_2O in a 96-well round-bottom plate. 5 µL of each dilution was then dropped onto duplicate TSB agar plates with streptomycin. After incubating these plates overnight at 37°C, colonies were counted, and cfu/mL values of the original solution were calculated. For tissue lysates these cfu values were then calibrated by dividing the mass of tissue from which each sample was derived, to arrive at a cfu per mL per gram of organ value (cfu mL^{-1} g^{-1}).

A.2.3 HITS-CLIP

HITS-CLIP analysis was performed on with mouse pan-Ago pulldown, on samples generated from bone-marrow-derived-macrophages stimulated with EMCV for 6 hour. The HITS-CLIP protocol was carried as described in [235] and [236]

A.3 Results

A.3.1 Investigating the role of PIR1 in other models of infection

Mouse model of infection with Listeria monocytogenes *Listeria monocytogenes* is an intracellular facultative anaerobe that can cause enteritis and encephalitis in children, adults, and especially fetuses. It is know that *L. monocytogenes*, since it is an intracellular pathogen, activates several intracellular PRRs as it infects a cell. In particular, *L. monocytogenes* has been shown to activate the type 1 IFN pathways via LGP2 and MDA5 [237]. Having evolved to grow inside human cells, *L. monocytogenes* has actually adapted to using the type 1 IFN response to its advantage, with decreased type 1 IFN signaling leading to slower bacterial replication and lessened disease.

To test whether PIR1, which is known to interact with LGP2 (see Figure 2.3), has any role in *L. monocytogenes* infection, I inoculated littermate control and PIR1KO mice with *L. monocytogenes* by intravenous injection, and assessed bacterial growth at 24 hours and 48 hours after infection. Spleen and liver samples were collected from each mouse, lysed, and live bacteria collected. The bacteria was then titered by serial dilution on TSB/streptomycin plates.

As can be seen in Figure A.1, at 48 hours post infection, the PIR1KO mice show a marked decreased in recovered *L monocytogenes* colonies from both the liver and spleen. This result suggests that PIR1KO plays an important role in promoting *L monocytogenes* infection in the mouse. Future studies should investigate whether this phenotype is a results of a lack of type 1 IFN signaling—as I originally hypothesized—or whether PIR1 is playing a different role.

Type 1 IFN is critical for supporting *L. monocytogenes* replications [238], and is stimulated by the activation of the RLR receptor LGP2 [237], presumably by the production of immunostimulatory RNA from bacterial DNA via cytosolic RNA polymerase III [155,237,239]. As this pathway for type 1 IFN involves RNA polymerase III (RNApolIII) products—known

ligands of PIR1 [96]—it stands to reason that PIR1 would likely play a role. However, the data presented in Figure A.1 would suggest that the removal of PIR1 limits type 1 IFN production. It is possible that the RNApolIII products, being fundamentally different from virus-derived RNAs, requires some amount of dephosphorylation or shuttling into the RLR pathway in order to properly stimulate an IFN response.

Mouse model of infection with Influenza A Virus Influenza A virus ([IAV]) is a human pathogenic orthomyxovirus (negative sense ssRNA), which elicits a robust innate immune response upon entering a cell. Since IAV is know to produced triphosphorylated RNAs during the course of infection, I chose to investigate whether PIR1 plays a role. PIR1 is hypothesized to function in processing viral RNAs, so I thought that PIR1KO mice would show more severe disease following inoculation with IAV.

We infected littermate control and PIR1KO mice with IAV by intrapharangyeal inoculation, and monitored death and weather loss. As can be seen in Figure A.2, the PIR1 KO mice do show some differences in disease progression. While the littermate control and PIR1KO mice show similar mortality rates, the PIR1KO actually exhibit significant less weight loss, and actually begin gaining weight as the disease progresses.

This is a counterintuitive result, and suggests that the mechanism of weight loss (which is often used as a surrogate measure for IAV disease severity) might be separate from the infectious processes ultimately responsible for mortality. The cause of IAV-induced weight loss in the mouse models is thought to be a consequence of cytokine-induced anorexia (which can be partially rescued by administration of a cyclooxygenase-2 inhibitor) [240], meaning that a decrease in circulating inflammatory cytokines without a concomitant decrease in lung damage and edema could theoretically lead to a less severe weight-loss phenotype without any observable difference in survival.

If PIR1 modulated viral progression, affecting the infection efficiency in certain tissues or cell types, its possible that the damage and lung dysfunction responsible for mortality could persist, while the mechanism for weight loss is mitigated, whether it be diffuse cy-

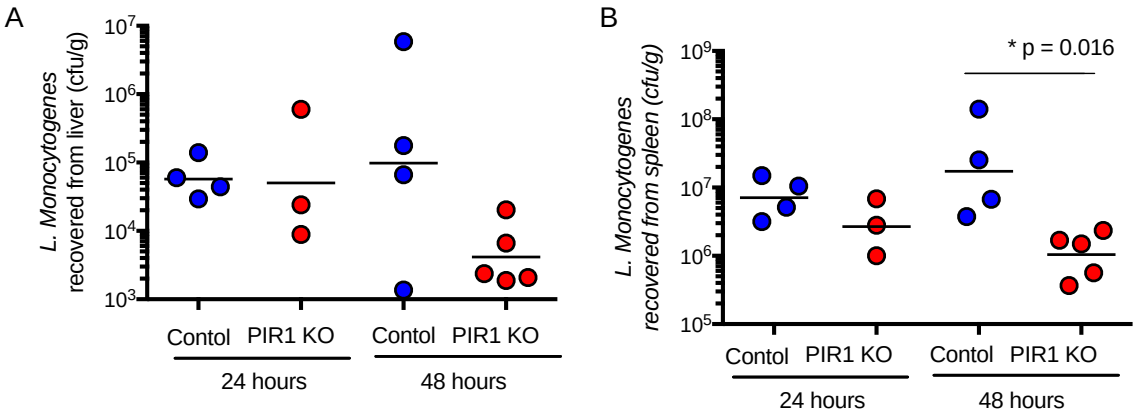

Figure A.1: PIR1-deficient mice show decreased rates of *L. monocytogenes* growth following infection. PIR1KO (N=6) and littermate control mice were each infected with *L. monocytogenes* by intravenous injection and organs were collected at 24 and 48 hours post infection. The burden of bacteria was then measured in each organ. Each ● represents a control mouse, each ● represents a PIR1KO, and for each group the geometric mean is also displayed. Control and PIR1KO groups were analyzed using the Mann-Whitney U test.

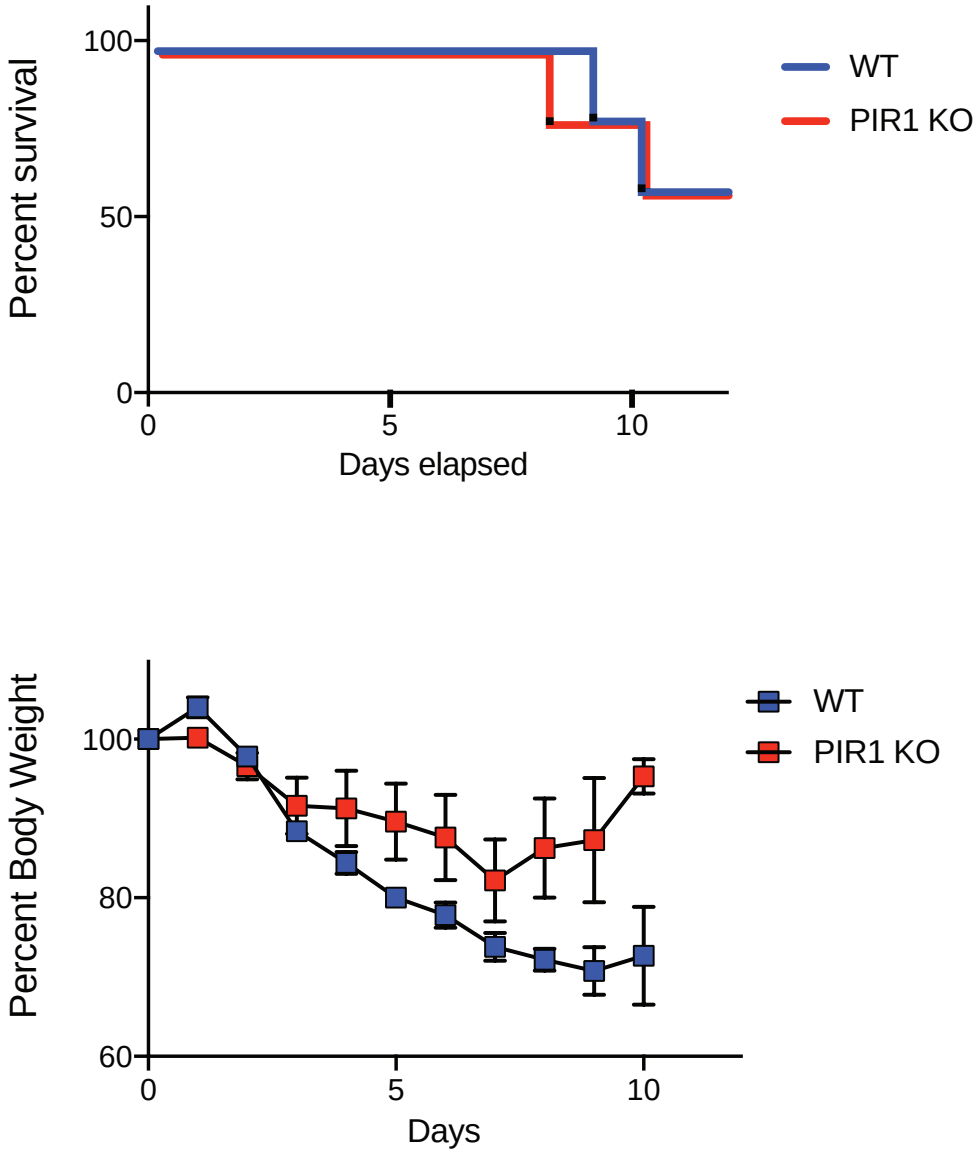

Figure A.2: PIR1-deficient show less weight loss, but similar survival kinetics following infection Influenza A. PIR1KO (N=6) and littermate control mice were infected with IAV PR8 by intrapharangyeal inoculation. Five mice per genotype were infected with 4000 pfu of influenza A virus (PR8 strain). (A) The ■ represents the mean weight loss of the littermate control mice, and ■ represents the mean weight loss of the PIR1KO mice. Error bars represent SEM.

tokine production, immobility. Future studies should look to repeat these experiments while monitoring for serum cytokine levels and assessing mouse mobility over the course of the infection. Additional studies to collect lung samples from IAV-infected mice and measure inflammation cytokine production and/or IAV replication in the lungs should also be done. I would hypothesize that there would not be much of a difference in the lung, as this would contradict the lack of a survival phenotype, as seen in Figure A.2.

A.3.2 High-throughput sequencing of argonaute-associated RNA molecules

Performing HITS-CLIP (high-throughput sequence cross-linked immunoprecipitation) with a pan-Argonaute antibody, I isolated and sequenced the RNAs fragments associated with an argonaute protein following infection with EMCV. Following sequencing the ago-associated sequences were aligned to the EMCV genome. As can be seen Figure 4.3, there does appear to a differential levels of EMCV-derived small RNAs bound to argonaute proteins, with PIR1KO showing substantially higher levels of RNA derived from certain regions of the EMCV genome, particularly in and round the L region.

While this experiment needs to be repeated, it does suggest that PIR1KO cells generate and load into RISC a different repertoire of virus-derived RNA molecules. As reads were normalized to all aligned reads, and I have previously seen by direct probe ligation that PIR1KO cells at baseline

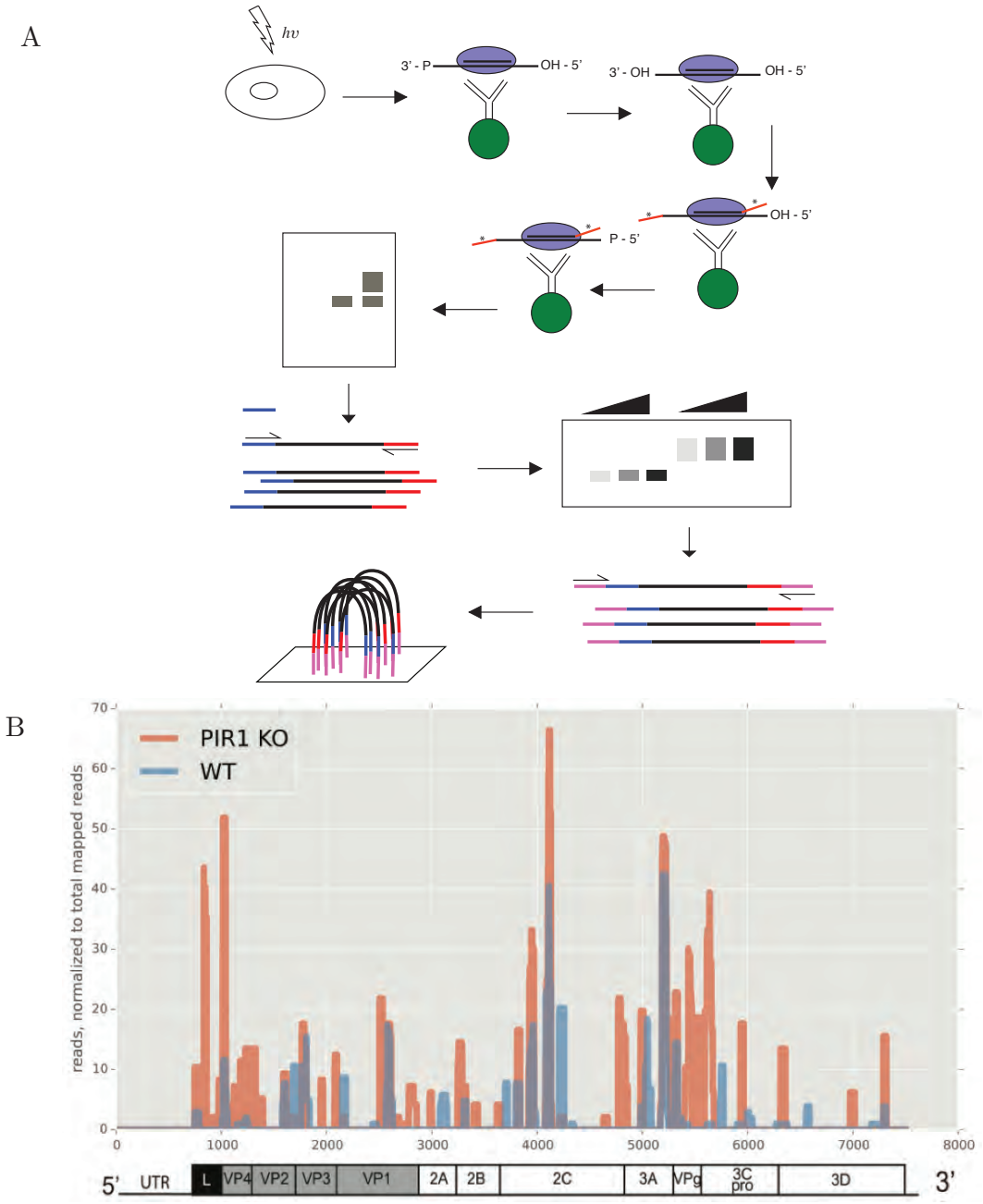

Figure 4.3: Analysis of argonuate-associated RNA molecules by HITS-CLIP. (A) An overview of the HITS-CLIP protocol. (B) all ago-associated RNA molecules which aligned to the EMCV genome were stacked along the genome. Reads were normalized to total mapped reads (mapped to the mouse or EMCV genomes). Blue tracks are aligned RNAs isolated from wild-type cells and red tracks are aligned RNAs isolated from PIR1KO cells. Positive and negative sense sequences are shown (positive sense above the x-axis and negative sense below the x-axis), but almost no negative sense sequences were found.

CHAPTER V: References

1. Rolfes MA, Foppa IM, Garg S, Flannery B, Brammer L, Singleton JA, Burns E, Jernigan D, Reed C, Olsen SJ, Bresee J. Estimated Influenza Illnesses, Medical Visits, Hospitalizations, and Deaths Averted by Vaccination in the United States [Internet]. 2016.

2. Janeway C, Travers P, Walport M, Shlomchik M. Immunobiology. 6th [Internet]. 2005.

3. O'Neill LAJ, Golenbock D, Bowie AG. The history of Toll-like receptors - redefining innate immunity. Nature reviews Immunology. 2013 Jun;13(6):453–460. PMID: 23681101 DOI: 10.1038/nri3446

4. Medzhitov R, Preston-Hurlburt P, Janeway CA. A human homologue of the Drosophila Toll protein signals activation of adaptive immunity. Nature. 1997 Jul;388(6640):394–397. PMID: 9237759 DOI: 10.1038/41131

5. Poltorak A, He X, Smirnova I, Liu MY, Van Huffel C, Du X, Birdwell D, Alejos E, Silva M, Galanos C, Freudenberg M, Ricciardi-Castagnoli P, Layton B, Beutler B. Defective LPS signaling in C3H/HeJ and C57BL/10ScCr mice: mutations in Tlr4 gene. Science (New York, NY). 1998 Dec;282(5396):2085–2088. PMID: 9851930

6. Takeuchi O, Kawai T, Mühlradt PF, Morr M, Radolf JD, Zychlinsky A, Takeda K, Akira S. Discrimination of bacterial lipoproteins by Toll-like receptor 6. International immunology. 2001 Jul;13(7):933–940. PMID: 11431423

7. Takeuchi O, Sato S, Horiuchi T, Hoshino K, Takeda K, Dong Z, Modlin RL, Akira S. Cutting edge: role of Toll-like receptor 1 in mediating immune response to microbial lipoproteins. The Journal of Immunology. 2002 Jul;169(1):10–14. PMID: 12077222

8. Leoni V, Gianni T, Salvioli S, Campadelli-Fiume G. Herpes simplex virus glycoproteins gH/gL and gB bind Toll-like receptor 2, and soluble gH/gL is sufficient to activate NF-κB. Journal of virology. 2012 Jun;86(12):6555–6562. PMCID: PMC3393584 DOI: 10.1128/JVI.00295-12

9. Casiraghi C, Gianni T, Campadelli-Fiume G. αvβ3 Integrin Boosts the Innate Immune Response Elicited in Epithelial Cells through Plasma Membrane and Endosomal Toll-Like Receptors. Journal of virology. 2016 Apr;90(8):4243–4248. PMCID: PMC4810540 DOI: 10.1128/JVI.03175-15

10. Gianni T, Leoni V, Campadelli-Fiume G. Type I interferon and NF-κB activation elicited by herpes simplex virus gH/gL via αvβ3 integrin in epithelial and neuronal cell lines. Journal of virology. 2013 Dec;87(24):13911–13916. PMCID: PMC3838217 DOI: 10.1128/JVI.01894-13

11. Gianni T, Leoni V, Chesnokova LS, Hutt-Fletcher LM, Campadelli-Fiume G.

αvβ3-integrin is a major sensor and activator of innate immunity to herpes simplex virus-1. Proceedings of the National Academy of Sciences of the United States of America. 2012 Nov;109(48):19792–19797. PMCID: PMC3511702 DOI: 10.1073/pnas.1212597109

12. Kenny EF, Talbot S, Gong M, Golenbock DT, Bryant CE, O'Neill LAJ. MyD88 adaptor-like is not essential for TLR2 signaling and inhibits signaling by TLR3. Journal of immunology (Baltimore, Md : 1950). 2009 Sep;183(6):3642–3651. PMID: 19717524 DOI: 10.4049/jimmunol.0901140

13. Wesche H, Henzel WJ, Shillinglaw W, Li S, Cao Z. MyD88: an adapter that recruits IRAK to the IL-1 receptor complex. Immunity. 1997 Dec;7(6):837–847. PMID: 9430229

14. Kawagoe T, Sato S, Matsushita K, Kato H, Matsui K, Kumagai Y, Saitoh T, Kawai T, Takeuchi O, Akira S. Sequential control of Toll-like receptor-dependent responses by IRAK1 and IRAK2. Nature immunology. 2008 Jun;9(6):684–691. PMID: 18438411 DOI: 10.1038/ni.1606

15. Keating SE, Maloney GM, Moran EM, Bowie AG. IRAK-2 participates in multiple toll-like receptor signaling pathways to NFkappaB via activation of TRAF6 ubiquitination. The Journal of biological chemistry. 2007 Nov;282(46):33435–33443. PMID: 17878161 DOI: 10.1074/jbc.M705266200

16. Deng L, Wang C, Spencer E, Yang L, Braun A, You J, Slaughter C, Pickart C, Chen ZJ. Activation of the IkappaB kinase complex by TRAF6 requires a dimeric ubiquitin-conjugating enzyme complex and a unique polyubiquitin chain. Cell. 2000 Oct;103(2):351–361. PMID: 11057907

17. Iwami KI, Matsuguchi T, Masuda A, Kikuchi T, Musikacharoen T, Yoshikai Y. Cutting edge: naturally occurring soluble form of mouse Toll-like receptor 4 inhibits lipopolysaccharide signaling. The Journal of Immunology. 2000 Dec;165(12):6682–6686. PMID: 11120784

18. Liew FY, Xu D, Brint EK, O'Neill LAJ. Negative regulation of toll-like receptor-mediated immune responses. Nature reviews Immunology. 2005 Jun;5(6):446–458. PMID: 15928677 DOI: 10.1038/nri1630

19. Mihrshahi R, Barclay AN, Brown MH. Essential Roles for Dok2 and RasGAP in CD200 Receptor-Mediated Regulation of Human Myeloid Cells. The Journal of Immunology. 2009 Oct;183(8):4879–4886. PMCID: PMC2788151 DOI: 10.4049/jimmunol.0901531

20. Mihrshahi R, Brown MH. Downstream of Tyrosine Kinase 1 and 2 Play Opposing Roles in CD200 Receptor Signaling. The Journal of Immunology. 2010 Dec;185(12):7216–7222. PMCID: PMC2999833 DOI: 10.4049/jimmunol.1002858

21. Zhang S, Phillips JH. Identification of tyrosine residues crucial for CD200R-mediated inhibition of mast cell activation. Journal of leukocyte biology. 2006 Feb;79(2):363–368.

PMID: 16330532 DOI: 10.1189/jlb.0705398

22. Shinohara H, Inoue A, Toyama-Sorimachi N, Nagai Y, Yasuda T, Suzuki H, Horai R, Iwakura Y, Yamamoto T, Karasuyama H, Miyake K, Yamanashi Y. Dok-1 and Dok-2 are negative regulators of lipopolysaccharide-induced signaling. Journal of Experimental Medicine. 2005 Feb;201(3):333–339. PMCID: PMC2213020 DOI: 10.1084/jem.20041817

23. Prigent M, Barlat I, Langen H, Dargemont C. IkappaBalpha and IkappaBalpha /NF-kappa B complexes are retained in the cytoplasm through interaction with a novel partner, RasGAP SH3-binding protein 2. The Journal of biological chemistry. 2000 Nov;275(46):36441–36449. PMID: 10969074 DOI: 10.1074/jbc.M004751200

24. Hoek RM, Ruuls SR, Murphy CA, Wright GJ, Goddard R, Zurawski SM, Blom B, Homola ME, Streit WJ, Brown MH, Barclay AN, Sedgwick JD. Down-Regulation of the Macrophage Lineage Through Interaction with OX2 (CD200). Science (New York, NY). 2000 Dec;290(5497):1768–1771. PMID: 11099416 DOI: 10.1126/science.290.5497.1768

25. Chen Z, Yu K, Zhu F, Gorczynski R. Over-Expression of CD200 Protects Mice from Dextran Sodium Sulfate Induced Colitis. PloS one. 2016;11(2):e0146681. PMCID: PMC4740450 DOI: 10.1371/journal.pone.0146681

26. Cortez M, Huynh C, Fernandes MC, Kennedy KA, Aderem A, Andrews NW. Leishmania Promotes Its Own Virulence by Inducing Expression of the Host Immune Inhibitory Ligand CD200. Cell host & microbe. 2011 Jun;9(6):463–471. PMCID: PMC3118640 DOI: 10.1016/j.chom.2011.04.014

27. Mukhopadhyay S, Plüddemann A, Hoe JC, Williams KJ, Varin A, Makepeace K, Aknin M-L, Bowdish DME, Smale ST, Barclay AN, Gordon S. Immune Inhibitory Ligand CD200 Induction by TLRs and NLRs Limits Macrophage Activation to Protect the Host from Meningococcal Septicemia. Cell host & microbe. 2010 Sep;8(3):236–247. PMID: 20833375 DOI: 10.1016/j.chom.2010.08.005

28. Deckert M, Sedgwick JD, Fischer E, Schlüter D. Regulation of microglial cell responses in murine Toxoplasma encephalitis by CD200/CD200 receptor interaction. Acta neuropathologica. 2006;111(6):548–558. PMID: 16718351 DOI: 10.1007/s00401-006-0062-z

29. Radoshevich L, Dussurget O. Cytosolic Innate Immune Sensing and Signaling upon Infection. Frontiers in microbiology. 2016;7(e1002934):313. PMCID: PMC4789553 DOI: 10.3389/fmicb.2016.00313

30. Onoguchi K, Yoneyama M, Fujita T. Retinoic Acid-Inducible Gene-I-Like Receptors. wwwliebertpubcom. 2011 Jan;31(1):27–31. DOI: 10.1089/jir.2010.0057

31. Wies E, Wang MK, Maharaj NP, Chen K, Zhou S, Finberg RW. Dephosphorylation of the RNA Sensors RIG-I and MDA5 by the Phosphatase PP1 Is Essential for Innate Immune Signaling. Immunity. 2013 Mar;38(3):437–449. PMCID: PMC3616631

DOI: 10.1016/j.immuni.2012.11.018

32. Davis ME, Gack MU. Ubiquitination in the antiviral immune response. Virology. 2015 May;479-480:52–65. PMCID: PMC4774549 DOI: 10.1016/j.virol.2015.02.033

33. Xu L-G, Wang Y-Y, Han K-J, Li L-Y, Zhai Z, Shu H-B. VISA is an adapter protein required for virus-triggered IFN-beta signaling. Molecular cell. 2005 Sep;19(6):727–740. PMID: 16153868 DOI: 10.1016/j.molcel.2005.08.014

34. Meylan E, Curran J, Hofmann K, Moradpour D, Binder M, Bartenschlager R, Tschopp J. Cardif is an adaptor protein in the RIG-I antiviral pathway and is targeted by hepatitis C virus. Nature. 2005 Oct;437(7062):1167–1172. PMID: 16177806 DOI: 10.1038/nature04193

35. Kawai T, Takahashi K, Sato S, Coban C, Kumar H, Kato H, Ishii KJ, Takeuchi O, Akira S. IPS-1, an adaptor triggering RIG-I- and Mda5-mediated type I interferon induction. Nature immunology. 2005 Oct;6(10):981–988. PMID: 16127453 DOI: 10.1038/ni1243

36. Seth RB, Sun L, Ea C-K, Chen ZJ. Identification and characterization of MAVS, a mitochondrial antiviral signaling protein that activates NF-kappaB and IRF 3. Cell. 2005 Sep;122(5):669–682. PMID: 16125763 DOI: 10.1016/j.cell.2005.08.012

37. Hou F, Sun L, Zheng H, Skaug B, Jiang Q-X, Chen ZJ. MAVS forms functional prion-like aggregates to activate and propagate antiviral innate immune response. Cell. 2011 Aug;146(3):461. PMCID: PMC3179916 DOI: 10.1016/j.cell.2011.06.041

38. McNab F, Mayer-Barber K, Sher A, Wack A, O'Garra A. Type I interferons in infectious disease. Nature reviews Immunology. 2015 Feb;15(2):87–103. PMID: 25614319 DOI: 10.1038/nri3787

39. Barik S. What Really Rigs Up RIG-I? Journal of innate immunity. 2016;8(5):429–436. PMID: 27438016 DOI: 10.1159/000447947

40. Peisley A, Wu B, Yao H, Walz T, Hur S. RIG-I forms signaling-competent filaments in an ATP-dependent, ubiquitin-independent manner. Molecular cell. 2013 Sep;51(5):573–583. PMID: 23993742 DOI: 10.1016/j.molcel.2013.07.024

41. Peisley A, Lin C, Wu B, Orme-Johnson M, Liu M, Walz T, Hur S. Cooperative assembly and dynamic disassembly of MDA5 filaments for viral dsRNA recognition. Proceedings of the National Academy of Sciences of the United States of America. 2011 Dec;108(52):21010–21015. PMCID: PMC3248507 DOI: 10.1073/pnas.1113651108

42. Wu B, Peisley A, Richards C, Yao H, Zeng X, Lin C, Chu F, Walz T, Hur S. Structural basis for dsRNA recognition, filament formation, and antiviral signal activation by MDA5. Cell. 2013 Jan;152(1-2):289. PMID: 23273991 DOI: 10.1016/j.cell.2012.11.048

43. Berke IC, Yu X, Modis Y, Egelman EH. MDA5 assembles into a polar helical filament on dsRNA. Proceedings of the National Academy of Sciences of the United States of

America. 2012 Nov;109(45):18437–18441. PMCID: PMC3494895
DOI: 10.1073/pnas.1212186109

44. Peisley A, Jo MH, Lin C, Wu B, Orme-Johnson M, Walz T, Hohng S, Hur S. Kinetic mechanism for viral dsRNA length discrimination by MDA5 filaments. Proceedings of the National Academy of Sciences of the United States of America. 2012 Dec;109(49):E3340–9. PMCID: PMC3523859 DOI: 10.1073/pnas.1208618109

45. Pichlmair A, Schulz O, Tan C-P, Rehwinkel J, Kato H, Takeuchi O, Akira S, Way M, Schiavo G, Reis e Sousa C. Activation of MDA5 requires higher-order RNA structures generated during virus infection. Journal of virology. 2009 Oct;83(20):10761–10769. PMCID: PMC2753146 DOI: 10.1128/JVI.00770-09

46. Lu H, Lu N, Weng L, Yuan B, Liu Y-J, Zhang Z. DHX15 senses double-stranded RNA in myeloid dendritic cells. Journal of immunology (Baltimore, Md : 1950). 2014 Aug;193(3):1364–1372. PMCID: PMC4108507 DOI: 10.4049/jimmunol.1303322

47. Bruns AM, Leser GP, Lamb RA, Horvath CM. The Innate Immune Sensor LGP2 Activates Antiviral Signaling by Regulating MDA5-RNA Interaction and Filament Assembly. Molecular cell. 2014 Aug; PMCID: PMC4156907
DOI: 10.1016/j.molcel.2014.07.003

48. Takahasi K, Kumeta H, Tsuduki N, Narita R, Shigemoto T, Hirai R, Yoneyama M, Horiuchi M, Ogura K, Fujita T, Inagaki F. Solution structures of cytosolic RNA sensor MDA5 and LGP2 C-terminal domains: identification of the RNA recognition loop in RIG-I-like receptors. The Journal of biological chemistry. 2009 Jun;284(26):17465–17474. PMCID: PMC2719387 DOI: 10.1074/jbc.M109.007179

49. Bruns AM, Pollpeter D, Hadizadeh N, Myong S, Marko JF, Horvath CM. ATP hydrolysis enhances RNA recognition and antiviral signal transduction by the innate immune sensor, laboratory of genetics and physiology 2 (LGP2). The Journal of biological chemistry. 2013 Jan;288(2):938–946. PMCID: PMC3543043
DOI: 10.1074/jbc.M112.424416

50. Takahasi K, Yoneyama M, Nishihori T, Hirai R, Kumeta H, Narita R, Gale Jr. M, Inagaki F, Fujita T. Nonself RNA-Sensing Mechanism of RIG-I Helicase and Activation of Antiviral Immune Responses. Molecular cell. 2008 Feb;29(4):428–440.
DOI: 10.1016/j.molcel.2007.11.028

51. Kato H, Takeuchi O, Mikamo-Satoh E, Hirai R, Kawai T, Matsushita K, Hiiragi A, Dermody TS, Fujita T, Akira S. Length-dependent recognition of double-stranded ribonucleic acids by retinoic acid-inducible gene-I and melanoma differentiation-associated gene 5. The Journal of experimental medicine. 2008 Jul;205(7):1601–1610. PMCID: PMC2442638 DOI: 10.1084/jem.20080091

52. Saito T, Owen DM, Jiang F, Marcotrigiano J, Gale Jr. M. Innate immunity induced by composition-dependent RIG-I recognition of hepatitis C virus RNA. Nature. 2008

Jul;454(7203):523–527. DOI: 10.1038/nature07106

53. Kato H, Takeuchi O, Sato S, Yoneyama M, Yamamoto M, Matsui K, Uematsu S, Jung A, Kawai T, Ishii KJ, Yamaguchi O, Otsu K, Tsujimura T, Koh C-S, Reis e Sousa C, Matsuura Y, Fujita T, Akira S. Differential roles of MDA5 and RIG-I helicases in the recognition of RNA viruses. Nature. 2006 May;441(7089):101–105. PMID: 16625202 DOI: 10.1038/nature04734

54. Venkataraman T, Valdes M, Elsby R, Kakuta S, Caceres G, Saijo S, Iwakura Y, Barber GN. Loss of DExD/H box RNA helicase LGP2 manifests disparate antiviral responses. Journal of immunology (Baltimore, Md : 1950). 2007 May;178(10):6444–6455. PMID: 17475874

55. Deddouche S, Goubau D, Rehwinkel J, Chakravarty P, Begum S, Maillard PV, Borg A, Matthews N, Feng Q, Kuppeveld FJM van, Reis e Sousa C. Identification of an LGP2-associated MDA5 agonist in picornavirus-infected cells. eLife. 2014;3:e01535. PMCID: PMC3967861

56. Onomoto K, Jogi M, Yoo J-S, Narita R, Morimoto S, Takemura A, Sambhara S, Kawaguchi A, Osari S, Nagata K, Matsumiya T, Namiki H, Yoneyama M, Fujita T. Critical role of an antiviral stress granule containing RIG-I and PKR in viral detection and innate immunity. PloS one. 2012;7(8):e43031. PMCID: PMC3418241 DOI: 10.1371/journal.pone.0043031

57. Sánchez-Aparicio MT, Ayllón J, Leo-Macias A, Wolff T, García-Sastre A. Subcellular Localizations of RIG-I, TRIM25, and MAVS Complexes. Journal of virology. 2017 Jan;91(2):e01155–16. PMCID: PMC5215348 DOI: 10.1128/JVI.01155-16

58. Langereis MA, Feng Q, Kuppeveld FJ van. MDA5 localizes to stress granules, but this localization is not required for the induction of type I interferon. Journal of virology. 2013 Jun;87(11):6314–6325. PMCID: PMC3648107 DOI: 10.1128/JVI.03213-12

59. Ashe A, Bélicard T, Le Pen J, Sarkies P, Frézal L, Lehrbach NJ, Félix M-A, Miska EA, Weigel D. A deletion polymorphism in the Caenorhabditis elegans RIG-I homolog disables viral RNA dicing and antiviral immunity. eLife. 2013 Oct;2:e00994. PMCID: PMC3793227 DOI: 10.7554/eLife.00994

60. Sijen T, Steiner FA, Thijssen KL, Plasterk RHA. Secondary siRNAs result from unprimed RNA synthesis and form a distinct class. Science (New York, NY). 2007 Jan;315(5809):244–247. PMID: 17158288 DOI: 10.1126/science.1136699

61. Lu R, Maduro M, Li F, Li HW, Broitman-Maduro G, Li WX, Ding SW. Animal virus replication and RNAi-mediated antiviral silencing in *Caenorhabditis elegans*. Nature. 2005 Aug;436(7053):1040–1043. DOI: 10.1038/nature03870

62. Guo X, Zhang R, Wang J, Ding S-W, Lu R. Homologous RIG-I-like helicase proteins direct RNAi-mediated antiviral immunity in C. elegans by distinct mechanisms. Proceedings of the National Academy of Sciences of the United States of America. 2013

Oct;110(40):16085–16090. PMCID: PMC3791698 DOI: 10.1073/pnas.1307453110

63. Coffman SR, Lu J, Guo X, Zhong J, Jiang H, Broitman-Maduro G, Li W-X, Lu R, Maduro M, Ding S-W. Caenorhabditis elegans RIG-I Homolog Mediates Antiviral RNA Interference Downstream of Dicer-Dependent Biogenesis of Viral Small Interfering RNAs. mBio. 2017 Mar;8(2):e00264–17. PMCID: PMC5362034 DOI: 10.1128/mBio.00264-17

64. Welker NC, Pavelec DM, Nix DA, Duchaine TF, Kennedy S, Bass BL. Dicer's helicase domain is required for accumulation of some, but not all, *C. elegans* endogenous siRNAs. RNA (New York, NY). 2010;16(5):893–903.

65. Welker NC, Maity TS, Ye X, Aruscavage PJ, Krauchuk AA, Liu Q, Bass BL. Dicer's helicase domain discriminates dsRNA termini to promote an altered reaction mode. Molecular cell. 2011 Mar;41(5):589–599. PMCID: PMC3061311 DOI: 10.1016/j.molcel.2011.02.005

66. Sijen T, Fleenor J, Simmer F, Thijssen KL, Parrish S, Timmons L, Plasterk RH, Fire A. On the role of RNA amplification in dsRNA-triggered gene silencing. Cell. 2001 Nov;107(4):465–476. PMID: 11719187

67. Pak J, Fire A. Distinct populations of primary and secondary effectors during RNAi in *C. elegans*. Science (New York, NY). 2007 Jan;315(5809):241–244. PMID: 17124291 DOI: 10.1126/science.1132839

68. Lu R, Yigit E, Li W-X, Ding S-W. An RIG-I-Like RNA helicase mediates antiviral RNAi downstream of viral siRNA biogenesis in *Caenorhabditis elegans*. PLoS pathogens. 2009 Feb;5(2):e1000286. PMCID: PMC2629121 DOI: 10.1371/journal.ppat.1000286

69. Wilkins C, Dishongh R, Moore SC, Whitt MA, Chow M, Machaca K. RNA interference is an antiviral defence mechanism in *Caenorhabditis elegans*. Nature. 2005 Aug;436(7053):1044–1047. PMID: 16107852 DOI: 10.1038/nature03957

70. Schott DH, Cureton DK, Whelan SP, Hunter CP. An antiviral role for the RNA interference machinery in *Caenorhabditis elegans*. Proceedings of the National Academy of Sciences of the United States of America. 2005 Dec;102(51):18420–18424. PMCID: PMC1317933 DOI: 10.1073/pnas.0507123102

71. Guo X, Zhang R, Wang J, Lu R. Antiviral RNA silencing initiated in the absence of RDE-4, a double-stranded RNA binding protein, in *Caenorhabditis elegans*. Journal of virology. 2013 Jul; PMID: 23885080 DOI: 10.1128/JVI.01305-13

72. Félix M-A, Ashe A, Piffaretti J, Wu G, Nuez I, Bélicard T, Jiang Y, Zhao G, Franz CJ, Goldstein LD, Sanroman M, Miska EA, Wang D. Natural and experimental infection of *Caenorhabditis* nematodes by novel viruses related to nodaviruses. PLoS biology. 2011;9(1):e1000586. PMCID: PMC3026760 DOI: 10.1371/journal.pbio.1000586

73. Saito K, Ishizuka A, Siomi H, Siomi MC. Processing of pre-microRNAs by the

Dicer-1-Loquacious complex in Drosophila cells. PLoS biology. 2005 Jul;3(7):e235. PMCID: PMC1141268 DOI: 10.1371/journal.pbio.0030235

74. Liu X, Jiang F, Kalidas S, Smith D, Liu Q. Dicer-2 and R2D2 coordinately bind siRNA to promote assembly of the siRISC complexes. RNA (New York, NY). 2006 Aug;12(8):1514–1520. PMCID: PMC1524895 DOI: 10.1261/rna.101606

75. Galiana-Arnoux D, Dostert C, Schneemann A, Hoffmann JA, Imler J-L. Essential function in vivo for Dicer-2 in host defense against RNA viruses in drosophila. Nature immunology. 2006 Jun;7(6):590–597. PMID: 16554838 DOI: 10.1038/ni1335

76. Wang X-H, Aliyari R, Li W-X, Li H-W, Kim K, Carthew R, Atkinson P, Ding S-W. RNA interference directs innate immunity against viruses in adult *Drosophila*. Science (New York, NY). 2006 Apr;312(5772):454. PMCID: PMC1509097 DOI: 10.1126/science.1125694

77. Zambon RA, Vakharia VN, Wu LP. RNAi is an antiviral immune response against a dsRNA virus in Drosophila melanogaster. Cellular microbiology. 2006 May;8(5):880–889. PMID: 16611236 DOI: 10.1111/j.1462-5822.2006.00688.x

78. Goic B, Vodovar N, Mondotte JA, Monot C, Frangeul L, Blanc H, Gausson V, Vera-Otarola J, Cristofari G, Saleh M-C. RNA-mediated interference and reverse transcription control the persistence of RNA viruses in the insect model *Drosophila*. Nature immunology. 2013 Apr;14(4):396–403. PMID: 23435119 DOI: 10.1038/ni.2542

79. Tassetto M, Kunitomi M, Andino R. Circulating Immune Cells Mediate a Systemic RNAi-Based Adaptive Antiviral Response in Drosophila. Cell. 2017 Apr;169(2):314–325.e13. PMID: 28388413 DOI: 10.1016/j.cell.2017.03.033

80. Rij RP van, Saleh M-C, Berry B, Foo C, Houk A, Antoniewski C, Andino R. The RNA silencing endonuclease Argonaute 2 mediates specific antiviral immunity in *Drosophila melanogaster*. Genes & development. 2006 Nov;20(21):2985–2995. PMCID: PMC1620017 DOI: 10.1101/gad.1482006

81. Deddouche S, Matt N, Budd A, Mueller S, Kemp C, Galiana-Arnoux D, Dostert C, Antoniewski C, Hoffmann JA, Imler J-L. The DExD/H-box helicase Dicer-2 mediates the induction of antiviral activity in drosophila. Nature immunology. 2008 Dec;9(12):1425–1432. PMID: 18953338 DOI: 10.1038/ni.1664

82. Maillard PV, Ciaudo C, Marchais A, Li Y, Jay F, Ding SW, Voinnet O. Antiviral RNA Interference in Mammalian Cells. Science (New York, NY). 2013 Oct;342(6155):235–238. PMID: 24115438 DOI: 10.1126/science.1241930

83. Li Y, Basavappa M, Lu J, Dong S, Cronkite DA, Prior JT, Reinecker H-C, Hertzog P, Han Y, Li W-X, Cheloufi S, Karginov FV, Ding S-W, Jeffrey KL. Induction and suppression of antiviral RNA interference by influenza A virus in mammalian cells. Nature microbiology. 2016 Dec;2:16250. PMID: 27918527

DOI: 10.1038/nmicrobiol.2016.250

84. Maillard PV, Van der Veen AG, Grass SD, Rogers NC, Merits A, Sousa CRE. Inactivation of the type I interferon pathway reveals long double-stranded RNA-mediated RNA interference in mammalian cells. The EMBO journal. 2016 Nov;35(23):e201695086–2518. PMCID: PMC5167344 DOI: 10.15252/embj.201695086

85. Leung AKL, Vyas S, Rood JE, Bhutkar A, Sharp PA, Chang P. Poly(ADP-Ribose) Regulates Stress Responses and MicroRNA Activity in the Cytoplasm. Molecular cell. 2011 May;42(4):489–499. DOI: 10.1016/j.molcel.2011.04.015

86. Seo GJ, Kincaid RP, Phanaksri T, Burke JM, Pare JM, Cox JE, Hsiang T-Y, Krug RM, Sullivan CS. Reciprocal inhibition between intracellular antiviral signaling and the RNAi machinery in mammalian cells. Cell host & microbe. 2013 Oct;14(4):435–445. PMCID: PMC3837626 DOI: 10.1016/j.chom.2013.09.002

87. Rascovan N, Duraisamy R, Desnues C. Metagenomics and the Human Virome in Asymptomatic Individuals. dxdoiorg. 2016 Sep;70(1):125–141. DOI: 10.1146/annurev-micro-102215-095431

88. Denu JM, Stuckey JA, Saper MA, Dixon JE. Form and Function in Protein Dephosphorylation. Cell. 1996 Nov;87(3):361–364. DOI: 10.1016/S0092-8674(00)81356-2

89. Yuan Y, Li D-M, Sun H. PIR1, a Novel Phosphatase That Exhibits High Affinity to RNARibonucleoprotein Complexes. The Journal of biological chemistry. 1998 Aug;273(32):20347–20353. DOI: 10.1074/jbc.273.32.20347

90. Romá-Mateo C, Ríos P, Tabernero L, Attwood TK, Pulido R. A Novel Phosphatase Family, Structurally Related to Dual-specificity Phosphatases, that Displays Unique Amino Acid Sequence and Substrate Specificity. Journal of molecular biology. 2007 Dec;374(4):899–909. DOI: 10.1016/j.jmb.2007.10.008

91. Deshpande T, Takagi T, Hao L, Buratowski S, Charbonneau H. Human PIR1 of the Protein-tyrosine Phosphatase Superfamily Has RNA 5'-Triphosphatase and Diphosphatase Activities. The Journal of biological chemistry. 1999 Jun;274(23):16590–16594. DOI: 10.1074/jbc.274.23.16590

92. Sankhala RS, Lokareddy RK, Cingolani G. Structure of human PIR1, an atypical dual-specificity phosphatase. Biochemistry. 2014 Feb;53(5):862–871. PMID: 24447265 DOI: 10.1021/bi401240x

93. Duchaine TF, Wohlschlegel JA, Kennedy S, Bei Y, Conte D, Pang K, Brownell DR, Harding S, Mitani S, Ruvkun G, Yates JR, Mello CC. Functional proteomics reveals the biochemical niche of C. elegans DCR-1 in multiple small-RNA-mediated pathways. Cell. 2006 Jan;124(2):343–354. PMID: 16439208 DOI: 10.1016/j.cell.2005.11.036

94. Chaves DM de A de M. The RNA 5 phosphatase PIR-1 cooperates with dicer to produce endogenous small RNAs and suppress viral replication in *C. elegans* [Internet]

[PhD thesis].

95. Caprara G, Zamponi R, Melixetian M, Helin K. Isolation and characterization of DUSP11, a novel p53 target gene. Journal of cellular and molecular medicine. 2009 Aug;13(8B):2158–2170. PMID: 19120688 DOI: 10.1111/j.1582-4934.2008.00616.x

96. Burke JM, Kincaid RP, Nottingham RM, Lambowitz AM, Sullivan CS. DUSP11 activity on triphosphorylated transcripts promotes Argonaute association with noncanonical viral microRNAs and regulates steady-state levels of cellular noncoding RNAs. Genes & development. 2016 Sep;30(18):2076–2092. PMCID: PMC5066614 DOI: 10.1101/gad.282616.116

97. Brewer LA, Lwamba HC, Murtaugh MP, Palmenberg AC, Brown C, Njenga MK. Porcine encephalomyocarditis virus persists in pig myocardium and infects human myocardial cells. Journal of virology. 2001 Dec;75(23):11621–11629. PMCID: PMC114749 DOI: 10.1128/JVI.75.23.11621-11629.2001

98. Hammoumi S, Guy M, Eloit M, Bakkali-Kassimi L. Encephalomyocarditis virus may use different pathways to initiate infection of primary human cardiomyocytes. Archives of virology. 2012 Jan;157(1):43–52. PMID: 21989795 DOI: 10.1007/s00705-011-1133-6

99. Huber SA. VCAM-1 is a receptor for encephalomyocarditis virus on murine vascular endothelial cells. Journal of virology. 1994 Jun;68(6):3453–3458. PMCID: PMC236847

100. Parks GD, Duke GM, Palmenberg AC. Encephalomyocarditis virus 3C protease: efficient cell-free expression from clones which link viral 5' noncoding sequences to the P3 region. Journal of virology. 1986 Nov;60(2):376–384. PMCID: PMC288903

101. Loughran G, Firth AE, Atkins JF. Ribosomal frameshifting into an overlapping gene in the 2B-encoding region of the cardiovirus genome. Proceedings of the National Academy of Sciences of the United States of America. 2011 Nov;108(46):E1111–9. PMCID: PMC3219106 DOI: 10.1073/pnas.1102932108

102. Virgen-Slane R, Rozovics JM, Fitzgerald KD, Ngo T, Chou W, Heden van Noort GJ van der, Filippov DV, Gershon PD, Semler BL. An RNA virus hijacks an incognito function of a DNA repair enzyme. Proceedings of the National Academy of Sciences of the United States of America. 2012 Sep;109(36):14634–14639. PMCID: PMC3437895 DOI: 10.1073/pnas.1208096109

103. Maciejewski S, Nguyen JHC, Gómez-Herreros F, Cortés-Ledesma F, Caldecott KW, Semler BL. Divergent Requirement for a DNA Repair Enzyme during Enterovirus Infections. mBio. 2015 Dec;7(1):e01931–15. PMCID: PMC4725011 DOI: 10.1128/mBio.01931-15

104. Papon L, Oteiza A, Imaizumi T, Kato H, Brocchi E, Lawson TG, Akira S, Mechti N. The viral RNA recognition sensor RIG-I is degraded during encephalomyocarditis virus (EMCV) infection. Virology. 2009 Oct;393(2):311–318.

DOI: 10.1016/j.virol.2009.08.009

105. Gamarnik AV, Andino R. Switch from translation to RNA replication in a positive-stranded RNA virus. Genes & development. 1998 Aug;12(15):2293–2304. DOI: 10.1101/gad.12.15.2293

106. Gerber K, Wimmer E, Paul AV. Biochemical and genetic studies of the initiation of human rhinovirus 2 RNA replication: identification of a cis-replicating element in the coding sequence of 2A(pro). Journal of virology. 2001 Nov;75(22):10979–10990. PMCID: PMC114678 DOI: 10.1128/JVI.75.22.10979-10990.2001

107. Montagnier L, SANDERS FK. Replicative form of Encephalomyocarditis Virus Ribonucleic Acid. Nature. 1963 Aug;199(4894):664–667. DOI: 10.1038/199664a0

108. Novak JE, Kirkegaard K. Improved method for detecting poliovirus negative strands used to demonstrate specificity of positive-strand encapsidation and the ratio of positive to negative strands in infected cells. Journal of virology. 1991 Jun;65(6):3384–3387. PMCID: PMC241002

109. Carocci M, Bakkali-Kassimi L. The encephalomyocarditis virus. Virulence. 2012 Jun;3(4):351–367. DOI: 10.4161/viru.20573

110. Higuchi H, Hara M, Yamamoto K, Miyamoto T, Kinoshita M, Yamada T, Uchiyama K, Matsumori A. Mast cells play a critical role in the pathogenesis of viral myocarditis. Circulation. 2008 Jul;118(4):363–372. PMID: 18606918 DOI: 10.1161/CIRCULATIONAHA.107.741595

111. Matsumori A, Yamamoto K, Shimada M. Cetirizine a histamine H1 receptor antagonist improves viral myocarditis. Journal of inflammation (London, England). 2010 Aug;7(1):39. PMCID: PMC2922108 DOI: 10.1186/1476-9255-7-39

112. Iwasaki A, Matsumori A, Yamada T, Shioi T, Wang W, Ono K, Nishio R, Okada M, Sasayama S. Pimobendan inhibits the production of proinflammatory cytokines and gene expression of inducible nitric oxide synthase in a murine model of viral myocarditis. Journal of the American College of Cardiology. 1999 Apr;33(5):1400–1407. DOI: 10.1016/S0735-1097(98)00692-5

113. Wang J-F, Meissner A, Malek S, Chen Y, Ke Q, Zhang J, Chu V, Hampton TG, Crumpacker CS, Abelmann WH, Amende I, Morgan JP. Propranolol ameliorates and epinephrine exacerbates progression of acute and chronic viral myocarditis. American Journal of Physiology - Heart and Circulatory Physiology. 2005 Oct;289(4):H1577–H1583. PMID: 15923319 DOI: 10.1152/ajpheart.00258.2005

114. Matsumori A, Nunokawa Y, Yamaki A, Yamamoto K, Hwang MW, Miyamoto T, Hara M, Nishio R, Kitaura Inenaga K, Ono K. Suppression of cytokines and nitric oxide production, and protection against lethal endotoxemia and viral myocarditis by a new NF-κB inhibitor. European Journal of Heart Failure. 2004 Mar;6(2):137–144.

DOI: 10.1016/j.ejheart.2003.10.007

115. Carocci M, Cordonnier N, Huet H, Romey A, Relmy A, Gorna K, Blaise-Boisseau S, Zientara S, Kassimi LB. Encephalomyocarditis virus 2A protein is required for viral pathogenesis and inhibition of apoptosis. Journal of virology. 2011 Oct;85(20):10741–10754. PMCID: PMC3187497 DOI: 10.1128/JVI.00394-11

116. LaRue R, Myers S, Brewer L, Shaw DP, Brown C, Seal BS, Njenga MK. A wild-type porcine encephalomyocarditis virus containing a short poly(C) tract is pathogenic to mice, pigs, and cynomolgus macaques. Journal of virology. 2003 Sep;77(17):9136–9146. PMCID: PMC187386 DOI: 10.1128/JVI.77.17.9136-9146.2003

117. Nasu-Nishimura Y, Taniuchi Y, Nishimura T, Sakudo A, Nakajima K, Ano Y, Sugiura K, Sakaguchi S, Itohara S, Onodera T. Cellular prion protein prevents brain damage after encephalomyocarditis virus infection in mice. Archives of virology. 2008;153(6):1007–1012. DOI: 10.1007/s00705-008-0086-x

118. Hirasawa K, Jun HS, Maeda K, Kawaguchi Y, Itagaki S, Mikami T, Baek HS, Doi K, Yoon JW. Possible role of macrophage-derived soluble mediators in the pathogenesis of encephalomyocarditis virus-induced diabetes in mice. Journal of virology. 1997 May;71(5):4024–4031. PMCID: PMC191555

119. Satoh T, Kato H, Kumagai Y, Yoneyama M, Sato S, Matsushita K, Tsujimura T, Fujita T, Akira S, Takeuchi O. LGP2 is a positive regulator of RIG-I- and MDA5-mediated antiviral responses. Proceedings of the National Academy of Sciences of the United States of America. 2010 Jan;107(4):1512–1517. PMCID: PMC2824407 DOI: 10.1073/pnas.0912986107

120. Triantafilou K, Vakakis E, Kar S, Richer E, Evans GL, Triantafilou M. Visualisation of direct interaction of MDA5 and the dsRNA replicative intermediate form of positive strand RNA viruses. Journal of cell science. 2012 Oct;125(Pt 20):4761–4769. PMID: 22797917 DOI: 10.1242/jcs.103887

121. Hato SV, Ricour C, Schulte BM, Lanke KHW, Bruijni M de, Zoll J, Melchers WJG, Michiels T, Kuppeveld FJM van. The mengovirus leader protein blocks interferon-alpha/beta gene transcription and inhibits activation of interferon regulatory factor 3. Cellular microbiology. 2007 Dec;9(12):2921–2930. PMID: 17991048 DOI: 10.1111/j.1462-5822.2007.01006.x

122. Ye J, Coulouris G, Zaretskaya I, Cutcutache I, Rozen S, Madden TL. Primer-BLAST: a tool to design target-specific primers for polymerase chain reaction. BMC bioinformatics. 2012 Jun;13(1):134. PMCID: PMC3412702 DOI: 10.1186/1471-2105-13-134

123. Lutz MB, Kukutsch N, Ogilvie AL, Rössner S, Koch F, Romani N, Schuler G. An advanced culture method for generating large quantities of highly pure dendritic cells from mouse bone marrow. Journal of immunological methods. 1999 Feb;223(1):77–92.

PMID: 10037236

124. Brandt K, Bulfone-Paus S, Foster DC, Rückert R. Interleukin-21 inhibits dendritic cell activation and maturation. Blood. 2003 Dec;102(12):4090–4098. PMID: 12893770 DOI: 10.1182/blood-2003-03-0669

125. Yamamoto M, Sato S, Hemmi H, Hoshino K, Kaisho T, Sanjo H, Takeuchi O, Sugiyama M, Okabe M, Takeda K, Akira S. Role of adaptor TRIF in the MyD88-independent toll-like receptor signaling pathway. Science (New York, NY). 2003 Aug;301(5633):640–643. PMID: 12855817 DOI: 10.1126/science.1087262

126. Hardy MP, Owczarek CM, Jermiin LS, Ejdebäck M, Hertzog PJ. Characterization of the type I interferon locus and identification of novel genes. Genomics. 2004 Aug;84(2):331–345.

127. Haspel RL, Salditt-Georgieff M, Darnell JE. The rapid inactivation of nuclear tyrosine phosphorylated Stat1 depends upon a protein tyrosine phosphatase. The EMBO journal. 1996 Nov;15(22):6262–6268. PMCID: PMC452449

128. Goubau D, Schlee M, Deddouche S, Pruijssers AJ, Zillinger T, Goldeck M, Schuberth C, Van der Veen AG, Fujimura T, Rehwinkel J, Iskarpatyoti JA, Barchet W, Ludwig J, Dermody TS, Hartmann G, Sousa CRE. Antiviral immunity via RIG-I-mediated recognition of RNA bearing 5'-diphosphates. Nature. 2014 Aug; PMCID: PMC4201573 DOI: 10.1038/nature13590

129. Soberman RJ, MacKay CR, Vaine CA, Ryan GB, Cerny AM, Thompson MR, Nikolic B, Primo V, Christmas P, Sheiffele P, Aronov L, Knipe DM, Kurt-Jones EA. CD200R1 supports HSV-1 viral replication and licenses pro-inflammatory signaling functions of TLR2. PloS one. 2012;7(10):e47740. PMCID: PMC3474780 DOI: 10.1371/journal.pone.0047740

130. Nahmias AJ, Josey WE, Naib ZM, LUCE CF. Antibodies to Herpesvirus hominis types 1 and 2 in humans. I. Patients with genital herpetic infections. American journal of 1970;

131. Wentworth BB, Alexander ER. Seroepidemiology of infectious due to members of the herpesvirus group. American Journal of Epidemiology. 1971 Nov;94(5):496–507. DOI: 10.1093/oxfordjournals.aje.a121347

132. Knipe DM, Howley PM. Fields Virology [Internet]. 2013.

133. Whitley RJ, Cobbs CG, Alford CA, Soong S-J, Hirsch MS, Connor JD, Corey L, Hanley DF, Levin M, Powell DA. Diseases That Mimic Herpes Simplex Encephalitis: Diagnosis, Presentation, and Outcome. Jama. 1989 Jul;262(2):234–239. DOI: 10.1001/jama.1989.03430020076032

134. Levitz RE. Herpes simplex encephalitis: A review. Heart & Lung: The Journal of Acute and Critical Care. 1998 May;27(3):209–212.

DOI: 10.1016/S0147-9563(98)90009-7

135. Whitley RJ, Soong S-J, Dolin R, Galasso GJ, Ch'ien LT, Alford CA, Group the CS. Adenine Arabinoside Therapy of Biopsy-Proved Herpes Simplex Encephalitis. dxdoiorg. 2010 Jan;297(6):289–294. DOI: 10.1056/NEJM197708112970601

136. Lundberg P, Ramakrishna C, Brown J, Tyszka JM, Hamamura M, Hinton DR, Kovats S, Nalcioglu O, Weinberg K, Openshaw H, Cantin EM. The immune response to herpes simplex virus type 1 infection in susceptible mice is a major cause of central nervous system pathology resulting in fatal encephalitis. Journal of virology. 2008 Jul;82(14):7078–7088. PMCID: PMC2446972 DOI: 10.1128/JVI.00619-08

137. Kwong AD, Kruper JA, Frenkel N. Herpes simplex virus virion host shutoff function. Journal of virology. 1988 Mar;62(3):912–921. PMCID: PMC253650

138. Nicoll MP, Proença JT, Efstathiou S. The molecular basis of herpes simplex virus latency. FEMS Microbiology Reviews. 2012 May;36(3):684–705. DOI: 10.1111/j.1574-6976.2011.00320.x

139. Efstathiou S, Minson AC, Field HJ, Anderson JR, Wildy P. Detection of herpes simplex virus-specific DNA sequences in latently infected mice and in humans. Journal of virology. 1986 Feb;57(2):446–455. PMCID: PMC252756

140. Deshmane SL, Fraser NW. During latency, herpes simplex virus type 1 DNA is associated with nucleosomes in a chromatin structure. Journal of virology. 1989 Feb;63(2):943–947. PMCID: PMC247770

141. Wagner EK, Bloom DC. Experimental investigation of herpes simplex virus latency. Clinical Microbiology Reviews. 1997 Jul;10(3):419–443. PMCID: PMC172928

142. Orr MT, Mathis MA, Lagunoff M, Sacks JA, Wilson CB. CD8 T Cell Control of HSV Reactivation from Latency Is Abrogated by Viral Inhibition of MHC Class I. Cell host & microbe. 2007 Sep;2(3):172–180. DOI: 10.1016/j.chom.2007.06.013

143. Freeman ML, Sheridan BS, Bonneau RH, Hendricks RL. Psychological Stress Compromises CD8+ T Cell Control of Latent Herpes Simplex Virus Type 1 Infections. The Journal of Immunology. 2007 Jul;179(1):322–328. PMCID: PMC2367250 DOI: 10.4049/jimmunol.179.1.322

144. Iwasaki A, Medzhitov R. Toll-like receptor control of the adaptive immune responses. Nature immunology. 2004 Oct;5(10):987–995. PMID: 15454922 DOI: 10.1038/ni1112

145. Kurt-Jones EA, Chan M, Zhou S, Wang J, Reed G, Bronson R, Arnold MM, Knipe DM, Finberg RW. Herpes simplex virus 1 interaction with Toll-like receptor 2 contributes to lethal encephalitis. Proceedings of the National Academy of Sciences of the United States of America. 2004 Feb;101(5):1315–1320. PMCID: PMC337050 DOI: 10.1073/pnas.0308057100

146. Weber F, Wagner V, Rasmussen SB, Hartmann R, Paludan SR. Double-stranded

RNA is produced by positive-strand RNA viruses and DNA viruses but not in detectable amounts by negative-strand RNA viruses. Journal of virology. 2006 May;80(10):5059–5064. PMCID: PMC1472073 DOI: 10.1128/JVI.80.10.5059-5064.2006

147. Guo Y, Audry M, Ciancanelli M, Alsina L, Azevedo J, Herman M, Anguiano E, Sancho-Shimizu V, Lorenzo L, Pauwels E, Philippe PB, Diego RP de, Cardon A, Vogt G, Picard C, Andrianirina ZZ, Rozenberg F, Lebon P, Plancoulaine S, Tardieu M, Doireau V, Jouanguy E, Chaussabel D, Geissmann F, Abel L, Casanova J-L, Zhang S-Y. Herpes simplex virus encephalitis in a patient with complete TLR3 deficiency: TLR3 is otherwise redundant in protective immunity. Journal of Experimental Medicine. 2011 Sep;208(10):jem.20101568–2098. PMCID: PMC3182056 DOI: 10.1084/jem.20101568

148. Zhang S-Y, Jouanguy E, Ugolini S, Smahi A, Elain G, Romero P, Segal D, Sancho-Shimizu V, Lorenzo L, Puel A, Picard C, Chapgier A, Plancoulaine S, Titeux M, Cognet C, Bernuth H von, Ku C-L, Casrouge A, Zhang X-X, Barreiro L, Leonard J, Hamilton C, Lebon P, Héron B, Vallée L, Quintana-Murci L, Hovnanian A, Rozenberg F, Vivier E, Geissmann F, Tardieu M, Abel L, Casanova J-L. TLR3 Deficiency in Patients with Herpes Simplex Encephalitis. Science (New York, NY). 2007 Sep;317(5844):1522–1527. PMID: 17872438 DOI: 10.1126/science.1139522

149. Paludan SR, Bowie AG, Horan KA, Fitzgerald KA. Recognition of herpesviruses by the innate immune system. Nature reviews Immunology. 2011 Feb;11(2):143–154. DOI: 10.1038/nri2937

150. Lund J, Sato A, Akira S, Medzhitov R, Iwasaki A. Toll-like Receptor 9mediated Recognition of Herpes Simplex Virus-2 by Plasmacytoid Dendritic Cells. Journal of Experimental Medicine. 2003 Aug;198(3):513–520. PMCID: PMC2194085 DOI: 10.1084/jem.20030162

151. Rasmussen SB, Sørensen LN, Malmgaard L, Ank N, Baines JD, Chen ZJ, Paludan SR. Type I interferon production during herpes simplex virus infection is controlled by cell-type-specific viral recognition through Toll-like receptor 9, the mitochondrial antiviral signaling protein pathway, and novel recognition systems. Journal of virology. 2007 Dec;81(24):13315–13324. PMCID: PMC2168887 DOI: 10.1128/JVI.01167-07

152. Takaoka A, Wang Z, Choi MK, Yanai H, Negishi H, Ban T, Lu Y, Miyagishi M, Kodama T, Honda K, Ohba Y, Taniguchi T. DAI (DLM-1/ZBP1) is a cytosolic DNA sensor and an activator of innate immune response. Nature. 2007 Jul;448(7152):501–505. PMID: 17618271 DOI: 10.1038/nature06013

153. Pham TH, Kwon KM, Kim Y-E, Kim KK, Ahn J-H. DNA sensing-independent inhibition of herpes simplex virus 1 replication by DAI/ZBP1. Journal of virology. 2013 Mar;87(6):3076–3086. PMCID: PMC3592125 DOI: 10.1128/JVI.02860-12

154. Furr SR, Chauhan VS, Moerdyk-Schauwecker MJ, Marriott I. A role for DNA-dependent activator of interferon regulatory factor in the recognition of herpes simplex virus type 1 by glial cells. Journal of neuroinflammation. 2011 Aug;8(1):99.

PMCID: PMC3168419 DOI: 10.1186/1742-2094-8-99

155. Chiu Y-H, Macmillan JB, Chen ZJ. RNA polymerase III detects cytosolic DNA and induces type I interferons through the RIG-I pathway. Cell. 2009 Aug;138(3):576–591. PMCID: PMC2747301 DOI: 10.1016/j.cell.2009.06.015

156. Johnson KE, Chikoti L, Chandran B. Herpes simplex virus 1 infection induces activation and subsequent inhibition of the IFI16 and NLRP3 inflammasomes. Journal of virology. 2013 May;87(9):5005–5018. PMCID: PMC3624293 DOI: 10.1128/JVI.00082-13

157. Wu J, Sun L, Chen X, Du F, Shi H, Chen C, Chen ZJ. Cyclic GMP-AMP Is an Endogenous Second Messenger in Innate Immune Signaling by Cytosolic DNA. Science (New York, NY). 2013 Feb;339(6121):826–830. PMCID: PMC3855410 DOI: 10.1126/science.1229963

158. Su C, Zhan G, Zheng C. Evasion of host antiviral innate immunity by HSV-1, an update. Virology journal. 2016 Mar;13(1):38. PMCID: PMC4782282 DOI: 10.1186/s12985-016-0495-5

159. Lint AL van, Murawski MR, Goodbody RE, Severa M, Fitzgerald KA, Finberg RW, Knipe DM, Kurt-Jones EA. Herpes simplex virus immediate-early ICP0 protein inhibits Toll-like receptor 2-dependent inflammatory responses and NF-kappaB signaling. Journal of virology. 2010 Oct;84(20):10802–10811. PMCID: PMC2950559 DOI: 10.1128/JVI.00063-10

160. Kalamvoki M, Roizman B. HSV-1 degrades, stabilizes, requires, or is stung by STING depending on ICP0, the US3 protein kinase, and cell derivation. Proceedings of the National Academy of Sciences of the United States of America. 2014 Feb;111(5):E611–7. PMCID: PMC3918790 DOI: 10.1073/pnas.1323414111

161. Orzalli MH, DeLuca NA, Knipe DM. Nuclear IFI16 induction of IRF-3 signaling during herpesviral infection and degradation of IFI16 by the viral ICP0 protein. Proceedings of the National Academy of Sciences of the United States of America. 2012 Oct;109(44):E3008–17. PMCID: PMC3497734 DOI: 10.1073/pnas.1211302109

162. Xing J, Wang S, Lin R, Mossman KL, Zheng C. Herpes simplex virus 1 tegument protein US11 downmodulates the RLR signaling pathway via direct interaction with RIG-I and MDA-5. Journal of virology. 2012 Apr;86(7):3528–3540. PMCID: PMC3302539 DOI: 10.1128/JVI.06713-11

163. Peri P, Mattila RK, Kantola H, Broberg E, Karttunen HS, Waris M, Vuorinen T, Hukkanen V. Herpes Simplex Virus Type 1 Us3 Gene Deletion Influences Toll-like Receptor Responses in Cultured Monocytic Cells. Virology journal. 2008 Nov;5(1):140. DOI: 10.1186/1743-422X-5-140

164. Sen J, Liu X, Roller R, Knipe DM. Herpes simplex virus US3 tegument protein inhibits Toll-like receptor 2 signaling at or before TRAF6 ubiquitination. Virology.

2013 May;439(2):65–73. DOI: 10.1016/j.virol.2013.01.026

165. Wang S, Wang K, Lin R, Zheng C. Herpes simplex virus 1 serine/threonine kinase US3 hyperphosphorylates IRF3 and inhibits beta interferon production. Journal of virology. 2013 Dec;87(23):12814–12827. PMCID: PMC3838156 DOI: 10.1128/JVI.02355-13

166. Wang K, Ni L, Wang S, Zheng C. Herpes Simplex Virus 1 Protein Kinase US3 Hyperphosphorylates p65/RelA and Dampens NF-κB Activation. Journal of virology. 2014 Jul;88(14):7941–7951. PMCID: PMC4097809 DOI: 10.1128/JVI.03394-13

167. Ma Y, Jin H, Valyi-Nagy T, Cao Y, Yan Z, He B. Inhibition of TANK binding kinase 1 by herpes simplex virus 1 facilitates productive infection. Journal of virology. 2012 Feb;86(4):2188–2196. PMCID: PMC3302378 DOI: 10.1128/JVI.05376-11

168. Verpooten D, Ma Y, Hou S, Yan Z, He B. Control of TANK-binding kinase 1-mediated signaling by the gamma(1)34.5 protein of herpes simplex virus 1. The Journal of biological chemistry. 2009 Jan;284(2):1097–1105. PMCID: PMC2613634 DOI: 10.1074/jbc.M805905200

169. Xing J, Ni L, Wang S, Wang K, Lin R, Zheng C. Herpes simplex virus 1-encoded tegument protein VP16 abrogates the production of beta interferon (IFN) by inhibiting NF-κB activation and blocking IFN regulatory factor 3 to recruit its coactivator CBP. Journal of virology. 2013 Sep;87(17):9788–9801. PMCID: PMC3754106 DOI: 10.1128/JVI.01440-13

170. Shen G, Wang K, Wang S, Cai M, Li M-l, Zheng C. Herpes simplex virus 1 counteracts viperin via its virion host shutoff protein UL41. Journal of virology. 2014 Oct;88(20):12163–12166. PMCID: PMC4178720 DOI: 10.1128/JVI.01380-14

171. Su C, Zhang J, Zheng C. Herpes simplex virus 1 UL41 protein abrogates the antiviral activity of hZAP by degrading its mRNA. Virology journal. 2015 Dec;12(1):203. DOI: 10.1186/s12985-015-0433-y

172. Zenner HL, Mauricio R, Banting G, Crump CM. Herpes simplex virus 1 counteracts tetherin restriction via its virion host shutoff activity. Journal of virology. 2013 Dec;87(24):13115–13123. PMCID: PMC3838292 DOI: 10.1128/JVI.02167-13

173. Whitley RJ, Alford CA, Hirsch MS. Vidarabine versus acyclovir therapy in herpes simplex encephalitis. ... England Journal of 1986;

174. Kamei S, Sekizawa T, Shiota H, Mizutani T, Itoyama Y, Takasu T, Morishima T, Hirayanagi K. Evaluation of combination therapy using aciclovir and corticosteroid in adult patients with herpes simplex virus encephalitis. Journal of Neurology, Neurosurgery & Psychiatry. 2005 Nov;76(11):1544–1549. PMCID: PMC1739396 DOI: 10.1136/jnnp.2004.049676

175. Lizarraga KJ, Alexandre LC, Ramos-Estebanez C, Merenda A. Are steroids a beneficial adjunctive therapy in the immunosuppressed patient with herpes simplex

virus encephalitis? Case Reports in Neurology. 2013 Jan;5(1):52–55. PMCID: PMC3635685 DOI: 10.1159/000350572

176. Sheridan PA, Beck MA. The immune response to herpes simplex virus encephalitis in mice is modulated by dietary vitamin E. The Journal of nutrition. 2008 Jan;138(1):130–137. PMCID: PMC2430048

177. Sarangi PP, Kim B, Kurt-Jones E, Rouse BT. Innate recognition network driving herpes simplex virus-induced corneal immunopathology: role of the toll pathway in early inflammatory events in stromal keratitis. Journal of virology. 2007 Oct;81(20):11128–11138. PMCID: PMC2045562 DOI: 10.1128/JVI.01008-07

178. Barnett EM, Jacobsen G, Evans G, Cassell M, Perlman S. Herpes simplex encephalitis in the temporal cortex and limbic system after trigeminal nerve inoculation. The Journal of infectious diseases. 1994 Apr;169(4):782–786. PMID: 8133092

179. Wang JP, Bowen GN, Zhou S, Cerny A, Zacharia A, Knipe DM, Finberg RW, Kurt-Jones EA. Role of specific innate immune responses in herpes simplex virus infection of the central nervous system. Journal of virology. 2012 Feb;86(4):2273–2281. PMCID: PMC3302371 DOI: 10.1128/JVI.06010-11

180. Dick AD, Broderick C, Forrester JV, Wright GJ. Distribution of OX2 Antigen and OX2 Receptor within Retina. Investigative Ophthalmology & Visual Science. 2001 Jan;42(1):170–176.

181. Chen DX, He H, Gorczynski RM. Synthetic peptides from the N-terminal regions of CD200 and CD200R1 modulate immunosuppressive and anti-inflammatory effects of CD200CD200R1 interaction. International immunology. 2005;

182. Gorczynski RM, Chen Z, Fu XM, Zeng H. Increased expression of the novel molecule OX-2 is involved in prolongation of murine renal allograft survival. Transplantation. 1998 Apr;65(8):1106–1114. PMID: 9583873

183. Snelgrove RJ, Goulding J, Didierlaurent AM, Lyonga D, Vekaria S, Edwards L, Gwyer E, Sedgwick JD, Barclay AN, Hussell T. A critical function for CD200 in lung immune homeostasis and the severity of influenza infection. Nature immunology. 2008 Sep;9(9):1074–1083. PMID: 18660812 DOI: 10.1038/ni.1637

184. Kurt-Jones EA, Sandor F, Ortiz Y, Bowen GN, Counter SL, Wang TC, Finberg RW. Use of murine embryonic fibroblasts to define Toll-like receptor activation and specificity. Journal of Endotoxin Research. 2016 Sep;10(6):419–424. DOI: 10.1177/09680519040100060701

185. Taylor TJ, McNamee EE, Day C, Knipe DM. Herpes simplex virus replication compartments can form by coalescence of smaller compartments. Virology. 2003 May;309(2):232–247.

186. Nilsen N, Nonstad U, Khan N, Knetter CF, Akira S, Sundan A, Espevik T, Lien E. Lipopolysaccharide and double-stranded RNA up-regulate toll-like receptor 2

independently of myeloid differentiation factor 88. The Journal of biological chemistry. 2004 Sep;279(38):39727–39735. PMID: 15190057 DOI: 10.1074/jbc.M405027200

187. Liu Y, Wang Y, Yamakuchi M, Isowaki S, Nagata E, Kanmura Y, Kitajima I, Maruyama I. Upregulation of toll-like receptor 2 gene expression in macrophage response to peptidoglycan and high concentration of lipopolysaccharide is involved in NF-kappa b activation. Infection and Immunity. 2001 May;69(5):2788–2796. PMCID: PMC98226 DOI: 10.1128/IAI.69.5.2788-2796.2001

188. Musikacharoen T, Matsuguchi T, Kikuchi T, Yoshikai Y. NF-kappa B and STAT5 play important roles in the regulation of mouse Toll-like receptor 2 gene expression. The Journal of Immunology. 2001 Apr;166(7):4516–4524. PMID: 11254708

189. MacKay CR, Wang JP, Kurt-Jones EA. Dicer's role as an antiviral: still an enigma. Current opinion in immunology. 2014 Feb;26:49–55. PMCID: PMC3932008 DOI: 10.1016/j.coi.2013.10.015

190. Louber J, Brunel J, Uchikawa E, Cusack S, Gerlier D. Kinetic discrimination of self/non-self RNA by the ATPase activity of RIG-I and MDA5. BMC biology. 2015 Jul;13(1):54. PMCID: PMC4517655 DOI: 10.1186/s12915-015-0166-9

191. Meister G. Argonaute proteins: functional insights and emerging roles. Nature Reviews Genetics. 2013 Jul;14(7):447–459. DOI: 10.1038/nrg3462

192. Li Y, Lu J, Han Y, Fan X, Ding S-W. RNA Interference Functions as an Antiviral Immunity Mechanism in Mammals. Science (New York, NY). 2013 Oct;342(6155):231–234. PMID: 24115437 DOI: 10.1126/science.1241911

193. Nejepinska J, Malik R, Filkowski J, Flemr M. dsRNA expression in the mouse elicits RNAi in oocytes and low adenosine deamination in somatic cells. Nucleic acids 2012;

194. Shimizu A, Nakatani Y, Nakamura T, Jinno-Oue A, Ishikawa O, Boeke JD, Takeuchi Y, Hoshino H. Characterisation of cytoplasmic DNA complementary to non-retroviral RNA viruses in human cells. Scientific Reports. 2014 May;4(1):5074. DOI: 10.1038/srep05074

195. Klenerman P, Hengartner H, Zinkernagel RM. A non-retroviral RNA virus persists in DNA form. Nature. 1997 Nov;390(6657):298–301. DOI: 10.1038/36876

196. Geuking MB, Weber J, Dewannieux M, Gorelik E, Heidmann T, Hengartner H, Zinkernagel RM, Hangartner L. Recombination of Retrotransposon and Exogenous RNA Virus Results in Nonretroviral cDNA Integration. Science (New York, NY). 2009 Jan;323(5912):393–396. PMID: 19150848 DOI: 10.1126/science.1167375

197. Painter MM, Morrison JH, Zoecklein LJ, Rinkoski TA, Watzlawik JO, Papke LM, Warrington AE, Bieber AJ, Matchett WE, Turkowski KL, Poeschla EM, Rodriguez M. Antiviral Protection via RdRP-Mediated Stable Activation of Innate Immunity. PLoS

pathogens. 2015 Dec;11(12):e1005311. DOI: 10.1371/journal.ppat.1005311

198. Nikonov A, Mölder T, Sikut R, Kiiver K, Männik A, Toots U, Lulla A, Lulla V, Utt A, Merits A, Ustav M. RIG-I and MDA-5 Detection of Viral RNA-dependent RNA Polymerase Activity Restricts Positive-Strand RNA Virus Replication. PLoS pathogens. 2013 Sep;9(9):e1003610. DOI: 10.1371/journal.ppat.1003610

199. Yu G-Y, He G, Li C-Y, Tang M, Grivennikov S, Tsai W-T, Wu M-S, Hsu C-W, Tsai Y, Wang LH-C, Karin M. Hepatic Expression of HCV RNA-Dependent RNA Polymerase Triggers Innate Immune Signaling and Cytokine Production. Molecular cell. 2012 Oct;48(2):313–321. DOI: 10.1016/j.molcel.2012.07.032

200. Arnold JJ, Ghosh SKB, Cameron CE. Poliovirus RNA-dependent RNA Polymerase (3Dpol): DIVALENT CATION MODULATION OF PRIMER, TEMPLATE, AND NUCLEOTIDE SELECTION. The Journal of biological chemistry. 1999 Dec;274(52):37060–37069. DOI: 10.1074/jbc.274.52.37060

201. Arnold JJ, Cameron CE. Poliovirus RNA-dependent RNA polymerase (3Dpol) is sufficient for template switching in vitro. The Journal of biological chemistry. 1999 Jan;274(5):2706–2716. PMID: 9915801 DOI: 10.1074/jbc.274.5.2706

202. Parameswaran P, Sklan E, Wilkins C, Burgon T, Samuel MA, Lu R, Ansel KM, Heissmeyer V, Einav S, Jackson W, Doukas T, Paranjape S, Polacek C, Santos FB dos, Jalili R, Babrzadeh F, Gharizadeh B, Grimm D, Kay M, Koike S, Sarnow P, Ronaghi M, Ding S-W, Harris E, Chow M, Diamond MS, Kirkegaard K, Glenn JS, Fire AZ. Six RNA viruses and forty-one hosts: viral small RNAs and modulation of small RNA repertoires in vertebrate and invertebrate systems. PLoS pathogens. 2010 Feb;6(2):e1000764. PMCID: PMC2820531 DOI: 10.1371/journal.ppat.1000764

203. Schopman NCT, Willemsen M, Liu YP, Bradley T, Kampen A van, Baas F, Berkhout B, Haasnoot J. Deep sequencing of virus-infected cells reveals HIV-encoded small RNAs. Nucleic acids research. 2012 Jan;40(1):414–427. PMCID: PMC3245934 DOI: 10.1093/nar/gkr719

204. Xu N, Segerman B, Zhou X, Akusjärvi G. Adenovirus virus-associated RNAII-derived small RNAs are efficiently incorporated into the rna-induced silencing complex and associate with polyribosomes. Journal of virology. 2007 Oct;81(19):10540–10549. PMCID: PMC2045446 DOI: 10.1128/JVI.00885-07

205. Aparicio O, Razquin N, Zaratiegui M, Narvaiza I, Fortes P. Adenovirus virus-associated RNA is processed to functional interfering RNAs involved in virus production. Journal of virology. 2006 Feb;80(3):1376–1384. PMCID: PMC1346933 DOI: 10.1128/JVI.80.3.1376-1384.2006

206. Andersson MG, Haasnoot PCJ, Xu N, Berenjian S, Berkhout B, Akusjärvi G. Suppression of RNA interference by adenovirus virus-associated RNA. Journal of virology. 2005 Aug;79(15):9556–9565. PMCID: PMC1181602

DOI: 10.1128/JVI.79.15.9556-9565.2005

207. Weng KF, Hung CT, Hsieh PT, Li ML. A cytoplasmic RNA virus generates functional viral small RNAs and regulates viral IRES activity in mammalian cells. Nucleic acids 2014;

208. Kok K-H, Lui P-Y, Ng M-HJ, Siu K-L, Au SWN, Jin D-Y. The Double-Stranded RNA-Binding Protein PACT Functions as a Cellular Activator of RIG-I to Facilitate Innate Antiviral Response. Cell host & microbe. 2011 Apr;9(4):299–309.

209. Ho T-H, Kew C, Lui P-Y, Chan C-P, Satoh T, Akira S, Jin D-Y, Kok K-H. PACT- and RIG-I-Dependent Activation of Type I Interferon Production by a Defective Interfering RNA Derived from Measles Virus Vaccine. Journal of virology. 2016 Feb;90(3):1557–1568. PMCID: PMC4719617 DOI: 10.1128/JVI.02161-15

210. Komuro A, Homma Y, Negoro T, Barber GN, Horvath CM. The TAR-RNA binding protein is required for immunoresponses triggered by Cardiovirus infection. Biochemical and biophysical research communications. 2016 Nov;480(2):187–193. DOI: 10.1016/j.bbrc.2016.10.023

211. Weber M, Sediri H, Felgenhauer U, Binzen I, Bänfer S, Jacob R, Brunotte L, García-Sastre A, Schmid-Burgk JL, Schmidt T, Hornung V, Kochs G, Schwemmle M, Klenk H-D, Weber F. Influenza Virus Adaptation PB2-627K Modulates Nucleocapsid Inhibition by the Pathogen Sensor RIG-I. Cell host & microbe. 2015 Mar;17(3):309–319.

212. Sato S, Li K, Kameyama T, Hayashi T, Ishida Y, Murakami S, Watanabe T, Iijima S, Sakurai Y, Watashi K, Tsutsumi S, Sato Y, Akita H, Wakita T, Rice CM, Harashima H, Kohara M, Tanaka Y, Takaoka A. The RNA Sensor RIG-I Dually Functions as an Innate Sensor and Direct Antiviral Factor for Hepatitis B Virus. Immunity. 2015 Jan;42(1):123–132. DOI: 10.1016/j.immuni.2014.12.016

213. Yao H, Dittmann M, Peisley A, Hoffmann H-H, Gilmore RH, Schmidt T, Schmid-Burgk JL, Hornung V, Rice CM, Hur S. ATP-Dependent Effector-like Functions of RIG-I-like Receptors. Molecular cell. 2015 May;58(3):541–548. DOI: 10.1016/j.molcel.2015.03.014

214. Gu W, Lee H-C, Chaves D, Youngman EM, Pazour GJ, Conte Jr. D, Mello CC. CapSeq and CIP-TAP Identify Pol II Start Sites and Reveal Capped Small RNAs as C. elegans piRNA Precursors. Cell. 2012 Dec;151(7):1488–1500. DOI: 10.1016/j.cell.2012.11.023

215. Li S, Wang L, Berman M, Kong Y-Y, Dorf ME. Mapping a dynamic innate immunity protein interaction network regulating type I interferon production. Immunity. 2011 Sep;35(3):426–440. PMCID: PMC3253658 DOI: 10.1016/j.immuni.2011.06.014

216. Hamzeh-Mivehroud M, Mahmoudpour A, Rezazadeh H, Dastmalchi S. Non-specific translocation of peptide-displaying bacteriophage particles across the gastrointestinal barrier. European Journal of Pharmaceutics and Biopharmaceutics. 2008

Oct;70(2):577–581. DOI: 10.1016/j.ejpb.2008.06.005

217. Bogaert D, Keijser B, Huse S, Rossen J, Veenhoven R, Gils E van, Bruin J, Montijn R, Bonten M, Sanders E. Variability and Diversity of Nasopharyngeal Microbiota in Children: A Metagenomic Analysis. PloS one. 2011 Feb;6(2):e17035. DOI: 10.1371/journal.pone.0017035

218. Patel A, Hanson J, McLean TI, Olgiate J, Hilton M, Miller WE, Bachenheimer SL. Herpes simplex type 1 induction of persistent NF-kappa B nuclear translocation increases the efficiency of virus replication. Virology. 1998 Aug;247(2):212–222. PMID: 9705914

219. Goodkin ML, Ting AT, Blaho JA. NF-kappaB is required for apoptosis prevention during herpes simplex virus type 1 infection. Journal of virology. 2003 Jul;77(13):7261–7280. PMCID: PMC164802 DOI: 10.1128/JVI.77.13.7261-7280.2003

220. Liu X, Fitzgerald K, Kurt-Jones E, Finberg R, Knipe DM. Herpesvirus tegument protein activates NF-kappaB signaling through the TRAF6 adaptor protein. Proceedings of the National Academy of Sciences of the United States of America. 2008 Aug;105(32):11335–11339. PMCID: PMC2516262 DOI: 10.1073/pnas.0801617105

221. Liang Y, Yang K, Guo J, Wroblewska J, Fu Y-X, Peng H. Innate lymphotoxin receptor mediated signaling promotes HSV-1 associated neuroinflammation and viral replication. Scientific Reports. 2015 May;5(1):10406. PMCID: PMC4438665 DOI: 10.1038/srep10406

222. Dietrich N, Lienenklaus S, Weiss S, Gekara NO. Murine toll-like receptor 2 activation induces type I interferon responses from endolysosomal compartments. PloS one. 2010 Apr;5(4):e10250. PMCID: PMC2857745 DOI: 10.1371/journal.pone.0010250

223. Jenmalm MC, Cherwinski H, Bowman EP, Phillips JH, Sedgwick JD. Regulation of myeloid cell function through the CD200 receptor. The Journal of Immunology. 2006 Jan;176(1):191–199. PMID: 16365410 DOI: 10.4049/jimmunol.176.1.191

224. Rijkers ESK, De Ruiter T, Buitenhuis M, Veninga H, Hoek RM, Meyaard L. Ligation of CD200R by CD200 is not required for normal murine myelopoiesis. European Journal of Haematology. 2007 Nov;79(5):410–416. DOI: 10.1111/j.1600-0609.2007.00920.x

225. Scheffzek K, Ahmadian MR, Kabsch W, Wiesmüller L, Lautwein A, Schmitz F, Wittinghofer A. The Ras-RasGAP complex: structural basis for GTPase activation and its loss in oncogenic Ras mutants. Science (New York, NY). 1997 Jul;277(5324):333–338. PMID: 9219684

226. Downer EJ, Johnston DGW, Lynch MA. Differential role of Dok1 and Dok2 in TLR2-induced inflammatory signaling in glia. Molecular and Cellular Neuroscience. 2013 Sep;56:148–158. DOI: 10.1016/j.mcn.2013.04.007

227. Peroval MY, Boyd AC, Young JR, Smith AL. A critical role for MAPK signalling

pathways in the transcriptional regulation of toll like receptors. PloS one. 2013;8(2):e51243. PMCID: PMC3566169 DOI: 10.1371/journal.pone.0051243

228. Richardson E, Wearsch P, Boom W. TLR2 and ERK signaling control macrophage responses to Mycobacterium tuberculosis and the balance of inflammatory mechanisms and Th1 activation (INC7P. 402 .... The Journal of 2014;

229. Lu Z, Xie D, Chen Y, Tian E, Muhammad I, Chen X, Miao Y, Hu W, Wu Z, Ni H, Xin J, Li Y, Li J. TLR2 mediates autophagy through ERK signaling pathway in Mycoplasma gallisepticum -infected RAW264.7 cells. Molecular Immunology. 2017 Jul;87:161–170. DOI: 10.1016/j.molimm.2017.04.013

230. Richardson ET, Shukla S, Sweet DR, Wearsch PA, Tsichlis PN, Boom WH, Harding CV. Toll-Like Receptor 2-Dependent Extracellular Signal-Regulated Kinase Signaling in Mycobacterium tuberculosis-Infected Macrophages Drives Anti-Inflammatory Responses and Inhibits Th1 Polarization of Responding T Cells. Infection and Immunity. 2015 Jun;83(6):2242–2254. PMCID: PMC4432743 DOI: 10.1128/IAI.00135-15

231. Underhill DM, Ozinsky A, Hajjar AM, Stevens A, Wilson CB, Bassetti M, Aderem A. The Toll-like receptor 2 is recruited to macrophage phagosomes and discriminates between pathogens. Nature. 1999 Oct;401(6755):811–815. DOI: 10.1038/44605

232. Nilsen NJ, Deininger S, Nonstad U, Skjeldal F, Husebye H, Rodionov D, Aulock S von, Hartung T, Lien E, Bakke O, Espevik T. Cellular trafficking of lipoteichoic acid and Toll-like receptor 2 in relation to signaling: role of CD14 and CD36. Journal of leukocyte biology. 2008 Jul;84(1):280–291. PMCID: PMC3178504 DOI: 10.1189/jlb.0907656

233. Schjetne KW, Thompson KM, Nilsen N, Flo TH, Fleckenstein B, Iversen J-G, Espevik T, Bogen B. Cutting Edge: Link Between Innate and Adaptive Immunity: Toll-Like Receptor 2 Internalizes Antigen for Presentation to CD4+ T Cells and Could Be an Efficient Vaccine Target. The Journal of Immunology. 2003 Jul;171(1):32–36. PMID: 12816980 DOI: 10.4049/jimmunol.171.1.32

234. Cohen M, Braun E, Tsalenchuck Y, Panet A, Steiner I. Restrictions that control herpes simplex virus type 1 infection in mouse brain ex vivo. Journal of General Virology. 2011 Oct;92(Pt 10):2383–2393. PMID: 21697348 DOI: 10.1099/vir.0.031013-0

235. Moore MJ, Zhang C, Gantman EC, Mele A, Darnell JC, Darnell RB. Mapping Argonaute and conventional RNA-binding protein interactions with RNA at single-nucleotide resolution using HITS-CLIP and CIMS analysis. Nature protocols. 2014 Feb;9(2):263–293. PMCID: PMC4156013 DOI: 10.1038/nprot.2014.012

236. Darnell JC, Van Driesche SJ, Zhang C, Hung KYS, Mele A, Fraser CE, Stone EF, Chen C, Fak JJ, Chi SW, Licatalosi DD, Richter JD, Darnell RB. FMRP stalls ribosomal translocation on mRNAs linked to synaptic function and autism. Cell. 2011

Jul;146(2):247–261. PMCID: PMC3232425 DOI: 10.1016/j.cell.2011.06.013

237. Pollpeter D, Komuro A, Barber GN, Horvath CM. Impaired cellular responses to cytosolic DNA or infection with Listeria monocytogenes and vaccinia virus in the absence of the murine LGP2 protein. PloS one. 2011 Apr;6(4):e18842. PMCID: PMC3077416 DOI: 10.1371/journal.pone.0018842

238. O'Connell RM, Saha SK, Vaidya SA, Bruhn KW, Miranda GA, Zarnegar B, Perry AK, Nguyen BO, Lane TF, Taniguchi T, Miller JF, Cheng G. Type I interferon production enhances susceptibility to Listeria monocytogenes infection. Journal of Experimental Medicine. 2004 Aug;200(4):437–445. PMCID: PMC2211937 DOI: 10.1084/jem.20040712

239. Ablasser A, Bauernfeind F, Hartmann G, Latz E, Fitzgerald KA, Hornung V. RIG-I-dependent sensing of poly(dA:dT) through the induction of an RNA polymerase III-transcribed RNA intermediate. Nature immunology. 2009 Oct;10(10):1065–1072. PMCID: PMC3878616 DOI: 10.1038/ni.1779

240. Swiergiel AH, Smagin GN, Dunn AJ. Influenza virus infection of mice induces anorexia: comparison with endotoxin and interleukin-1 and the effects of indomethacin. Pharmacology, biochemistry, and behavior. 1997 May;57(1-2):389–396. PMID: 9164599